# FREQUENCY-STABILIZED $CO_2$ LASERS

PHASE ONE REPORT

Contract NAS 8-20631

12 August 1966



Prepared For

National Aeronautics
and
Space Administration
Huntsville, Alabama

SESW-G534

SYLVANIA ELECTRONIC SYSTEMS-WESTERN OPERATION
Post Office Box 205
Mountain View, California 94042

# FREQUENCY-STABILIZED $CO_2$ LASERS

PHASE ONE REPORT

Contract NAS 8-20631

12 August 1966

Authors:

R.S. Reynolds
A.E. Siegman
J.D. Foster
R. Rogers

APPROVED BY: Dr. B. J. McMurtry
Mgr. Advanced Technology
Laboratory

Prepared For

National Aeronautics and Space Administration
Huntsville, Alabama

## FOREWORD

This is the Phase I engineering report, covering studies toward the best techniques for design of a frequency stabilized laser prepared under NASA Contract No. NAS8-20631. This report was prepared by the Electronic Systems Division of Sylvania Electric Products Inc., Mountain View, California and describes work performed in the Optics Department of the Advanced Technology Laboratory. Mr. Richard Reynolds is the principal investigator in this program.

All the work in this report was administered under the Astrionics Laboratory, NASA George C. Marshall Space Flight Center, Huntsville, Alabama. Dr. J. R. Randall is the principal technical representative for the laboratory.

## ABSTRACT

This report covers the work performed on a study effort to establish the best techniques for attaining a $1:10^{10}$ frequency-stabilized $CO_2$ laser. The report discusses several electronic and mechanical stabilization schemes, control loop techniques, wavelength and mode control techniques, and general laser construction and operation approaches. It appears that a technique which stabilizes the $CO_2$ laser frequency to an external $CO_2$ amplifier is capable of providing the required frequency stability.

TABLE OF CONTENTS

TABLE OF CONTENTS (Continued)

TABLE OF CONTENTS (Continued)

## LIST OF ILLUSTRATIONS

## LIST OF ILLUSTRATIONS (Continued)



## LIST OF TABLES

# Section 1

# INTRODUCTION

This Phase Report covers the work performed on the first phase of a two-phase program. The objectives of the program are to undertake a study and investigation directed toward disclosure of the most economical, practical, and feasible method of accomplishing the design, fabrication, testing, and demonstration of a frequency stabilized $CO_2$ gas laser. This report covers the study and investigation phase of the program.

The specific objectives of the program are to develop $CO_2$ laser fabrication and stabilization techniques which would be capable of providing a $CO_2$ laser stabilized in frequency to 1 part in $10^{10}$ for an indefinite period of time in a normal laboratory environment. This figure is for both long- and short-term stabilities. The laser output power shall be as high as possible consistent with the stabilization requirements and shall occur in a single frequency.

Most of the laser stabilization techniques which have been used in the past were reviewed for possible use with the $CO_2$ laser. Most schemes were not found to be applicable to the $CO_2$ laser, and the schemes which were applicable would not meet the requirements. Fortunately, a new scheme was devised for use with the $CO_2$ laser which can satisfy, at a minimum, the requirements set forth on the laser. This scheme is discussed at length in the body of this report.

Also, techniques for mechanically stabilizing the structure so as to reduce the problems inherent with ambient vibrations and thermal drift are discussed. Preferred laser construction techniques, mode and wavelength control techniques peculiar to the $CO_2$ laser are discussed at length.

Control loop techniques are also discussed and some examples of the expected performance of the stabilization system are presented based on the expected performance of typical components.

Section 2.0 offers background material on the characteristics of molecular lasers directly applicable to the present problems; Section 3 surveys many of the available stabilization techniques and Section 4 discusses in detail the technique chosen for this program with estimates on its sensitivity; Section 5 reviews control loop problems associated with laser stabilization; Section 6 discusses laser wavelength and mode control techniques applicable to the $CO_2$ laser; Section 7 describes several laser tube excitation and design techniques;

1. (Continued)

Section 8 analyzes mechanical stabilization techniques; Section 9 contains the concluding remarks and recommendations; Section 10 indicates our plans for the next period, and Section 11 contains the references. An appendix with a Molecular Laser Bibliography is included for completeness.

For ease of reading, each major section has a set of summary paragraphs at the end of the section so that the essence of the section can be obtained quickly.

# Section 2

# BACKGROUND DISCUSSION

## 2.1 GENERAL

The purpose of this section is to establish, in a coherent fashion and in one convenient location, a summary of molecular laser characteristics, the understanding of which is necessary for the complete evaluation of the limitations of the $CO_2$ laser and amplifier. Paragraph 2.2 describes the energy levels associated with infrared laser action and discusses the nomenclature used in describing these levels for the case of the $CO_2$ molecule. The vibrational and rotational level schemes are discussed, and the qualifications required for transitions between levels explained. It is not necessary to study this section to fully understand the stabilization techniques proposed later.

Paragraphs 2.3 and 2.4 summarize the practical characteristics of the $CO_2$ laser and cover the areas of inherent frequency shifts in the $CO_2$ laser line. For convenience, this section may be bypassed until later study is warranted; however, thorough understanding of this material is necessary for complete understanding of the limitations and peculiarities of the $CO_2$ laser as applied to the proposed program.

## 2.2 MOLECULAR LASER CHARACTERISTICS

### 2.2.1 Molecular Laser Energy Levels

Perhaps the most striking advance in gas laser technology to date has been the discovery of laser action at middle infrared wavelengths on the vibrational-rotational transitions of molecules, with the $CO_2$ molecule as the currently most important example.

To understand the energy levels on which molecular lasers operate, consider the schematic representation of a typical molecule, $CO_2$, as shown in Figure 2-1. The quantum states and energy levels of such a molecule originate from three main sources:

2.2.1 (Continued)

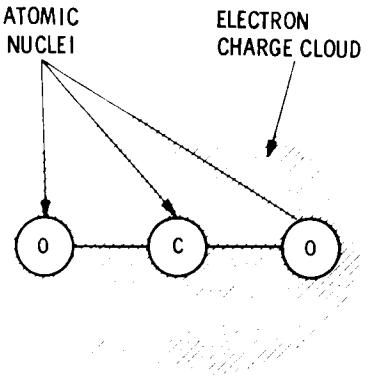


Figure 2-1. Pictorial Representation of a $CO_2$ Molecule

a. Electronic motions

The electronic charge cloud surrounding the fixed atomic nuclei can be represented by a quantum mechanical wave function, which has certain allowed energy states and associated wave functions, just as does the electronic charge cloud surrounding the nucleus in a single atom. These different electronic energy states are rather widely separated in energy, so that transitions between different electronic energy levels correspond to transition frequencies (generally in the visible and UV portions of the spectrum). The visible and UV laser action observed in various molecules in pulsed discharges comes from transitions involving electronic energy changes.

b. Vibrational motions

The atomic nuclei embedded in the electronic charge cloud are held in their rest positions by the molecular binding forces. However, the nuclei can vibrate about their equilibrium positions, more or less independently of the electronic quantum state of the electronic charge cloud. These vibrational frequencies are typically in the near and middle IR range. Of course, these vibrations must be quantized also, leading to vibrational energy levels. Thus, each widely spaced electronic level is actually split into a series of more closely spaced vibrational levels that indicate the state of vibrational motion of the molecule.

## Appendix C

## GaAs PHASE OR FREQUENCY MODULATOR

One electro-optic material known to be useful at 10.6 $\mu$m is gallium arsenide, GaAs. The peak phase delay $\delta$ for radiation transversing a GaAs crystal polarized along one of the birefringent axes is given by

$$\delta = \frac{\pi\, n_0^{\,3}\, r_{41}\, \ell V}{\lambda d}$$

where $n_0$ is the index of refraction; $r_{41}$, the electro-optic coefficient; $\ell$, the modulator length; $V$, the applied voltage; $\lambda$, the laser wavelength; and $d$, the modulator width.

The electro-optic coefficient for GaAs in the range 1.0 - 1.7 $\mu$m is given by Ho and Buhrer* as

$$n_0^{\,3}\, r_{41} \approx 6 \times 10^{-6} \text{ cm/kv}$$

More recent data at 10.6 $\mu$m (RCA Laboratories, unpublished) indicates that

$$r_{41} \approx 10^{-7} \text{ cm/kv}$$

$$n_0^{\,3}\, r_{41} \approx 3 \times 10^{-6} \text{ cm/kv} \qquad (n_0 \approx 3.1)$$

The latter value is probably more relevant to our problem.

Suppose that we use a modulator of length $\ell$ which is double-passed (by placing a mirror at one end of the modulator), the total retardation will then be

$$\delta = \frac{2\pi\, n_0^{\,3}\, r_{41}\, \ell V}{\lambda d}$$

Putting in numerical values yields,

$$\delta \approx 0.02 \times \frac{\ell}{d} \times V(\text{kV})$$

---

*L. Ho and C. F. Buhrer, "Electro-Optic Effect of Gallium Arsenide," Applied Optics 2, 647 (June 1963).

C. (Continued)

The $\ell/d$ (length over width) ratio can probably be made equal to 20, allowing a modulation index of

$$\delta \approx 1 \text{ radian per } 2.5 \text{ kV}$$

For a peak modulation index of, say, 1 radian we require the large but not impossible modulation voltage of 2.5 kV peak. (Ho and Buhrer, in fact, used 2 kV peak voltages at 1 MHz across a 4 mm square bar in their measurements on GaAs.)

2.2.1 (Continued)

c. Rotational motions

Finally, while all of these electronic and vibrational motions are going on, the molecule, as a whole, can also be slowly rotating about various axes in space, at rotation rates characteristic of far infrared frequencies. These rotational motions, by quantum rules, must have quantized angular momentum and hence quantized energy levels, with a relatively small energy spacing. Hence, each electronic-vibrational level is further subdivided into numerous closely spaced rotational levels.

The sketch of Figure 2-2 indicates diagrammatically this general energy level scheme. When one considers all of the multiple oscillations, vibrations, and rotations of a complex polyatomic molecule, one sees that the overall energy spectrum can become exceedingly complex.*

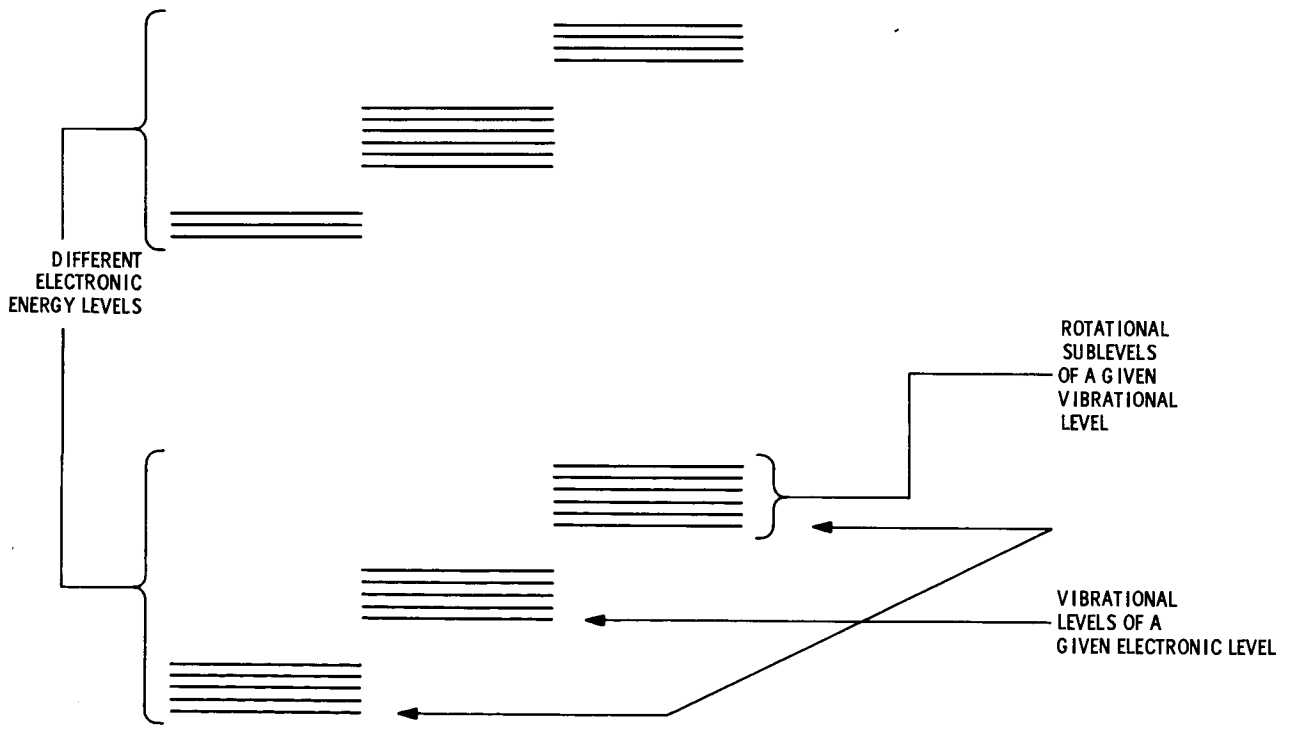


Figure 2-2. General Structure of Molecular Energy Levels

*If one goes one step further and includes nuclear spin effects, one adds even another stage of hyperfine splitting. Fortunately, we can neglect this in the cases of interest to us.

### 2.2.2 Vibrational-Rotational Laser Action in Molecules

The type of vibrational-rotational molecular laser action of interest to us generally follows the steps shown in Figure 2-3. The molecule is initially excited or pumped in the discharge from its ground level up to (very) many of its higher electronic levels. From these levels, the molecules relax or trickle down into various of the vibrational-rotational levels of the ground electronic state. Depending on the details of relaxation rates and lifetimes, population inversion between various vibrational-rotational levels in the ground electronic state will ensue and make laser action possible, as shown in Figure 2-3.

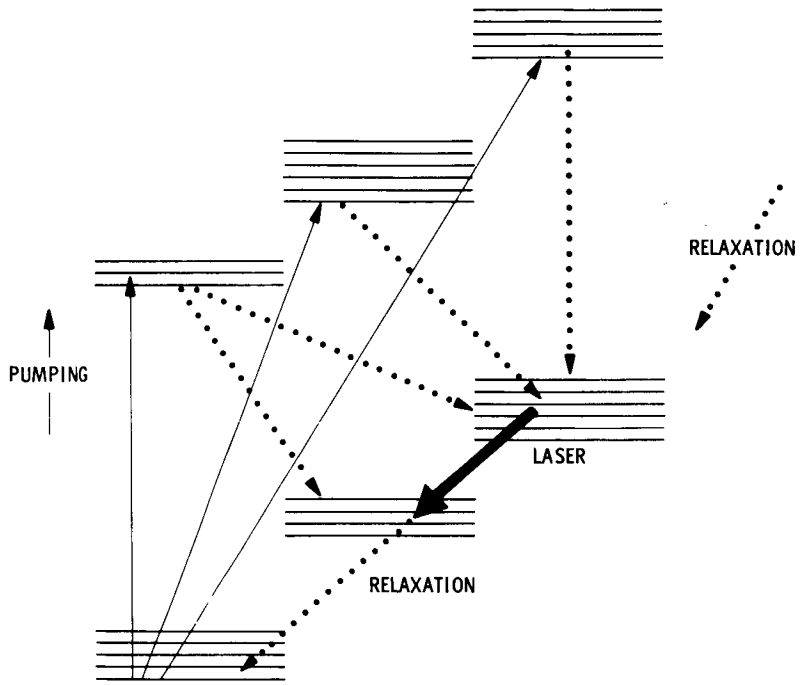


Figure 2-3. General Features of Molecular Laser Action on Vibrational-Rotational Transitions

Not indicated in the figure is the fact that other molecules in the discharge may also assist the laser action. In general, different molecules in the discharge will collide, and exchange energy in the process, especially if two transitions in the different molecules have nearly the same transition frequency. For instance, another molecule of type B may be more easily excited to high energy levels by the discharge than are the laser molecules of type A. Excited B molecules will then collide with ground state A molecules and give energy to them, thereby providing an indirect pumping mechanism for the laser. Type B molecules

2.2.2 (Continued)

may also help to empty out the lower laser level in type A laser molecules, by taking away energy and thus assisting the A molecule to get back to its ground state. In general, the situation seems to be that the presence of other molecules very often greatly enhances molecular laser action; e.g., the $CO_2$ laser is enhanced by the simultaneous presence of He, $N_2$, $H_2O$, and probably other gases.

## 2.2.3 Vibrational-Rotational Levels of the $CO_2$ Molecule

### 2.2.3.1 Vibrational Motions

The $CO_2$ molecule is an excellent molecule to examine in detail because it is complicated enough to be interesting and yet simple enough to be understood. As illustrated in Figure 2-1, the $CO_2$ molecule is a symmetric, linear molecule.* We will not attempt any discussion of its electronic states, but will turn immediately to the vibrational-rotational states of the ground electronic level.

The $CO_2$ molecule has three possible elementary modes of vibrational motion, as indicated in Figure 2-4. Note that the first of these, $\nu_1$, is a purely symmetric motion that has no net electric dipole moment. Hence, this motion (and associated transitions) will not couple directly to electromagnetic radiation, although this motion will appear strongly in Raman scattering. The $\nu_2$ motion can occur equally in two directions perpendicular to the molecular axis, and hence there is a twofold degeneracy associated with $\nu_2$. The quantum number, $n_2$, gives the total transverse vibration, while a second quantum number, $\ell \leq n_2$, then indicates the net angular momentum about the molecular axis that is associated with the $\nu_2$ vibrational motion.

Each of these vibrations is like a simple harmonic oscillator, and the overall energy of the molecule can be viewed as consisting of some integer number of quanta of energy $h\nu$ at each of these frequencies. The vibrational quantum states are thus labelled by an overall quantum label which is written in the form

$$\left| n_1, n_2^{\ell}, n_3 \right|$$

* In technical terms, its point group symmetry is $D_{\infty h}$. The D means "dihedral," i.e., there are (an infinite number of) twofold symmetry axes passing through the middle of the molecule perpendicular to the molecule's axis of symmetry. The $\infty$ means essentially infinite-fold symmetry about the symmetry axis, and the h means there is a "horizontal" plane of symmetry through the middle of the molecule perpendicular to the symmetry axis.

2.2.3.1 (Continued)

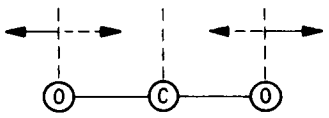

$\nu_1 \approx 1337\ cm^{-1}$ | $n_1$ | SYMMETRIC -- NO ELECTRIC DIPOLE MOMENT -- QUANT NO. $n_1$ | RAMAN ACTIVE

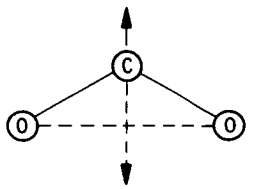

$\nu_2 \approx 667\ cm^{-1}$ | $n_2, \ell$ | UNSYMMETRIC -- DIPOLE MOMENT -- TWOFOLD DEGENERACY | IR ACTIVE

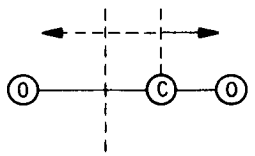

$\nu_3 \approx 2349\ cm^{-1}$ | $n_3$ | UNSYMMETRIC -- LARGE DIPOLE MOMENT | STRONGLY IR ACTIVE

TOTAL QUANTUM NUMBER: $\left\{ n_1, n_2^{\ell}, n_3 \right\}$

Figure 2-4. Vibrational Motions of the $CO_2$ Molecule

The energy associated with an $(n_1, n_2^{\ell}, n_3)$ vibrational state is then given to first order by

$$E_{vibr}(n_1 n_2^{\ell} n_3 \text{ state}) = (n_1 + \tfrac{1}{2})h\nu_1 + (n_2 + \tfrac{1}{2})h\nu_2 + (n_3 + \tfrac{1}{2})h\nu_3$$

The 1/2 factors represent zero-point energies, as in the usual quantized simple harmonic oscillator.

For example, Figure 2-5 shows some of the important lowest vibrational levels of the $CO_2$ molecule, together with the strong laser lines of $CO_2$. The meaning of the vibrational (00°1), and so forth, notation now becomes clear.

One fine point in the $CO_2$ spectrum is that, essentially by accident, $\nu_1 \approx 2\nu_2$. Hence the (100) and (020) levels are nearly degenerate. As a result, there is a quantum-mechanical "coupling" of these levels that tends to split them apart or repel them. A check will show that the (10°0) and (02°0) levels in Figure 2-5 are not exactly at $\nu_1$ and at $2\nu_2$; but the mean value of the two energies does come at $\nu \approx \nu_1 \approx 2\nu_2$.

2.2.3.1 (Continued)

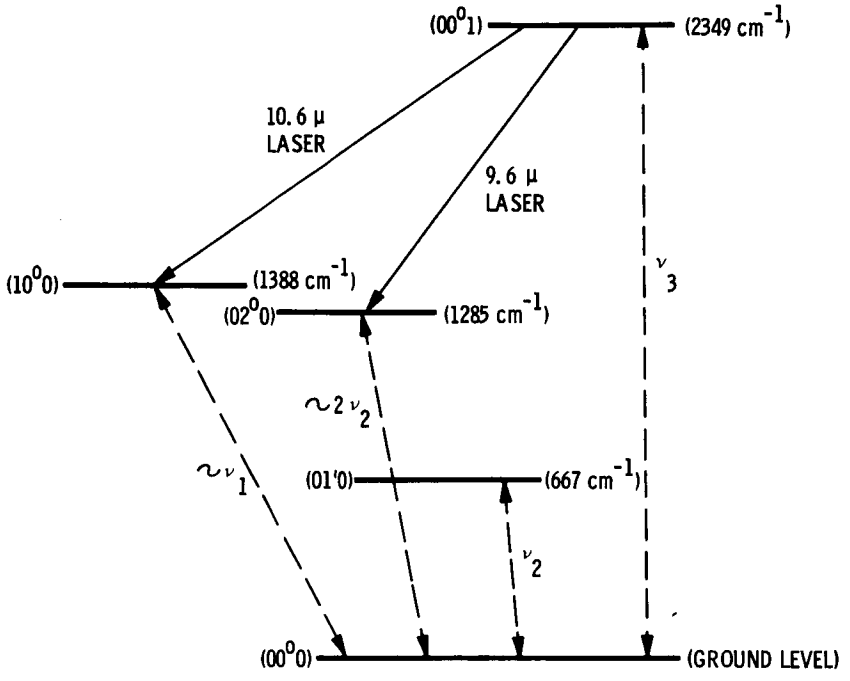


Figure 2-5. Some Vibrational Energy Levels of the $CO_2$ Molecule

In general, more refined values of the vibrational energy levels, especially for higher overtones of $\nu_1$, $\nu_2$, and $\nu_3$, are given by more complicated expressions of the form

$$E_{vibr}(n_1 n_2{}^{\ell} n_3) = \sum_{i=1}^{3} h\nu_i \left(n_i + \frac{1}{2}\right) + \sum_{i,j} x_{ij} \left(n_i + \frac{1}{2}\right)\left(n_j + \frac{1}{2}\right)$$

$$+ \sum_{i,j} g_{ij} \ell_i \ell_j$$

The first additional sum, containing the $x_{ij}$ terms and double products of $(n_i + 1/2)$, represents the effects of small anharmonicity or nonlinearity in the restoring forces of the molecular vibrations. The second additional sum represents the fact that levels of the same $n_1$, $n_2$, $n_3$ but different $\ell$ values will, in general, be split slightly in energy. These topics are of great importance to spectroscopists, but are not of great importance to us here.

2.2.3.2 Rotational Motions

The $CO_2$ molecule is a rigid rotor that can rotate about any axis normal to the molecular symmetry axis. From the quantum theory of rotation and angular momentum, the energy levels of the rotational motions are given, at least to first order, by

$$E_{rot}(J) = B\,J(J+1), \qquad J = 0, 1, 2, \ldots.$$

where J is the angular momentum or rotational quantum number.

Refinements to this picture occur when one takes into account that the molecule will stretch, and hence its moment of inertia will change slightly, when it rotates faster. This can be included by writing

$$E_{rot}(J) = B\,J(J+1) - D\,J^2(J+1)^2$$

The correction due to D is usually fairly small, and we will not discuss it in detail.

In addition, the coefficients B and D depend slightly on which vibrational level the molecule is in. This is taken into account by writing

$$E_{rot}(n_1, n_2^{\ell}, n_3, J) = B_v J(J+1) - D_v J^2(J+1)^2$$

where v is shorthand for the vibrational quantum numbers $(n_1, n_2^{\ell}, n_3)$. For instance, Herzberg[1*] gives for the $CO_2$ molecule

$$B_{00^0 0} = 0.3937\ cm^{-1}$$

$$B_{00^0 1} = 0.3866\ cm^{-1}$$

$$B_{10^0 0} = 0.3897\ cm^{-1}$$

$$B_{02^0 0} = 0.3899\ cm^{-1}$$

*See List of References, Section 11.

2.2.3.3 (Continued)

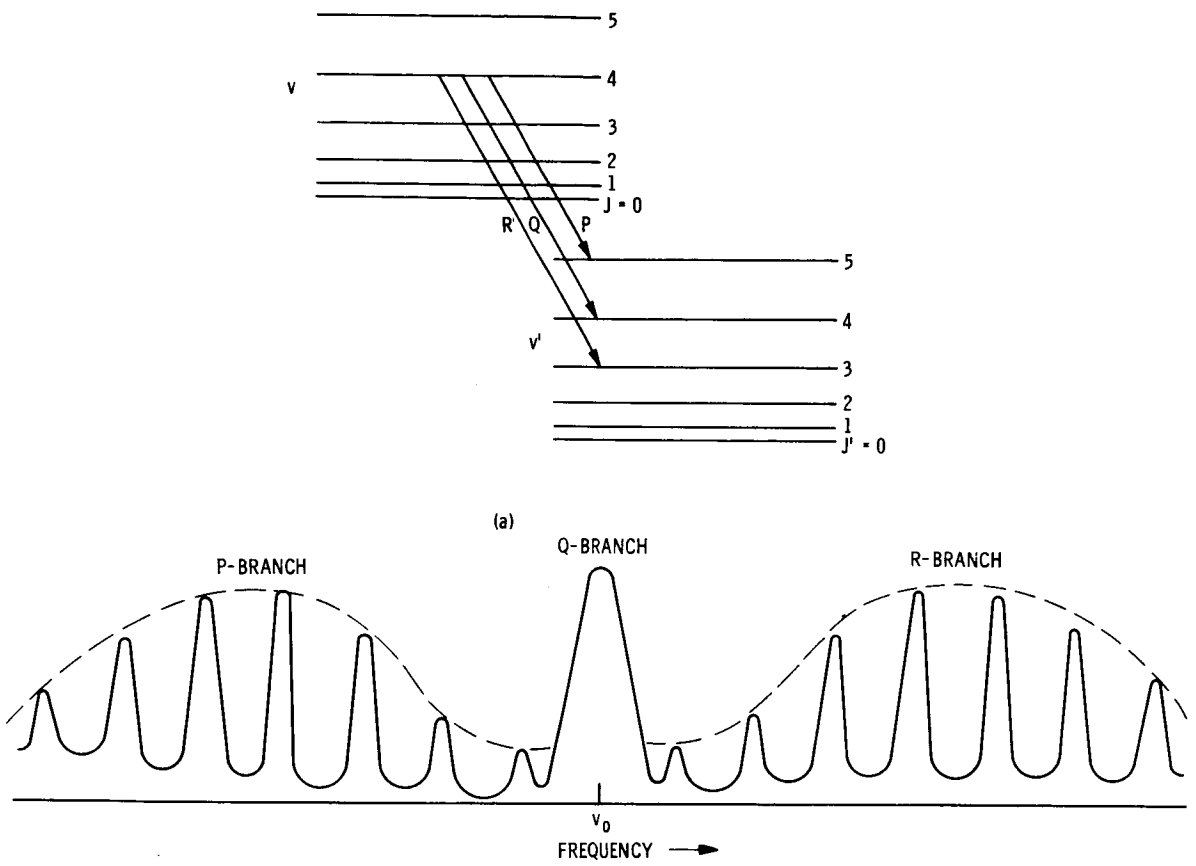


Figure 2-6. Vibrational-Rotational Transitions–P, Q, and R Branches

Carbon dioxide follows the above description, with some important exceptions. Because $CO_2$ is an exactly symmetrical molecule, and is without nuclear spin, the Q-branch or J = 0 transitions are absolutely forbidden by symmetry restrictions. Also, J to J ± 1 transitions within a single vibrational state are absolutely forbidden in $CO_2$ energy level diagram of Figure 2-7, in which the dashed lines indicate radiative transitions that are allowed by electric dipole considerations. The $\Sigma^+$ and $\pi$ notations have to do with the electronic-vibrational state of the molecule, and the subscripts g and u indicate whether the vibrational state is symmetric or antisymmetric with respect to vibrational motion.

Consider a molecule initially in an even J rotational level of the ground state. Inspection will show that by making allowed P- or R-branch transitions to other vibrational levels, this molecule can only get to odd J levels in the u states, or to even J levels in any g states.

2.2.3.2 (Continued)

We will see later that the observed lines in a vibrational-rotational spectrum are almost, but not quite, equally spaced. The difference in $B_v$ values accounts in part for the nonequal spacing, together with the $D_v$ correction term.

2.2.3.3 Combined Vibrational-Rotational Levels

Consider two different vibrational levels of a molecule, with their associated rotational sublevels as shown in Figure 2-6(a). In general, transitions from the rotational sublevels of one vibrational level to the rotational sublevels of another are governed by selection rules as to the allowed change in J; and these transitions are classified into "branches" by the change in J as follows:

| Transitions from | v, J(upper) to | v', J'(lower) |
|---|---|---|
| P-branch: | $J' = J + 1$ | $P(J')$ |
| Q-branch: | $J' = J$ | $Q(J')$ |
| R-branch: | $J' = J - 1$ | $R(J')$ |

The associated transition frequencies are given by

$$h\nu = E_v(J) - E_{v'}(J')$$

$$= \left|E_v(0) + B_v J(J+1)\right| - \left|E_{v'}(0) + B_{v'} J'(J'+1)\right|$$

$$= \left|E_v(0) - E_{v'}(0)\right| + B\left|J(J+1) - J'(J'+1)\right|$$

If we call the frequency $(1/h)\left|E_v(0) - E_{v'}(0)\right|$ the band center frequency $\nu_0$, then the transition frequencies can be written

$$\nu = \begin{cases} \nu_0 - (2B/h)J & P(J+1) \\ \nu_0 & Q \\ \nu_0 + (2B/h)J & R(J-1) \end{cases}$$

Thus, the Q branch is concentrated exactly at the band center, while the P and R branches form a series of lines evenly spaced (to first order) below and above the band center frequency. Figure 2-6(b) shows the typical appearance of a vibrational-rotational absorption or spontaneous emission with the P, Q, and R branches.

2.2.3.3 (Continued)

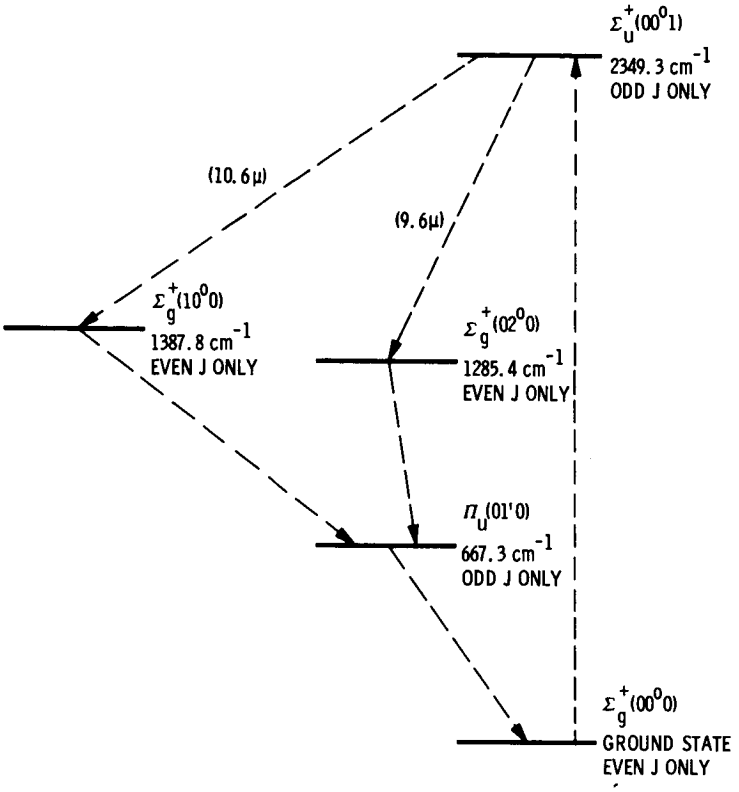


Figure 2-7. Low-Lying $CO_2$ Energy Levels in Greater Detail

Similarly, any molecules initially in ground state at odd J levels will always go to even J levels in u states or odd J levels in g states. Thus, we might divide all $CO_2$ molecules into two classes, depending upon whether they could reach even or odd J levels in a g state. So highly forbidden (by parity conservation) are all transitions connecting these classes that the two classes (if both do exist) will remain separated for all time.*

In fact, the experimental evidence plainly shows that only the "even J in g states" class of $CO_2$ molecules seems to be in existence. This is certainly to be expected because of the fact that the two oxygen atoms are spinless, symmetrically located, indistinguishable particles. From concepts of symmetry, interchange of two indistinguishable particles must either leave the wave function of a system totally unchanged or must change the sign of the wave functions. If the former holds true, the particle is called a boson, and the system obeys Bose-Einstein statistics. If the latter case (i.e., sign change) applies, the particles are called fermions, and the system obeys Fermi-Dirac statistics.** If $CO_2$ molecules did exist in "odd J in g state" or "even J in u state" levels, these $CO_2$ molecules would be Fermi-Dirac particles, which would give them very odd properties.

*Another example of this same concept is the existence of ortho- and para-hydrogen, except that the ortho-to-para conversion process is there not so highly forbidden because of the existence of nuclear spins.

**See Dicke and Wittke, Introduction to Quantum Mechanics, Addison-Wesley; Chapter 17.

2.2.3.3 (Continued)

We conclude, therefore, that all $CO_2$ g states have rotational levels with even J values only, while all u states have odd J values only. Only even J' values appear in $CO_2$ P- and R-branch spectra; and no Q-branches ever appear.*

## 2.3 $CO_2$ LASER CHARACTERISTICS

As already noted, high-power, single-frequency CW laser action is readily obtained in $CO_2$ on the following transitions:

| | | |
|---|---|---|
| 00°1 - 10°0 | ~10.6$\mu$ | P(even), R(even) |
| 00°1 - 02°0 | ~ 9.6$\mu$ | P(even), R(even) |

The general features of this laser action have been described extensively in the literature, by Patel [2, 4, 5, 7] and others.[3, 6, 8, 9] Hence, we will not try to repeat all of the laser characteristics here, but will concentrate on those that are especially relevant to our prime concern – frequency stability.

### 2.3.1 Basic $CO_2$ Laser Characteristics

We will skip over many questions such as optimum pressures, gas fills, and so forth. These are obviously important, but at the same time they are not critical to first order and will be considered only when they are directly relevant to frequency stabilization.

Figure 2-8 indicates two vibrational levels, each with a total population $N_v$ and $N_{v'}$, and with Boltzmann distributions over the rotational sublevels in each vibrational band. Thermalization of populations by relaxation is known to take place rapidly among the rotational sublevels, so that the Boltzmann distribution with a temperature $T_{rot}$ is appropriate. In mild discharges such as are used in molecular lasers, $T_{rot}$ should not be far from the overall molecular temperature, and this should be considerably influenced by the wall temperature.

Figure 2-8 is presented chiefly to show that even with no total population inversion between $N_v$ and $N_{v'}$ ($N_{v'} \lesssim N_v$), and hence with a positive vibrational temperature $T_{vibr}$, there can still be net population inversion between a v, J level and a v', J' = J + 1 level,

*It is interesting to note that a mixed-isotope $CO_2$ molecule, e.g., $O^{16}CO^{18}$, is not quite perfectly symmetric; hence the intervening J values do reappear.

2.3.1 (Continued)

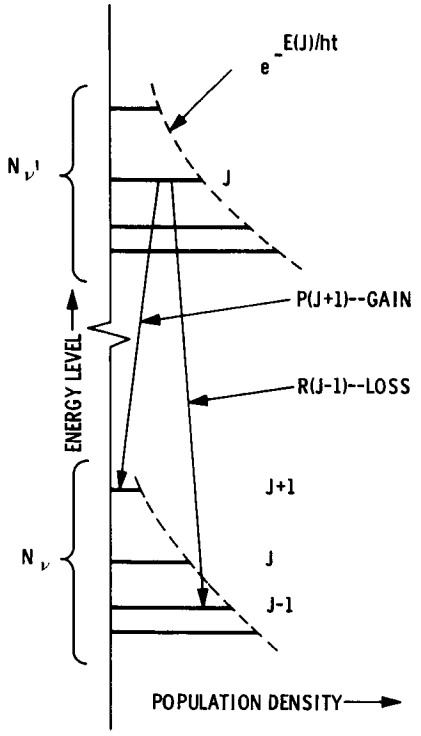


Figure 2-8. Illustrating that High Gain is More Probable on P-Branch than on R-Branch Transitions

essentially because the J' level is higher up the Boltzmann curve. Hence, P-branch oscillation is much more likely than R-branch oscillation under usual circumstances, as is clearly observed in experiments.

The complete details of the gain as a function of J for P(J + 1) and R(J - 1) transitions have been worked out by Patel,[10] taking into account the degeneracies of the J levels, the matrix elements, the Boltzmann partition factors, and so forth. The important conclusion is that the P-branch gain is positive over a range of J levels that varies with molecular temperature and pumping level (i.e., with $N_{v'}/N_v$). For example, in one experiment Patel found the following oscillations on the nominal 10.6$\mu$ transition:

2.3.1 (Continued)

| | | |
|---|---|---|
| P(14) | 949.47 $cm^{-1}$ | 10.5322$\mu$ |
| P(16) | 947.70 $cm^{-1}$ | 10.5519$\mu$ |
| P(18) | 945.93 $cm^{-1}$ | 10.5716$\mu$ |
| P(20) | 944.15 $cm^{-1}$ | 10.5915$\mu$ |
| P(22) | 942.34 $cm^{-1}$ | 10.6119$\mu$ |
| P(24) | 940.49 $cm^{-1}$ | 10.6327$\mu$ |
| P(26) | 938.64 $cm^{-1}$ | 10.6537$\mu$ |

The P(20) transition was the strongest of these. By using wavelength selection methods to suppress stronger transitions and allow weaker transitions to oscillate, and by varying pumping conditions, others [11] have obtained oscillations over J levels as high as P(52).

It is vitally important to note that these transitions all compete for molecules in the upper laser level. Once one transition begins oscillation it "steals" atoms from all of the other rotational levels by the fast relaxation among rotational levels.

We have not yet mentioned specifically that the Doppler-broadened linewidth of the $CO_2$ transitions, is given by the usual Doppler formula,

$$\Delta\nu_D = \frac{2\sqrt{2\ell n 2}}{\lambda}\sqrt{\frac{kT_{mol}}{M}} \approx 50 \text{ Mc}$$

where M is the molecular mass, and $T_{mol}$ the molecular temperature in the discharge. The axial mode spacing for a cavity of reasonable length will be several times this frequency. Hence, there is a good chance that an axial resonant cavity mode may not be present inside the P(J) line with the highest gain. In this case, laser action will occur in some other lower-gain P(J) transition. Indeed, the observation is that, as the laser mirrors vibrate and the axial modes shift in frequency, the laser oscillation jumps from one P(J) line to another, with oscillation at any one time in a single P(J) line only. Figure 2-9 shows three P(J) lines and a possible set of cavity modes, drawn very much not to scale, in order to show how one P(J) line may have a cavity mode within its linewidth, while other P(J) lines do not.

This will obviously be a major design problem for a stabilized laser. The laser will have to be initially set, and then locked, to one selected P(J) line. Mechanical vibrations

2.3.1 (Continued)

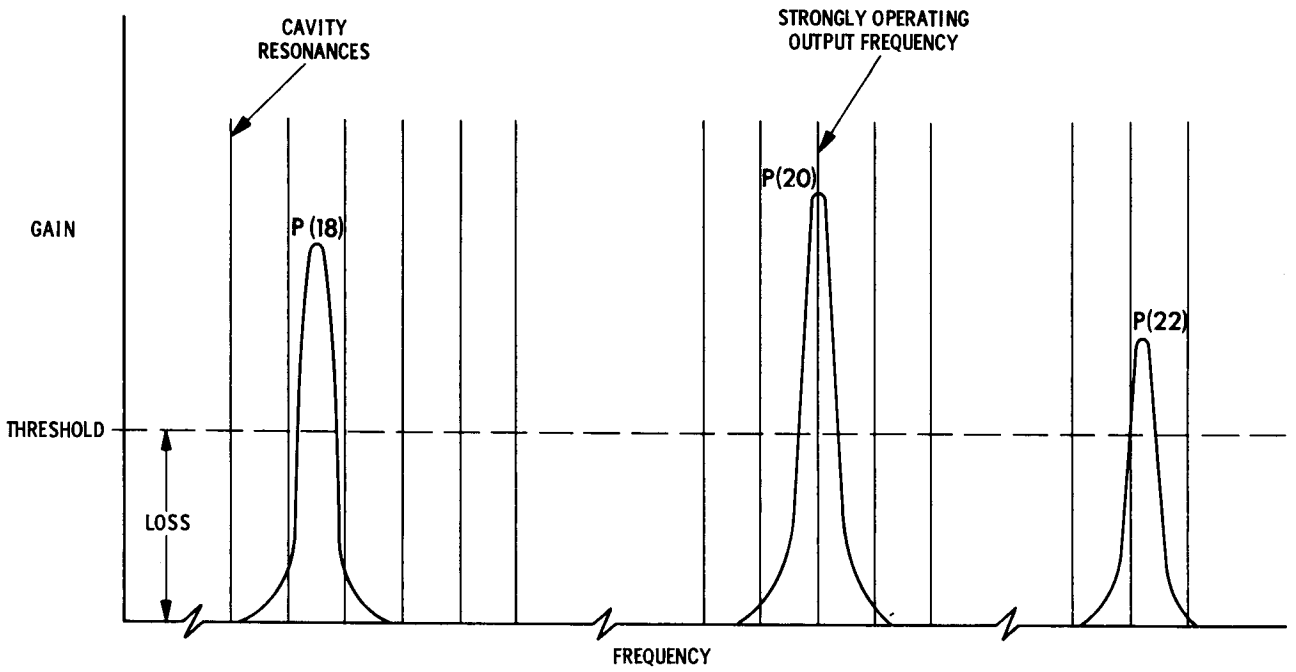


Figure 2-9. Single-Pass Gain versus Frequency for Three Lines of the $CO_2$ Laser, Showing Cavity Modes and P(J) Transitions

will have to be minimized, and thermal length changes compensated (either mechanically or electrically) to ensure very long-term operation in one single P(J) line.

2.3.2 Laser Excitation Techniques

The energy transfer process has been found to be extremely efficient, relative to other gas laser systems, and efficiencies as high as 13 percent have been reported for multiline operation[9] with multimode power outputs over 200 watts CW. The laser tubes producing these powers were about 6 meters long and about 2.2 cm in diameter.

The energy of a photon at 10.6$\mu$ is approximately 0.1 ev. The energy which is transferred from an electron in the discharge to a molecule, when the molecule is excited to an upper electronic level by collision with the electron, is several ev. Therefore, even if every such excited atom eventually returned to the ground state by passing through the laser transition, the power efficiency would only be ~5 percent or less – and it is not likely that every excited $CO_2$ molecule does participate in laser action, since some decay by other routes.

2.3.2 (Continued)

The remarkable efficiency of the $CO_2$ laser appears to be explained in part by the fact that the nitrogen molecule has a vibrational transition – and hence a ladder of vibrational energy levels – with frequency spacing very close to the (00°1) transition of the $CO_2$ molecule. The nitrogen molecules are excited to a high level on this "ladder" of energy levels by electron impact. The nitrogen molecules then drop back down this ladder, step by step, by successive collisions with unexcited $CO_2$ molecules. At each collision, the $CO_2$ molecule is excited to the upper 10.6-$\mu$ laser level; and the $N_2$ molecule drops down one more rung in energy. Thus, each excited $N_2$ molecule can pump multiple $CO_2$ molecules, leading to the observed pumping efficiency.

As noted, $CO_2$ 10.6-$\mu$ laser action is aided by addition of several other gases. Some of these aid the pumping process to the upper $CO_2$ laser level in a manner analogous to $N_2$. Others aid rather in relaxing $CO_2$ molecules out of the lower laser level. Information relevant to these processes was presented by C.K.N. Patel at the Fourth International Conference on Quantum Electronics in Phoenix, April 1966.

## 2.4 SECOND-ORDER FREQUENCY SHIFTS IN $CO_2$ LASER AMPLIFIERS

When one's objective is high frequency stability, consideration of first-order frequency shifts is not sufficient, and one must be prepared to closely examine more difficult second-order effects that will have an effect on the oscillation frequency. We now consider some of these effects.

### 2.4.1 Discharge Conditions: Pressure and Temperature Broadening and Shifts

For the case of a frequency stabilized laser, one will want to carefully stabilize the discharge conditions, the pressure, and the wall temperature in the laser proper. It is not possible at this point to predict the sensitivity to these parameters in detail, and this will form one aspect of the development program. However, we can carry out some very rough estimates, as follows.

The dominant source of inhomogeneous broadening in the $CO_2$ laser is the random Doppler broadening arising from the random thermal velocities of the $CO_2$ molecules. The full linewidth $\Delta\nu_D$ of any transition due to Doppler broadening was given earlier. For the 10.6$\mu$ $CO_2$ transition, $\Delta\nu_D \approx 50$ Mc.

2.4.1 (Continued)

However, there will also be both a certain amount of homogeneous line broadening $\Delta\nu_L$ and a transition frequency shift $\Delta\nu_S$ resulting from collisions of $CO_2$ molecules with other gas atoms and with each other. The broadening is called Lorentz broadening, or by some, Holtzmark broadening where it is due to collisions of an atom with other atoms of the same kind. There is a standard kinetic theory expression for the number of collisions per second (per unit volume) in a mixture of gases of types 1 and 2, namely,

$$Z = 2N_1N_2\sigma^2 \sqrt{2\pi kT\left(\frac{1}{M_1} + \frac{1}{M_2}\right)}$$

where $N_1$ and $N_2$ are the concentrations of the two types, and $M_1$ and $M_2$ are the molecular masses. The parameter $\sigma^2$ is the effective cross-section for the process; typical values of this parameter are $\sigma^2 \approx (20 - 80) \times 10^{-16}$ cm$^2$. Gerry and Leonard have recently measured this quantity to be $57 \times 10^{-16}$ cm$^2$ for $CO_2$ molecules.[12] If Z is the total number of collisions in unit volume, the average number of collisions per unit time for a single molecule is

$$Z_L = \frac{Z}{N_1}$$

The full linewidth $\Delta\nu_L$ due to Lorentz or collision broadening is then given by

$$\Delta\nu_L = \frac{Z_L}{\pi}$$

$$= \frac{2}{\pi}N_2\sigma^2 \sqrt{2\pi kT\left(\frac{1}{M_1} + \frac{1}{M_2}\right)}$$

This says that the Lorentz broadening of a transition in molecules of type 1 is directly proportional to the concentration (or pressure) $N_2$ of any other gas of type 2; and this can be experimentally verified. At the same time, by simply changing $N_2$ and $M_2$ to $N_1$ and $M_1$ one can get a reasonable idea of the Lorentz (or Holtzmark) broadening resulting from self-collisions with molecules of the same kind. Putting rough numbers into the expression above gives

$$\Delta\nu_L \approx 1 - 10 \text{ Mc per Torr}$$

2.4.1 (Continued)

as the amount of Lorentz or collision broadening for a given gas pressure. The higher figure, that is, ~10 Mc per Torr, seems to be close to correct for $CO_2$, so that at a pressure of several Torr the homogeneous linewidth of the $CO_2$ vibrational transitions is several tens of Mc. The lifetime of the (00°1) state is roughly $10^{-3}$ seconds. This makes the natural width of the radiated line roughly 1 kc, a small width compared to the collision broadening.

Other measurements by Gerry and Leonard indicate that the cross-sections for collisions of $CO_2$ with $N_2$ or CO are nearly the same as for collisions of $CO_2$ with itself; i.e., $\sigma^2 \approx 50$ to $56 \times 10^{-16}$ $cm^2$. The cross-section against He seems to be noticeably smaller, $\sigma^2 \approx 18 \times 10^{-16}$ $cm^2$.

There is also a Lorentz shift in the line center frequency resulting from collisions, which causes the overall line to be shifted to lower frequencies. This shift results because when two molecules come near each other, the transition frequencies of either molecule tend to be pulled downward because of the nature of the Franck-Condon potential-vs-radius curves. If every molecule undergoes occasional collisions, its transition frequencies tend on the average to be pulled slightly lower in frequency, since the molecule spends some fraction of its time near other molecules.

The theory of this shift is very involved, but the net result is that the Lorentz shift $\Delta\nu_S$ and the Lorentz broadening $\Delta\nu_L$ are related by

$$\frac{\Delta\nu_S}{\Delta\nu_L} \approx 0.2 - 0.4$$

in many gases. Actually, we have some data on the pressure shift in $CO_2$. Patel notes that $CO_2$ laser wavelengths, measured at less than 1 Torr, are shifted from earlier $CO_2$ wavelengths measured in absorption or spontaneous emission at 1 atmosphere (760 Torr) by about 0.17 $cm^{-1}$ = $5.1 \times 10^9$ cps. This corresponds to a pressure shift

$$\frac{\Delta\nu_S}{P} \approx \frac{5 \times 10^9 \text{ cps}}{760 \text{ Torr}} \approx 6.6 \frac{\text{Mc}}{\text{Torr}}$$

2.4.1 (Continued)

Since an optimum $CO_2$ laser discharge will contain perhaps a few Torr of other gases such as $N_2$ and He, in addition to the $CO_2$, it appears that very careful pressure (and temperature) control will be necessary in order to eliminate frequency shifts due to pressure variations.

2.4.2 Isotope Shifts

Naturally occurring oxygen has two isotopes $O^{14}$ and $O^{15}$, with natural abundances of 99.63 percent and 0.37 percent, respectively, while the common natural isotopes of carbon are $C^{12}$(98.89 percent) and $C^{13}$(1.11 percent). Therefore, one needs to consider possible line shifts and/or asymmetries because of isotope shifts, such as are well known in He-Ne lasers.

Actually, the isotope shifts in vibrational-rotational bands are quite large, because the changed mass of the nucleus significantly changes both the vibrational frequency and the rotational moment of inertia. For instance, the isotope shift in $\nu_3$ between $C^{12}O_2{}^{16}$ and $C^{13}O_2{}^{16}$ is ~3 percent. Hence, the isotopically shifted components are probably moved entirely outside the frequency range of interest, and we can probably ignore completely any effects because of the very small natural concentrations of $C^{13}$ and $O^{15}$.

2.4.3 Zeeman Shifts

Each of the J rotational levels of the $CO_2$ molecule is still (2J + 1) fold degenerate (space degeneracy) because of the multiple allowed orientations of the angular momentum vector in space. Application of a dc magnetic field $B_0$ will cause this degeneracy to be lifted. Each J level, and its associated transitions, will be split into 2J + 1 components.

The amount of this Zeeman splitting between two adjacent components can be written as

$$\Delta f = g_J(\beta/h)B_0$$

where $\beta$ is the nuclear magneton, and $g_J$ is a numerical factor, called simply "the g value," (or the spectroscopic splitting factor). For a single nuclear spin, for example, $g_J$ has the value 2.0, and the levels split at the rate $\Delta f/B_0 \approx 1.5$ kc/gauss.

However, the magnetic dipole moment produced by a rotating molecule is relatively small, because both the positive nuclear charges and the negative electron cloud rotate around together. Thus, the net circulating current and the associated magnetic dipole

2.4.3 (Continued)

moment are small. While detailed $g_J$ values for the $CO_2$ levels are not available, typical values for rotating molecules are

$$g_J \approx 0.02 - 0.05$$

Therefore, the Zeeman splitting rate is

$$\frac{\Delta f}{B_0} \approx (0.02 - 0.05)\ \frac{\beta}{h}$$

$$\approx (15 - 35)\ \frac{\text{cps}}{\text{gauss}}$$

It should be easy to keep ambient magnetic fields well below 1 gauss. In any case, the first-order effect of the Zeeman effect will be simply to broaden the $CO_2$ lines very slightly, since the lines split symmetrically with components being shifted both upwards and downwards. Hence, it does appear that Zeeman effects should not be a serious obstacle to good frequency stability.

2.4.4 Stark Effect Shifts

There are dc (and possibly also RF) electric fields present in the $CO_2$ laser, and hence the possibility of Stark frequency shifts in the $CO_2$ line must be considered. However, it appears that any Stark perturbations will, in fact, be extremely small. First, because the $CO_2$ molecule has no permanent electric dipole moment, there will be no first-order Stark effect, but only a second-order effect in which the splitting goes as $E_0^2$ for small electric fields $E_0$. Secondly, Stark splitting decreases rapidly with increasing J values, and $CO_2$ lasers operate on relatively large-J transitions, e.g., P(20). Thirdly, both upper and lower laser levels may be shifted in the same direction, so that their difference may be very little changed.

By examining the limited data available on second-order Stark splitting of molecular levels, we conclude that Stark shifts due to the dc discharge fields should not be a problem.

Section 3

# SURVEY OF STABILIZATION SCHEMES

## 3.1 INTRODUCTION

This section surveys some of the techniques which have been used in the past for the active stabilization of the frequency of a gas laser and discusses their applicability to the $CO_2$ laser. A good review article which covers in more detail some of the schemes mentioned in the following sections has been written recently by A.D. White.[13]

In most cases, the end result in a feedback stabilization scheme has been the control and movement of one of the laser cavity mirrors. Since the laser operating frequency is primarily determined by the optical path length between mirrors, other schemes which have control over this parameter could be used. These schemes might include the use of an electro-optic phase retardation crystal inside the optical cavity or a variable pressure gas cell, also in the cavity, to achieve a variable optical path length. With various practical limitations in these schemes, the technique of mirror position control has had the most attention due primarily to the readily available piezoelectric crystal.

Because of the present difficulties in materials and techniques at the 10$\mu$m wavelength, no internal cavity modulation schemes have been considered as possible approaches for $CO_2$ laser stabilization. Instead, only techniques which involve mirror movement have been studied. The following sections briefly discuss possible techniques for laser frequency stabilization with comments on the degree of applicability to the present objectives of stabilizing a $CO_2$ laser.

## 3.2 POWER SENSING

For the case of the 10-micron laser lines, the Doppler broadened line is so narrow (approximately 50 MHz) that a stabilization scheme involving a power-output-frequency correlation can be used. Figure 3-1 shows such a scheme. When one is frequency tuned away from the top of the Doppler curve, the side of the curve for estimating purposes can be approximated by a straight line, giving a near linear power-frequency correlation. To obtain a 3 kHz stability on such a curve, a sensing circuit capable of detecting power variations of about 1 part in $10^4$ is required. Although difficult, this is not an unreasonable demand on a null detection system.

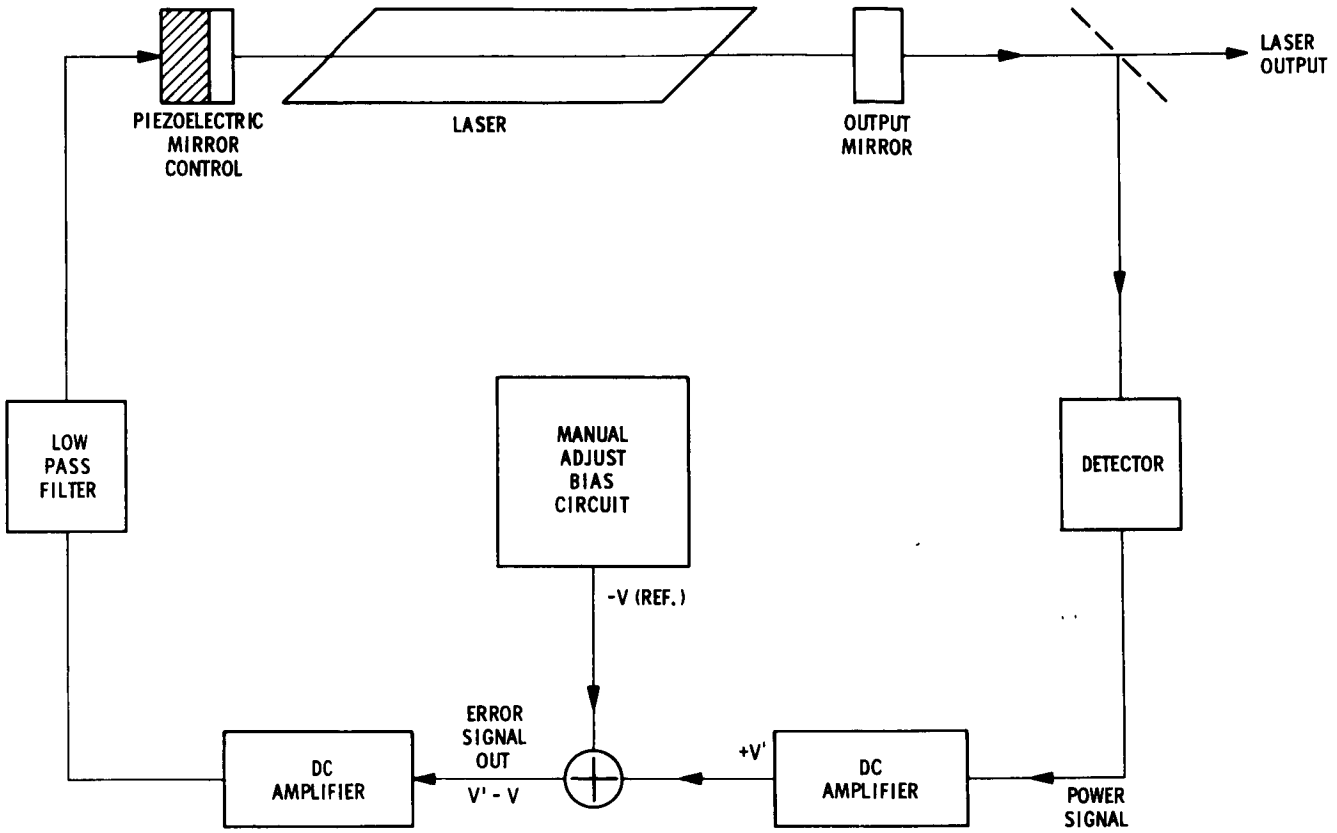


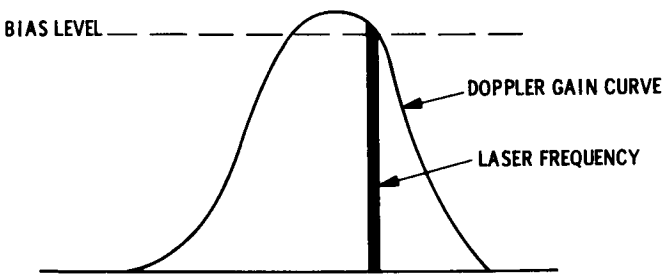


Figure 3-1. Power Sensing Stabilization Scheme

3.2 (Continued)

However, in this case, the frequency is only being inferred from the measurement of laser power and, therefore, the power from the laser must be stable to better than 1 part in $10^4$, not only for short periods but also for long periods of time if long-term stability is to be maintained. This is an extremely difficult requirement, making this scheme unsuitable for the stability goals of 1 part in $10^{10}$. For lesser requirements, this scheme appears promising, especially since it does not introduce any intentional FM and AM on the laser beam.

## 3.3 EXTERNAL FABRY-PEROT CAVITY

Frequency stabilization based on the use of high-Q resonant cavities as discriminators has been used in the optical region for stabilizing the output of lasers. In this case, the discriminators have generally been based on the power transmission or reflection properties of the cavity.

The Q factor of optical cavities is approximately $2\pi\ L/\lambda_o T$, where L is the mirror spacing, $\lambda_o$ the cavity center wavelength, and T is the composite single-pass loss in the cavity. For the case where wavelengths fall in the visible region, good quality mirrors can give a cavity Q as high as about $10^8$ for a 0.05m (5 cm) long cavity. Since the resonant width, $\Delta\nu$, of the cavity is given by $\nu_o/Q$, this Q corresponds to a width of less than 10 MHz for visible wavelengths. It can be easily seen that $\Delta\nu$ is independent of $\nu_o$ and is given by $\Delta\nu = \frac{cT}{2\pi L}$ where c is the speed of light.

Such cavities may be used as a sensitive optical frequency discriminator by sensing the transmission peak of the cavity by modulating the cavity center frequency $\nu_o$ at some lower frequency f. The amplitude and phase of the intensity-modulated component at f in the transmitted beam is proportional to the deviation of the laser frequency from $\nu_o$ and may be used as a suitable error signal to control the laser frequency. This approach does not introduce any intentional FM on the laser output.

Since the passive high-Q optical cavities may be extremely compact, they may be made with much less susceptibility to environmental disturbances than long laser cavities. The temperature detuning, however, is the same for any length of cavity made of the same materials. Therefore, the cavity discriminator has high sensitivity and good short-term stability, but lacks long-term stability primarily because of temperature detuning.

Assuming the reflecting quality of the optics at a wavelength of 10$\mu$m can be made as high as in the visible (a difficult job at the present state-of-the-art), the cavity passband $\Delta\nu$

3.3 (Continued)

could be made the same width for either case. Present techniques limit this passband to values greater than about 10 MHz. Unfortunately, this value is only slightly narrower than the 50 MHz Doppler linewidth of the laser transition. That is, the transmission characteristics of the external cavity to be used as a frequency discriminator would only give a slight advantage over the laser Doppler line itself. This technique would, therefore, hardly be worth pursuing, especially since it would also have to be coupled with a technique providing good long-term stability.

## 3.4 SELF DISPERSION

A technique for stabilization, which utilizes the hole burning and mode pulling effects in a gas laser, has been proposed by Bennett [14] and tested by Bennett, [15] et al. In principle, either the dispersive or gain properties of the inverted population of the laser may be used to construct an optical frequency discriminator. The method is based on a shift of in-cavity resonance introduced by a change in gain of the laser medium. The shift in cavity resonance vanishes at line center and is of opposite sign on either side of line center. By modulating the cavity gain, the cavity resonance can be modulated. Then, by beating this laser with an auxiliary laser, offset by an intermediate frequency (say, 10.7 MHz) stabilized with an AFC loop, the modulating frequency can be phase detected, thus providing an error signal to be used to adjust the length of the main laser.

This system was successfully operated to provide a long-term (eight hours) stability of 1 part in $10^{10}$ for the 3.39$\mu$ He-Ne laser line. Short-term stability was not measured. Extrapolating this technique for use with the $CO_2$ laser, a slight advantage can be realized. The undesirable increase in wavelength by about a factor of three is offset by the narrow homogeneous linewidth ($\sim$10 MHz) of $CO_2$ as compared to the 3.39$\mu$ line of He-Ne ($\sim$115 MHz). These factors extrapolate approximately linearly to give about a factor of three enhancement. It appears possible that this approach could be made successful in stabilizing the long term drift of the $CO_2$ laser line to 1 part in $10^{10}$.

However, this approach suffers strongly because of the complexity of the stabilization scheme. It not only requires a second complete laser and an optical heterodyne system, it also requires stabilization and tracking of the second laser to the first by an automatic frequency control system. As will be seen later, a simpler scheme is available for stabilizing to the required level.

## 3.5 ZEEMAN SPLIT ABSORPTION CELL DISCRIMINATION

In a recently developed scheme,[16] in which the same atomic line is used in a way that is completely independent of the laser discharge, stabilities on the order of 1 part in $10^9$ were obtained at 6328 Angstroms. The technique involves the use of an external absorption cell that is placed in a solenoidal magnetic field. The magnetic field causes Zeeman splitting of the Doppler line, giving rise to two polarization sensitive absorption profiles. By chopping the output of a laser beam into alternately left then right circularly polarized light before passing the beam through the absorption cell, the output of the cell will be composed of different amplitudes of polarized light. When the laser is operating on line center, the amplitudes of each polarization will be the same. The system is also phase sensitive so that the direction of line movement can be determined. It is expected that this approach will be extended to provide a frequency stability factor for the He-Ne laser to about 2 parts in $10^{12}$.

Unfortunately, this approach may not be directly extended to the $CO_2$ laser since the 10.6 micron laser transitions cannot be appreciably split by a magnetic field (see Section 2). However, a similar approach, utilizing an external gas cell, can be used for stabilization of the $CO_2$ laser. It is discussed in Section 3.8. A big advantage with this type of stabilization scheme is that no direct modulation of the laser cavity is necessary, thus providing a "clean" laser output signal.

## 3.6 RING LASER

An approach, which has been used for frequency stabilizing a He-Ne 6328 Angstrom laser, utilizes a laser placed in one arm of a triangular mirror system. Figure 3-2A depicts the scheme. For the ring laser, two independent traveling-wave oscillations (Beams A and B) can circulate within the laser cavity, each at the same frequency if the ring cavity is not rotating. When the operating frequency of the laser is appreciably off the center of the Doppler line, these two traveling-wave oscillations can exist simultaneously, since each oscillation burns a separate hole on one side only of the Doppler profile. However, when the operating frequency is at or near the Doppler line center, the two oscillations must share the same group of slow atoms near the center of the Doppler profile. Actually, the two oscillations will then compete for atoms, and the weaker oscillation will be suppressed by the stronger. (Chance circumstances will determine which one of the two is weaker or stronger.)

In general therefore, if the operating frequency is removed from the center of the Doppler line by as much or more than the homogeneous linewidth of the particular laser transition, there is no competition for the same atoms and both beams oscillate independently. If, however, one of the mirrors is moved slightly with a piezoelectric transducer so that the

3.6 (Continued)

operating frequency approaches line center, then Beam A and Beam B begin to compete for the same atoms, and one beam will begin to predominate in power over the other beam. When the mirror position is adjusted so that both lines are within the same homogeneous linewidth, one beam suppresses the other, driving its output to zero. This effect is depicted in Figure 3-2B.

A scheme is therefore available for stabilizing the laser frequency. If a servo-loop is used to keep the intensity of Beam B at zero, then Beam A will be stabilized in frequency to an accuracy of about the homogeneous linewidth. Unfortunately, this "dead region," the width of the homogeneous line, is fairly broad – on the order of 70 MHz for the 6328 Angstrom line in He-Ne and about 10 MHz for the $CO_2$ 10.6 $\mu$m lines. Stabilizing to this limit will only give about 3 parts in $10^7$ frequency stabilization for the $CO_2$ laser.

One can improve the stabilization levels somewhat by taking advantage of the relatively sharp cut-on point of the blanked-out beam. By biasing and controlling the voltage applied to the control mirror so as to allow Beam B to oscillate at a very low level near the cut-off point, an increase in frequency stability is possible. However, the problems inherent here are the same as those described in Section 3.1 on stabilization by power sensing; i.e., the laser power must be stabilized to a fractional percentage.

A dither scheme could also be utilized to drive the operating frequency back and forth across the cut-off region and measure the time ratio of power-on to power-off. By driving this ratio to one, the frequency could be stabilized to the cut-off point. This approach still requires utmost power stability since the position of the cut-off point will vary with laser gain. Also, this approach has the undesirable characteristic of considerable FM and AM on the output beam (Beam A).

## 3.7 INTERNAL FM SIDEBAND GENERATION

If a phase modulator is operated inside a laser cavity or one of the laser mirrors is oscillated at some frequency, f, the laser beam becomes frequency modulated and typical FM sidebands are generated inside the laser. The basic sideband amplitude and spacing is determined by the modulating frequency and index. However, because of the nonlinear Doppler gain curve, the sidebands are not amplified by the same factor when the carrier is off the center of the gain curve and the FM'd laser beam becomes distorted. Demodulation of the beam by direct detection external to the laser then will have beat frequencies between the various sidebands of the FM signal; i.e., there would be no beats in the case of an ideal, undistorted FM signal.

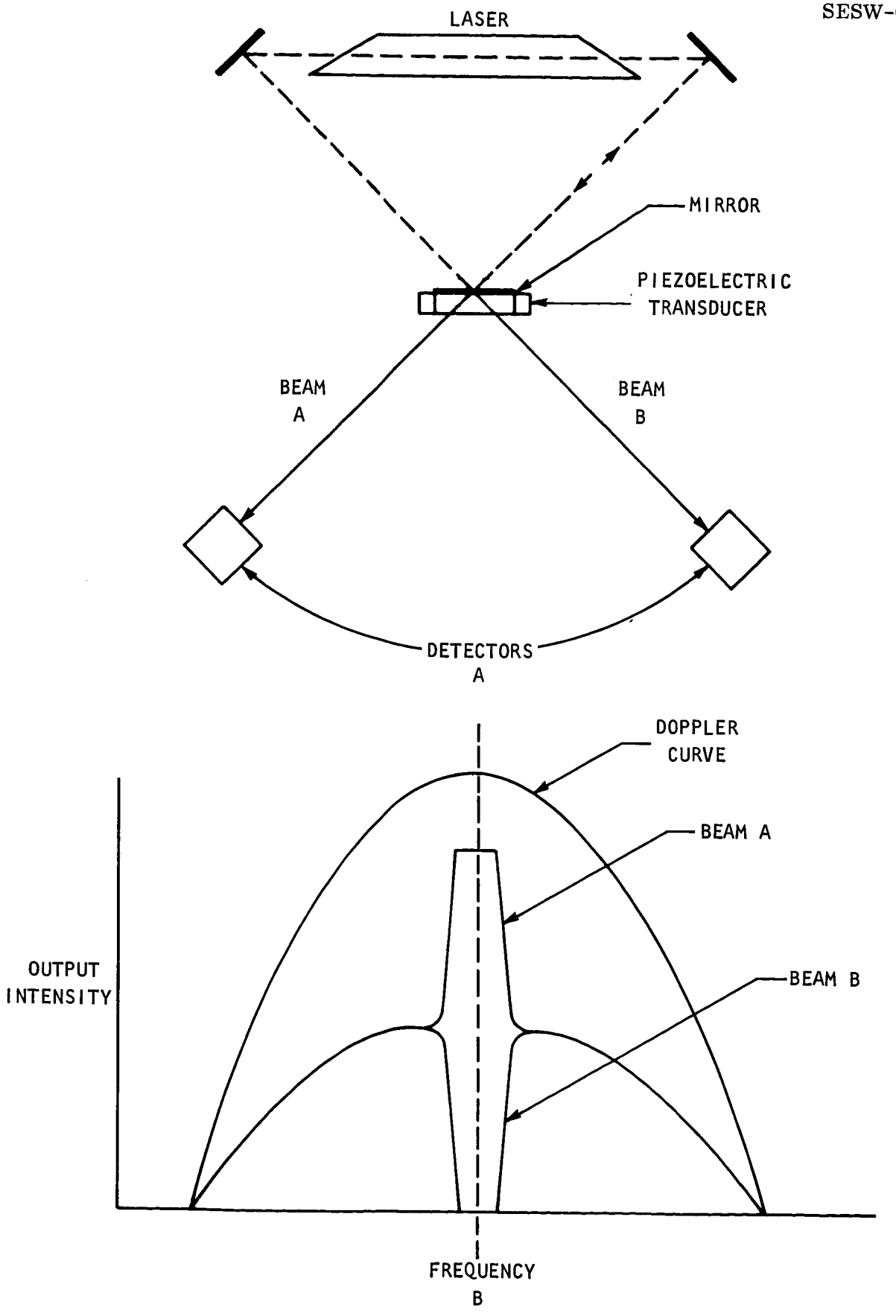


Figure 3-2. Ring Laser Stabilization Technique

3.7 (Continued)

These characteristics are then immediately applicable for absolute frequency stabilization of the laser output. One merely detects the amplitude of the beat at f and uses this amplitude as an indication of the position of the FM carrier. As long as the beat remains zero, then the carrier is at the center of the gain curve. If the beat increases to some nonzero value, then one mirror of the laser is moved so that the carrier is once again centered. In practice, this could be accomplished by attaching a piezoelectric transducer to one of the laser mirrors and controlling the voltage on the transducer by feedback electronics from the detected beat signal.

With proper design of the control loop, this scheme appears to have the capability of providing long-term stability of the order required. However, the short-term stability would be rather poor since the output beam of the laser would be frequency modulated at f due to the required dither frequency. A similar technique discussed in the following section removes the disadvantage of a modulated output.

## 3.8 FM SIDEBAND DETECTION USING A SEPARATE $CO_2$ LASER AMPLIFIER

Each of the schemes discussed so far has certain real disadvantages as described. Although any conceivable technique will have some disadvantages, we do not feel that any of the previously described methods will be satisfactory for the proposed program.

Fortunately, we have succeeded in devising a new scheme that appears to be quite satisfactory. The credit for this suggestion belongs to Professor A. E. Siegman, our consultant, who conceived the technique at Sylvania several months ago. Siegman's approach is diagrammed in Figure 3-3; in this approach, the frequency of the $CO_2$ laser oscillator is stabilized to the center of the $CO_2$ atomic transition with the aid of a separate nonregenerative $CO_2$ laser amplifier. As shown in the sketch, a small fraction of the main laser's output is tapped off and then frequency modulated at a modulation frequency, $\omega_m$, for example, by a vibrating mirror. This frequency-modulated signal is then amplified in a nonregenerative $CO_2$ laser amplifier, and detected with a detector tuned to the modulation frequency, $\omega_m$.

The nonregenerative $CO_2$ laser amplifier will have a gain profile determined only by the atomic gain profile of the $CO_2$ transition. The pure FM laser signal entering the laser amplifier will have no AM component or beat at the modulation frequency, $\omega_m$. If the main laser signal is exactly at the center of the atomic gain profile, then the FM sidebands will see a balanced gain, i.e., the same gain for corresponding upper and lower sidebands, and no AM at the modulation frequency will develop (although AM at $2\omega_m$ and higher, even harmonics will develop).

3.8 (Continued)

If, however, the main laser signal is slightly off the atomic line center, as in Figure 3-3, then upper and lower sidebands will be differently amplified and will become unbalanced and an AM component or beat at $\omega_m$ will develop. This beat will be detected by the photodetector. The unbalance will result both from amplitude and phase unbalance in the amplification of the opposite sidebands.

The beat at $\omega_m$ will increase in amplitude the further the carrier drifts off line center, go to zero at line center, and change phase by 180° as the main laser signal passes through line center. Hence, it provides an ideal and sensitive frequency discriminant. A proportional error signal for feedback control of the main laser oscillator is easily developed, using a phase-sensitive receiver as indicated.

This technique has the major advantage that no unwanted modulation sidebands of any sort need be present on the main laser output. With the power levels available from $CO_2$ lasers, the fraction of the main laser output tapped off for the stabilization system can be negligible. Nonregenerative gains in the $CO_2$ laser system are believed to be high, [17] e.g., on the order of 20% per meter in a closed system which gives this scheme good sensitivity. The scheme furnishes a stable long-term absolute stabilization to the unchanging $CO_2$ transition itself. With high enough gain, high enough modulation frequency, and fast enough electronics, it would provide good short-term stability as well.

The major disadvantage would seem to be the necessity for a second $CO_2$ laser tube in the system. However, this could be a small, low-power tube, and no stable mirror structure is required. Some reasonable care will also be required to see that the vibrating mirror at $\omega_m$ does not cause unwanted vibrations at this frequency in the main laser structure.

A big advantage to this approach is that no intentional FM or AM is introduced on the main laser beam and good sensitivity can be obtained. It appears that this stabilization scheme is the most suitable for the envisioned program.

## 3.9 SUMMARY

In the search for a suitable frequency stabilization scheme to be used for the $CO_2$ laser, the following criteria have been used:

(1) The scheme should be capable of both long- and short-term stabilization.

(2) No intentional AM or FM should appear on the laser output beam.

(3) Long- and short-term frequency stability levels are to be less than 1 part in $10^{10}$ (better than 3kHz for the $CO_2$ Laser).

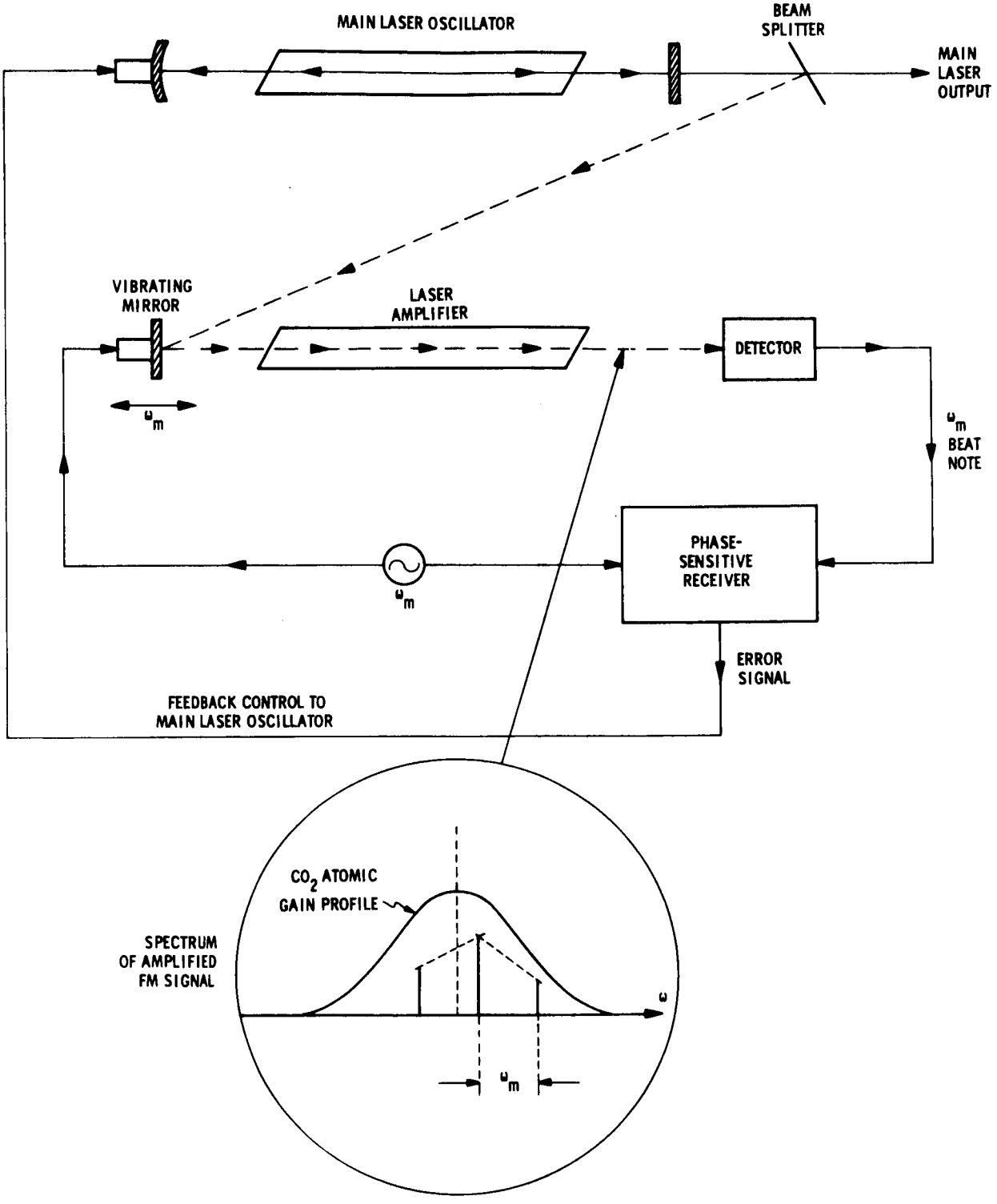


Figure 3-3. Stabilization Scheme Utilizing an External $CO_2$ Amplifier

3.9 (Continued)

(4) The scheme should be capable of operating continuously for long periods of time.

(5) The scheme should be relatively simple and not costly to build and/or maintain.

(6) Standard or proven components should be used throughout.

(7) The scheme should not inherently limit the power output of the laser.

The technique described in Section 3.7 (FM Sideband Detection Using a Separate $CO_2$ Laser Amplifier) fulfills the above criteria in all respects and has definite advantages over all the other schemes considered. Early studies on the external amplifier technique have indicated that the scheme is capable of the desired stability of 1 part in $10^{10}$. Further analysis has proceeded on this scheme, and a detailed analysis of the technique is presented in the following section.

Section 4

# ANALYSIS OF EXTERNAL $CO_2$ AMPLIFIER STABILIZATION SCHEME

## 4.1 INTRODUCTION

The desired long-term frequency stability can clearly not be obtained by stabilization to any purely mechanical structure, but must be locked to an atomic transition, specifically to the $CO_2$ laser transition itself. Furthermore, it is desirable to avoid internal modulation or "dither" in the master laser oscillator, if possible. With these points in mind, we propose that the laser frequency be locked to a separate $CO_2$ laser amplifier, as described in more detail in this section.

Other significant advantages of this scheme include the following:

a. The master laser oscillator, since it is not the main frequency determining element, can be designed to best meet other objectives, such as power output or modulation capability.

b. The separate laser amplifier, since it need not supply any power, can have its structure, gas fill, discharge, and other parameters all adjusted for maximum long-term stability, without worrying about other performance characteristics.

c. Since the separate laser amplifier is nonregenerative, cavity pulling effects and other cavity-related disturbances are entirely absent, and only the atomic line itself is involved.

The following sections contain the analytical treatment of the scheme first for the case of a homogeneously broadened gain curve and secondly, for the more real, and difficult case of a doppler broadened gain curve. The sensitivity functions are developed and typical operating parameters from available devices are used to estimate the sensitivity of the scheme.

## 4.2 THE SEPARATE $CO_2$ AMPLIFIER STABILIZATION SCHEME

The scheme to be investigated is best described with reference to Figure 4-1. As noted, a fraction of the main $CO_2$ oscillator's power output is tapped off, phase-modulated at some modulation frequency $f_m$, and passed through a separate $CO_2$ laser amplifier. A detector

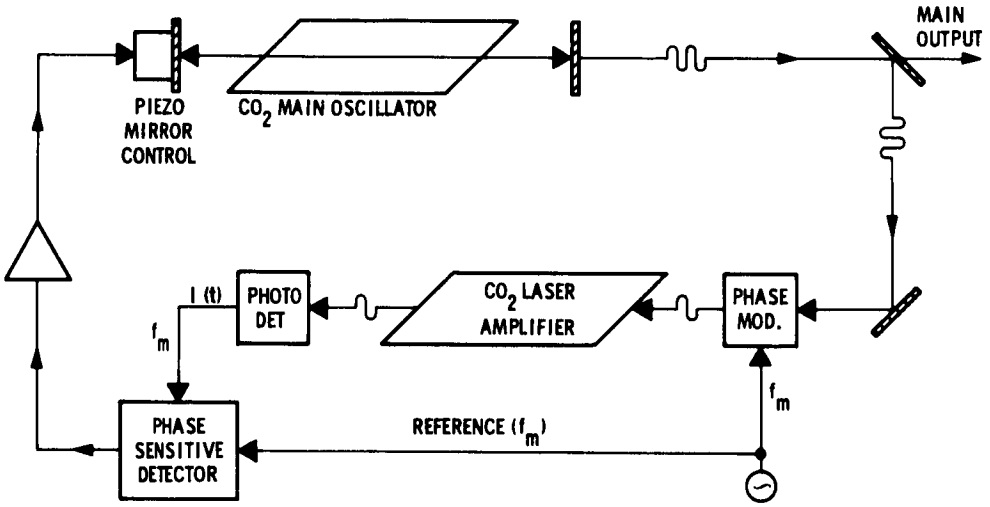


Figure 4-1. Schematic of the Main Frequency Control Loop

4.2 (Continued)

at the amplifier output looks for beat signals at frequency $f_m$ and compares them with the phase modulation, the objective being to have pure FM or zero beat in the amplifier's output. A servo system controls the main oscillator's cavity length by piezoelectric tuning, in such a way as to bring the observed beat to zero.

If the main laser frequency is exactly on the $CO_2$ line center, then the FM sidebands are symmetrically located on the atomic line, and they remain balanced in such a fashion that there is no AM beat signal generated at the fundamental frequency $f_m$. If, however, the main oscillation or carrier drifts off the $CO_2$ line center, then the FM sidebands are asymmetrically amplified. They become unbalanced, and a fundamental beat note is generated, more or less proportional to the deviation from line center. Moreover, the phase of this beat relative to the original FM modulating signal changes sign depending on which way the drift occurs. Hence, one can identify to which side of the line the carrier has drifted.

Note that both the gain and phase shift characteristics of the inhomogeneous line are important in determining the asymmetric amplification for a signal off resonance. The long-term stability of this scheme should depend only on the long-term frequency stability of the $CO_2$ molecular transition itself. We have already identified the factors that will limit or determine the long-term stability of the molecular line. The actual frequency modulation method may be electro-optic, if suitable materials are available, or it may be accomplished with a piezoelectrically vibrated mirror.

The basic elements of this stabilization scheme are the incident frequency-modulated (FM) laser signal; a single-pass laser amplifier; and a photodetector tuned to the first beat note, i.e., to the FM modulation frequency.

## 4.3 GENERATION OF A BEAT SIGNAL

We suppose that the incident laser beam is an FM signal with carrier frequency $\omega_c$, modulation frequency $\omega_m$, and FM modulation index $\delta$, so that the incident complex amplitude $\tilde{u}_1(t)$ may be written

$$\tilde{u}_1(t) = u_o e^{j\left[\omega_c t + \delta \sin \omega_m t\right]} = u_o \sum_{n=-\infty}^{\infty} J_n(\delta)\, e^{j(\omega_c + n\omega_m)t} \qquad (4.1)$$

4.3 (Continued)

If the complex voltage gain of the amplifier for a sideband at frequency $\omega$ is denoted by $\tilde{g}(\omega)$, then the complex output signal from the amplifier will be

$$\tilde{u}_2(t) = u_o \sum_{n=-\infty}^{\infty} J_n(\delta)\, \tilde{g}(\omega_c + n\omega_m) e^{j(\omega_c + n\omega_m)t} \tag{4.2}$$

The instantaneous intensity striking the output detector (and hence presumably the photocurrent from this detector) will be given by

$$I(t) = \tilde{u}_2^{\,*}(t)\, \tilde{u}_2(t) \tag{4.3}$$

If we adopt the shorthand notation

$$\tilde{g}_n \equiv \tilde{g}_n(\omega_c) = \tilde{g}(\omega_c + n\omega_m)\ , \tag{4.4}$$

then the photodetector output becomes

$$I(t) = u_o^2 \sum_{n=-\infty}^{\infty} \sum_{k=-\infty}^{\infty} \tilde{g}_n \tilde{g}_k^{\,*}\, J_n(\delta)\, J_k(\delta)\, e^{j(n-k)\omega_m t}$$

$$= I_o + \frac{1}{2}\left[\tilde{I}_1 e^{j\omega_m t} + cc\right] + \frac{1}{2}\left[\tilde{I}_2 e^{j2\omega_m t} + cc\right] + \ldots \tag{4.5}$$

where we have specifically indicated the expected dc photoresponse $I_o$ and the complex amplitudes of the beat-frequency components at the first two multiples of the modulation frequency $\omega_m$. The symbol cc indicates the complex conjugate. Sorting out the appropriate terms then yields for the dc and the first two beat components

$$I_o = u_o^2 \sum_{n=-\infty}^{\infty} \left|\tilde{g}_n\right|^2 J_n^{\,2} \tag{4.6a}$$

4.3 (Continued)

$$\tilde{I}_1 = 2u_o^2 \sum_{n=-\infty}^{\infty} \tilde{g}_{n+1}\, \tilde{g}_n^*\, J_{n+1}\, J_n \qquad (4.6b)$$

$$\tilde{I}_2 = 2u_o^2 \sum_{n=-\infty}^{\infty} \tilde{g}_{n+2}\, \tilde{g}_n^*\, J_{n+2}\, J_n \qquad (4.6c)$$

Note that the beat amplitudes are the complex peak values, and that we may as well set the incident intensity $u_o^2 = 1$. We now consider specific forms for the gain $\tilde{g}(\omega)$, and calculate the output current terms.

## 4.4 HOMOGENEOUS BROADENING

We will consider in this section the case of an amplifier having a homogeneously broadened atomic transition with center frequency $\omega_o$ and full homogeneous linewidth $\Delta\omega_H$. Therefore, the laser amplifier's complex gain $\tilde{g}(\omega)$ may be written

$$\tilde{g}(\omega) = \exp\left[\ell n\, g_o \frac{1}{1+j2\,(\omega - \omega_o)/\Delta\omega_H}\right] \qquad (4.7)$$

where $g_o$ is the midband voltage gain. The gain for the n-th sideband of the FM signal then becomes

$$\tilde{g}_n = \exp\left[\ell n\, g_o \frac{1}{1+j2\,(\omega_c - \omega_o + n\omega_m)/\Delta\omega_H}\right] \qquad (4.8)$$

where $\omega_c - \omega_o$ is the detuning between the FM signal's carrier frequency $\omega_c$ and the atomic line center $\omega_o$. It will be convenient to express this detuning and also the modulation frequency $\omega_m$ in normalized form by defining the dimensionless variables

$$D \equiv \frac{\text{Frequency detuning}}{\text{Full atomic linewidth}} \qquad (4.9a)$$

$$M \equiv \frac{\text{Modulation frequency}}{\text{Full atomic linewidth}} \qquad (4.9b)$$

4.4 (Continued)

In the present homogeneous case, we thus have

$$D = \frac{\omega_c - \omega_o}{\Delta\omega_H} \quad , \quad M = \frac{\omega_m}{\Delta\omega_H}$$

However, we emphasize that according to the basic definition the denominators are the full atomic linewidth, so that these denominators will become the doppler rather than the homogeneous width when we move to the inhomogeneous doppler case.

The gain expression now becomes

$$\tilde{g}_n (D,M) = \exp \left[ \ell n \, g_o \frac{1}{1+j2 (D + nM)} \right] \tag{4.10}$$

and we can evaluate the first three photocurrent components as functions of the parameters $g_o$ , $\delta$ , $D$ , and $M$ . Figure 4-2 shows how the magnitudes of these photocurrents vary as a function of detuning from line center. It will be noted in particular that the fundamental beat $\tilde{I}_1$ is identically zero when $D = 0$ . The magnitude of this beat current varies linearly with $D$ in the range about $D = 0$ . This beat is, of course, the output parameter that we intend to use as the discriminant, to indicate any detuning of the optical carrier $\omega_c$ from the atomic line center $\omega_o$ . Note also that the dc current $I_o$ decreases gradually with increasing detuning, $D$ , because the signal carrier is then moved away from the gain peak. There is also a weak second-harmonic component $I_2$ at frequency $2\omega_m$ . This component has a more complex variation with $D$ , and does not appear to be of utility as a frequency discriminant.

Examination of the phase $\tilde{I}_1$ shows that it changes by 180° in passing through line center, as would be expected. This discriminant beat signal reaches a maximum when the detuning reaches a value

$$D \equiv \frac{\omega_c - \omega_o}{\Delta\omega_H} \approx 0.28$$

and then decreases for still larger amounts of detuning. This value for the location of the maximum of $\tilde{I}_1$ is observed to remain nearly the same over wide ranges of modulation index $\delta$ and modulation frequency $\omega_m$ .

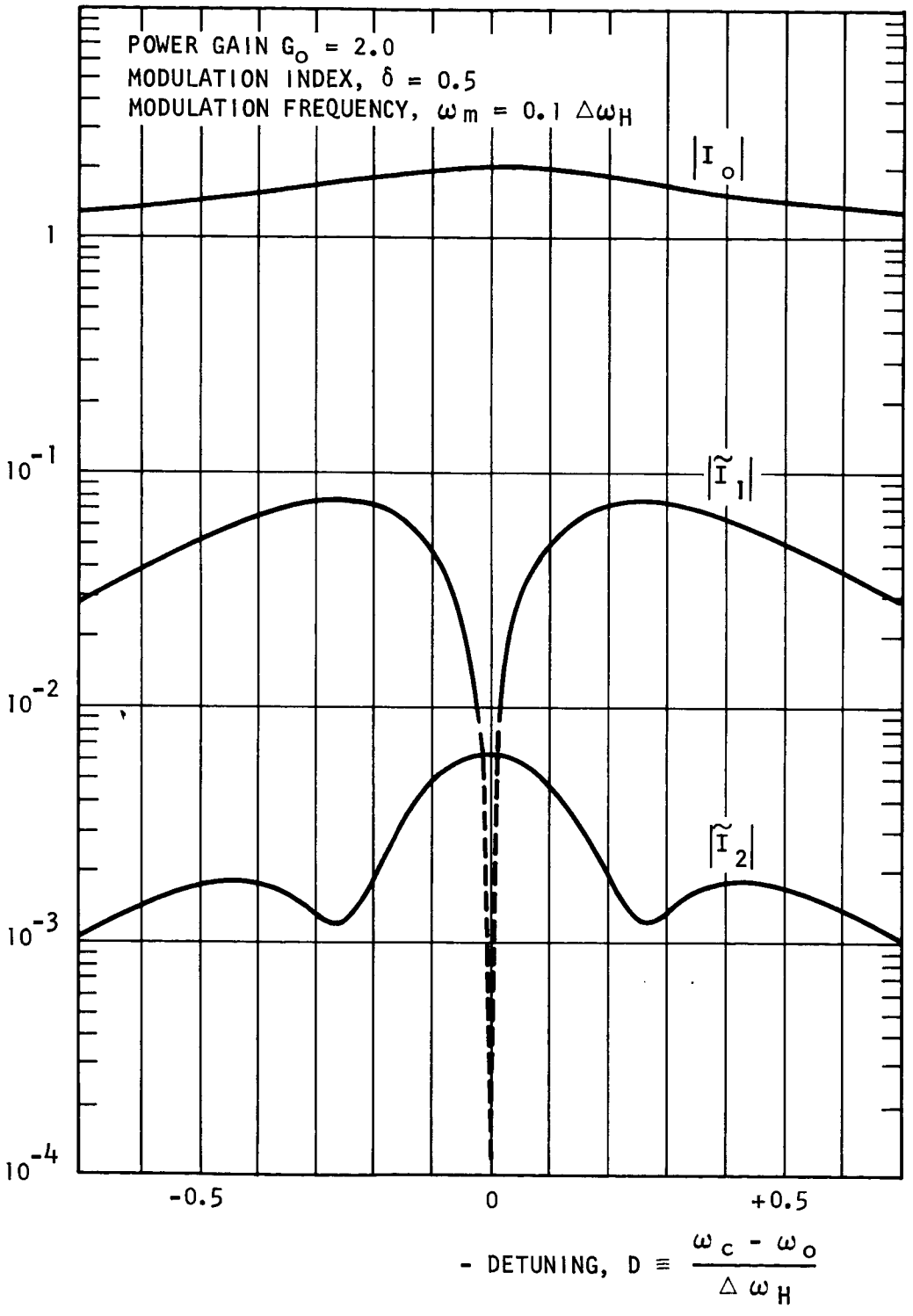


Figure 4-2. DC Output and Magnitude of the First Two Beat Currents Vs. Detuning D for a Typical Homogeneously Broadened Case

4.4 (Continued)

For stabilization purposes we are particularly interested in the midband sensitivity, i.e., the variation of the beat note $\tilde{I}_1$ with the detuning parameter D for small values of D . We can write for small D

$$\tilde{I}_1 \approx 2D \sum_{n=-\infty}^{\infty} (\tilde{g}_{n+1} \tilde{g}_n'^* + \tilde{g}_{n+1}' \tilde{g}_n^*) J_{n+1}(\delta) J_n(\delta) \qquad (4.11)$$

where the derivative $\tilde{g}_n'$ of $\tilde{g}_n$ in the homogeneous case is given by

$$\tilde{g}_n' \equiv \left. \frac{\partial \tilde{g}_n}{\partial D} \right|_{D=0} = - \frac{2j \ell n\, g_o}{(1+2jnM)^2} \exp \left[ \ell n\, g_o \frac{1}{1+2jnM} \right] \qquad (4.12)$$

and both $\tilde{g}_n$ and $\tilde{g}_n'$ are evaluated at D = 0. From the symmetry properties of $\tilde{g}_n$ and $J_n$ for negative n, it is easy to show that the midband sensitivity can also be written

$$\tilde{I}_1/D \approx 4 \sum_{n=0}^{\infty} (\tilde{g}_{n+1} \tilde{g}_n'^* + \tilde{g}_{n+1}' \tilde{g}_n^*) J_{n+1}(\delta) J_n(\delta) \qquad (4.13)$$

This expression can be easily approximated for the case of small FM modulation index, $\delta << 1$. In this case the only significant spectral components are the carrier, with $J_o(\delta) \approx 1$, and the first sidebands, with $J_1(\delta) \approx \delta/2$. The midband sensitivity can then be written

$$\frac{\tilde{I}_1}{D} \approx 4j\delta \ell n\, g_o \left[ \frac{M + jM^2}{M + j(M^2 - 1/4)} \right] e^{\ell n\, g_o} e^{\ell n\, g_o / (1+2jM)}, \quad (\delta << 1) \qquad (4.14)$$

The magnitude of the factor in rectangular brackets increases linearly with M for small M; passes through a maximum; and drops back asymptotically to 1 for large M . Its asymptotic and peak values are given by

4.4 (Continued)

$$\left[\frac{M + jM^2}{M + j(M^2 - 1/4)}\right] \begin{cases} \approx 4jM, & M << 1 \\ = (4/3)^{1/2} \exp\left[j \arctan(\sqrt{2}/5)\right], & M = M_{opt} = (2)^{-1/2} \\ \approx 1 & M >> 1 \end{cases} \quad (4.15)$$

For small $\delta$ a modulation frequency almost as large as the atomic linewidth is obviously desirable (although an FM modulation frequency this high may not be technically feasible, especially if the modulation is accomplished with an oscillating mirror). In physical terms, the largest sideband unbalance is obtained by placing the modulation sidebands well out on the sides of the atomic line, where the gain slope $(d/d\omega)\ \chi''(\omega)$ is largest and where the phase-shifting effects $\chi'(\omega)$ are also largest.

The midband slope or <u>discriminant</u> may thus be written for small $M$ and $\delta$ as

$$\left|\frac{\tilde{I}_1}{D}\right| \approx 8M\delta\, G_o\, \ell n\, G_o \quad (4.16)$$

where $G_o \equiv g_o^{\,2}$ is the single-pass midband power gain of the amplifier. More generally, we may write for the midband slope

$$\left|\frac{\tilde{I}_1}{D}\right| = \left[8M\delta\, G_o\, \ell n\, G_o\right] \times F(M, \delta, G_o) \quad (4.17)$$

where the factor $F(M, \delta, G_o)$ is unity for small $M$ and $\delta$, and decreases at larger values. Computer runs have shown that this factor is nearly unity over wide ranges of $M$ and $\delta$, as illustrated in Figure 4-3. It begins to fall below unity only for combinations of modulation index $\delta$ and modulation frequency $M$ which put a significant fraction of the laser energy into sidebands falling outside the main portion of the gain curve.

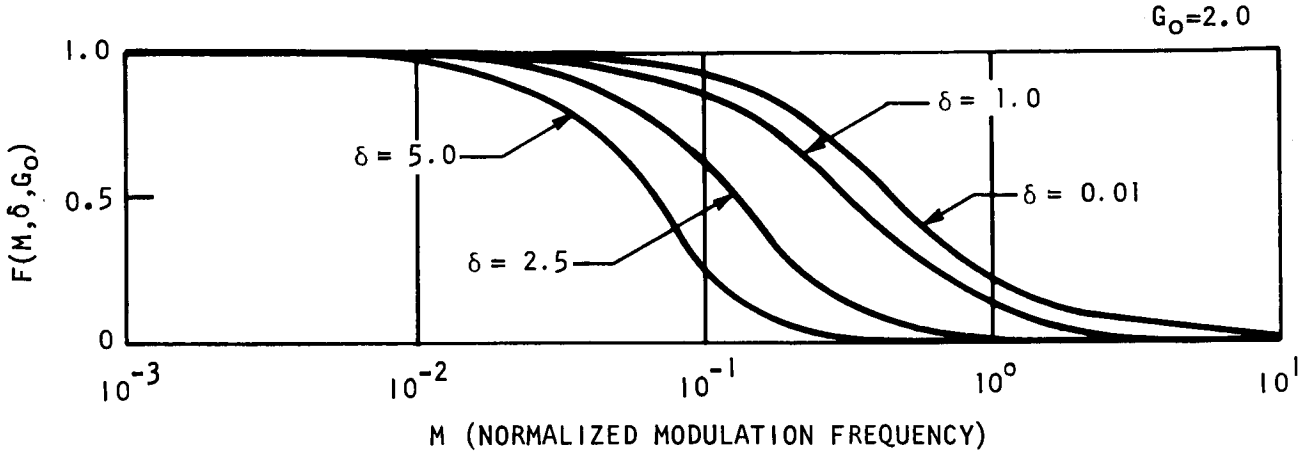


Figure 4-3. The Midband Discriminant Reduction Factor, $F(M, \delta, G_o)$ for Several Values of $\delta$

## 4.5 INHOMOGENEOUS (OR DOPPLER) BROADENING

We now need to consider the more realistic case of an inhomogeneously broadened atomic transition, such as is characteristic of doppler-broadened gas lasers. The gain in this case may be written

$$\tilde{g}(\omega) = \exp\left[-j\frac{1}{2}kL\,\tilde{\chi}(\omega)\right] \tag{4.18}$$

Here $k$ is the propagation constant neglecting any atomic interaction; $L$ is the amplifier length; and $\tilde{\chi}(\omega)$ is the complex atomic laser susceptibility, given by

$$\tilde{\chi}(\omega) = j\chi_o'' \frac{2}{\Delta\omega_D}\sqrt{\frac{\ell n\,2}{\pi}}\int_{-\infty}^{\infty}\frac{1}{1+2j(\omega-\omega_o')/\Delta\omega_H}\exp$$

$$\left[-\left(\frac{2\sqrt{\ell n 2}}{\Delta\omega_D}\right)^2(\omega_o'-\omega_o)^2\right]d\omega_o' \tag{4.19}$$

In this expression $j\chi_o''$ is the midband susceptibility of a single homogeneous line or "spectral packet" having homogeneous linewidth $\Delta\omega_H$. The first factor inside the integral gives the frequency variation of $\chi(\omega)$ for a single homogeneous packet centered at $\omega_o'$. The second (exponential) factor gives the distribution of packet center frequencies $\omega_o'$ about the line center $\omega_o$, with doppler linewidth $\Delta\omega_D$.

If we use the same basic definitions for normalized detuning and normalized modulation frequency as above, we will now have

$$D \equiv \frac{\text{Frequency detuning}}{\text{Atomic (doppler) linewidth}} = \frac{\omega_c - \omega_o}{\Delta\omega_D} \tag{4.20a}$$

$$M \equiv \frac{\text{Modulation frequency}}{\text{Atomic (doppler) linewidth}} = \frac{\omega_m}{\Delta\omega_D} \tag{4.20b}$$

Note that $\Delta\omega_H$ is now replaced by $\Delta\omega_D$ in these definitions. We also define the homogeneous broadening parameter

4.5 (Continued)

$$H \equiv \frac{\text{Homogeneous linewidth}}{\text{Inhomogeneous linewidth}} = \frac{\Delta\omega_H}{\Delta\omega_D} \tag{4.20c}$$

The laser susceptibility expression, evaluated at a sideband frequency $\omega = \omega_c + n\omega_m$, may now be written

$$\tilde{\chi}(\omega=\omega_c+n\omega_m) = jH\chi_o'' \sqrt{\frac{\ell n\, 2}{\pi}} \int_{-\infty}^{\infty} \frac{1}{\sqrt{\ell n 2}\ H + 2j(D+nM) - jy} e^{-y^2}\, dy$$

$$= jH\chi_o'' \sqrt{\frac{\ell n\, 2}{\pi}}\ \tilde{K}\ \left(\sqrt{\ell n 2}\ \left[H + 2j\ (D+nM)\right]\right) \tag{4.21}$$

where we define the new function

$$\tilde{K}\ (\tilde{\alpha}) \equiv \int_{-\infty}^{\infty} \frac{1}{\tilde{\alpha} - jy}\ e^{-y^2}\, dy \tag{4.22}$$

The argument $\tilde{\alpha}$ of this function will, in general, be complex. The problem now reduces to evaluating the rather complicated function $\tilde{K}\ (\tilde{\alpha})$ ; we will give various series expansions for $\tilde{K}\ (\tilde{\alpha})$ shortly.

The gain seen by a sideband at $\omega = \omega_c + n\omega_m$ in an inhomogeneous line can now be written

$$\tilde{g}_n(D, M, H) = \exp\left[\ell n\, g_o \frac{\tilde{K}\ \left(\sqrt{\ell n 2}\ \left[H + 2j\ (D+nM)\right]\right)}{\tilde{K}\ (\sqrt{\ell n 2}\ H)}\right] \tag{4.23}$$

We also will need the derivative of this gain with respect to $D$, evaluated at $D = 0$, which takes the form

$$\tilde{g}_n'(M,H) = 4j\ \sqrt{\ell n\, 2}\ \ell n\, g_o \frac{\tilde{\beta}_n \tilde{K}\ (\tilde{\beta}_n) - \sqrt{\pi}}{\tilde{K}\ (\sqrt{\ell n\, 2}\ H)} \exp\left[\ell n\, g_o \frac{\tilde{K}\ (\tilde{\beta}_n)}{\tilde{K}\ (\sqrt{\ell n\, 2}\ H)}\right] \tag{4.24}$$

4.5 (Continued)

where $\tilde{\beta}_n$ is the combination

$$\tilde{\beta}_n \equiv \sqrt{\ell n\, 2}\ (H + 2jnM) \tag{4.25}$$

These expressions for $\tilde{g}_n$ and $\tilde{g}_n'$ may now be used to compute the output signal from the laser amplifier.

In the present case extensive calculations carried out for wide ranges of M, D, H and $\delta$ would be largely academic. As a practical matter we are concerned with values $<< 1$ for all of these variables. Within this degree of approximation we can expand $\tilde{K}(\tilde{\alpha})$ in the form (see Appendix A)

$$\tilde{K}(\tilde{\alpha}) \approx \pi - 2\sqrt{\pi}\,\tilde{\alpha}\ , \quad |\tilde{\alpha}| << 1 \tag{4.26}$$

and the series expansion for the beat signal $\tilde{I}$, can also be expanded, in the same manner as was done for the homogeneous case. The result of this approximation is

$$\tilde{I}_1 \approx -(8\ \ell n\ 2)\ (G_o\ \ell n\ G_o)\ MD\delta \tag{4.27}$$

Hence the midband slope or discriminant is

$$\frac{|\tilde{I}_1|}{D} \approx -(8\ \ell n\ 2)\ (G_o\ \ell n\ G_o)\ M\delta \tag{4.28}$$

Note that this is exactly the same, except for a minor numerical difference, as the homogeneous result. The homogeneous linewidth parameter H drops out entirely – as might be expected since no saturation phenomena are taking place. By analogy with the homogeneous case we may expect this expression to remain valid for a wide range of values of $G_o$, M and $\delta$.

## 4.6 CALCULATION OF SYSTEM SENSITIVITY

In this section we calculate the sensitivity of the FM amplifier frequency stabilization method assuming a real infrared detector, with its many performance limitations.

From our previous analysis we have found that the peak value of the modulation-frequency beat Note I, is related to the input beam intensity $I_o$, the detuning factor D, and other parameters by

$$I_1 = (8 \ln 2)\,(G_o \ln G_o)\, I_o M D \delta \tag{4.29}$$

If we use a photoconductive IR detector with a responsivity R (measured in volts/watt), the rms signal voltage $V_s$ from the detector at the modulation frequency will be

$$V_s = \frac{1}{\sqrt{2}}\, R I_1 \tag{4.30}$$

If we express $I_1$ in terms of the modulation frequency $f_m$, doppler linewidth at half height $\Delta f_D$, and detuning $\Delta f = f_c - f_o$, this becomes

$$V_s = (4\sqrt{2} \ln 2) \left[\frac{(G_o \ln G_o)\, R I_o\, f_m \delta}{\Delta f_D^2}\right] \Delta f \tag{4.31}$$

$$= \frac{4(G_o \ln G_o)\, R I_o\, f_m \delta}{\Delta f_D^2}\, \Delta f$$

The signal voltage is, of course, linear in the frequency detuning or frequency error $\Delta f$ .

The rms noise voltage $V_n$ from an IR detector within a detection bandwidth B can be related to the specified responsivity R and noise equivalent power (NEP) of the detector by

$$V_n = R \times NEP \times \sqrt{B} \tag{4.32}$$

where the NEP is specified by the detector manufacturer assuming a 1 Hz detection bandwidth. The noise voltage can also be written in terms of the detector area A and the specified D* of the detector, in the form

$$V_n = \frac{R\sqrt{A}\sqrt{B}}{D^*} \tag{4.33}$$

In using these expressions one must be careful to use values of R, NEP and D* all determined for the same experimental conditions.

If we combine the above expressions for $V_s$ and $V_n$ we can obtain the signal to noise ratio in the form

4.6 (Continued)

$$\frac{V_s}{V_n} = \frac{4(G_o \ell n\, G_o)\, I_o\, f_m \delta}{NEP\, \sqrt{B}\, \Delta f_D^2}\, \Delta f \tag{4.34}$$

Suppose that we take as the minimum detectable signal criterion a signal-to-noise ratio of unity. Then, the minimum detectable frequency error ($V_s/V_n = 1$) for the real IR detector case is given by

$$\boxed{\Delta f_{min} = \frac{NEP\, \sqrt{B}\, \Delta f_D^2}{4(G_o \ell n G_o)\, I_o\, f_m \delta}} \tag{4.35}$$

or, alternatively,

$$\boxed{\Delta f_{min} = \frac{\sqrt{A}\, \sqrt{B}\, \Delta f_D^2}{4D^*(G_o \ell n G_o)\, I_o\, f_m \delta}} \tag{4.36}$$

Our next step is to put realistic numbers into these expressions.

Certain parameters in the experiment are fairly firmly determined. For example, the maximum gain in a $CO_2$ laser amplifier is known to be approximately 40% per meter.

Therefore, by constructing a simple optical system to provide, say, a triple pass of the optical beam through a 60 cm long amplifier tube, the gain would be

$$\left.\begin{aligned} G_o &\approx 2.0 \\ \ell n\, G_o &\approx .693 \end{aligned}\right\} \quad \begin{aligned} L &= 60 \text{ cm}, \\ &3 \text{ passes}. \end{aligned}$$

Also, the doppler linewidth in a $CO_2$ laser is well established

$$\Delta f_D \approx 45 \text{ MHz} \quad .$$

The detector parameters depend, of course, on the detector chosen. One IR detector that is available, fairly simple, and requires only liquid nitrogen cooling, is the Philco GPC-215. The important parameters of this gold-doped germanium photoconductor are summarized in Table 4-1. The important number for our purposes here is

$$NEP\ (\lambda = 10.6\mu) \approx 3.3 \times 10^{-10} \text{ watt}/\sqrt{\text{Hz}}$$

This value is estimated by extrapolation, but is believed to be fairly reliable.

4.6 (Continued)

System parameters are somewhat subject to our design control, and must be chosen within feasible angles. We will specify, for example, a modulation frequency of

$$f_m = 1 \text{ MHz} = 10^6 \text{ Hz}$$

It is proposed that the modulator should be of the electro-optic type, using Ga As (See Appendix C). Modulation of 10.6 $\mu$ radiation using this material has been demonstrated, with good performance. We suppose that a reasonable modulation index will be

$$\delta = 1 \text{ radian}$$

Table 4-1. PHILCO GPC-215 INFRARED DETECTOR
P-Type Ge:Au Photoconductor
$A = 10^{-2}$ cm$^2$ $T = 77°K$ [1]

| Parameter | $\lambda = 5.5\ \mu$ | $\lambda = 10.6\ \mu$ [2] |
|---|---|---|
| Responsivity [3] R | $14 \times 10^3$ volts/watt | $7 \times 10^2$ volts/watt |
| Detectivity D* | $6 \times 10^9$ cm$\sqrt{\text{Hz}}$/watt | $3 \times 10^8$ cm$\sqrt{\text{Hz}}$/watt |
| NEP | $1.7 \times 10^{-11}$ watt/$\sqrt{\text{Hz}}$ | $3.3 \times 10^{-10}$ watt/$\sqrt{\text{Hz}}$ |

Notes:

1). Performance is significantly improved if the operating temperature is reduced to T = 65°K

2). Values for $\lambda = 10.6\ \mu$ are estimated by slight extrapolation of published curves; they may possibly be improved with better windows and design of the detector specifically for $\lambda = 10.6\ \mu$

3). At ~100$\mu$a bias. Responsivity varies linearly with bias, while D* and NEP remain very nearly unchanged.

The detection bandwidth is more or less arbitrarily chosen as

$$B = 100 \text{ Hz}$$

This is a compromise between sensitivity and speed of response.

We have finally to choose the total intensity $I_o$ incident on the detector. The manufacturer specifies that for 500°K blackbody radiation the GPC-215 is linear to signal levels $I_o$ (500°K) $\geq 10^{-6}$ watts, with a responsivity to this radiation of R(500°K) $\approx 7 \times 10^3$ volts/watt.

4.6 (Continued)

This implies linear response up to signal voltages of at least $V_s = 7 \times 10^{-3}$ volts. In fact, since the bias voltage on the detector is approximately 20 volts in normal operation, it seems safe to assume that the signal voltage could go at least as high as 0.2 volts without too much departure from linearity. (The manufacturer also specifies no damage from, and very rapid recovery from, even "massive radiation overloads").

Our chief problem is that the desired beat signal $I_1$ rides on top of a very large dc input $I_o$, and the dc response of the detector to $I_o$ is the limiting factor. It seems reasonable to assume that we can operate with an input $I_o$ at 10.6$\mu$ which, when multiplied by the 10.6$\mu$ responsivity, causes a dc signal voltage of less than 0.2 volts. Therefore, we specify

$$I_o(10.6\mu) = \frac{0.2 \text{ volt}}{R(10.6\mu)} \tag{4.37}$$

$$= \frac{2 \times 10^{-1} \text{ volt}}{7 \times 10^{2} \text{ volt/watt}}$$

$$= 280\mu \text{ watt}$$

This is certainly well within the available power from the laser amplifier.

If we combine all of the above numbers, the final result for the minimum detectable frequency error is

$$\Delta f_{min} \approx 4.3 \times 10^{3} \text{ Hz} \tag{4.38}$$

The fractional frequency stability which this number represents is

$$\frac{\Delta f_{min}}{f_o} = \frac{4.3 \times 10^{4}}{3 \times 10^{13}} = 1.4 \times 10^{-10} \tag{4.39}$$

Therefore, this value very nearly, but not quite, achieves the objective of 1 part in $10^{10}$ frequency stability.

We have, however, deliberately chosen values for all of the system parameters which were not pushed to their maximum values, in order to obtain a fairly realistic estimate. In Table 4-2, we have tabulated both these somewhat conservative design choices, and also the results of a reevaluation using a "stretched" set of system parameters. The result with the stretched parameters is

$$\Delta f_{min} = 20 \text{ Hz} \tag{4.40}$$

and hence a frequency stability of

Table 4-2. Estimation of Minimum Frequency Error

$$\Delta f_{min} \approx \frac{NEP \sqrt{B}\, \Delta f_D^{\,2}}{4(G_o \ell n\, G_o)\, I_o\, f_m\, \delta}$$

| Parameter | Initial Design | "Stretched" Design |
|---|---|---|
| Detector NEP | $3.3 \times 10^{-10}$ Watts $(Hz)^{1/2}$ | $2 \times 10^{-10}$ Watts $(Hz)^{1/2}$ |
| Detection Bandwidth B | 100 Hz | 1 Hz |
| Doppler Linewidth $\Delta f_D$ | 45 MHz | 40 MHz |
| Laser Gain $G_o$ | 2.0 | 2.0 |
| Laser Power $I_o$ | 0.28 mw | 1 mw |
| Modulation Frequency fm | 1 MHz | 1.5 MHz |
| Modulation Index $\delta$ | 1 | 2 |
| Minimum Frequency Error $\Delta f_{min}$ | 4.3 kHz | 20 Hz |
| Frequency Stability $\Delta f_{min}/fo$ | $1.4 \times 10^{-10}$ | $6.7 \times 10^{-13}$ |

4.6 (Continued)

$$\frac{\Delta f_{min}}{f_o} = 6.7 \times 10^{-13} \qquad (4.41)$$

This result is not to be taken as a design prediction, but is only intended to show that with some optimizing of the system parameters the original design objective is feasible.

There also appear to be some "safety factors" which are available to compensate for any overly optimistic assumptions in our choices of parameters. These "safety factors" can be invoked if and when required to compensate for any other unforeseen difficulties. A list of possible "safety factors" includes:

1) If detector performance is a seriously limiting factor, it is possible to go to a helium-cooled detector, thereby gaining greatly improved detectivity (at a considerable cost in practical convenience). Typically these detectors will offer about a factor of 20 reduction in NEP.

2) Cooling the walls of the $CO_2$ laser amplifier will reduce the doppler width $\Delta f_D$, and probably also increase the available gain $G_o$.

3) The performance of the simpler nitrogen-cooled detectors should be capable of at least some improvement, by limiting the field of view to the very small angle needed for this application; optimizing the choice of window material; optimizing the detector geometry; and pumping on the nitrogen to cool below 77°K.

4) Concentration on modulator design and optimization should permit either higher modulation frequency $f_m$ (if detector limitations permit), and/or substantially higher modulation index $\delta$.

5) Use of the detector as a combined photodetector and modulation-frequency mixer, by using rf detector bias, will permit higher modulation frequencies, and may also improve noise performance. This is an important point, and should be checked experimentally early in the program.

6) Even higher values of the power $I_o$ from the $CO_2$ amplifier may be usable, especially with rf bias. The usable response range of available detectors should be checked early in the program.

## 4.7 SUMMARY

An analysis for the external $CO_2$ amplifier stabilization scheme has been carried out for both the homogeneously broadened and inhomogeneously (doppler) broadened amplifier gain curve. Only slight numerical differences in the midband discriminant function appeared, especially for the case of a $CO_2$ laser amplifier in which the ratio of doppler linewidth to homogeneous linewidth is relatively small.

For the case where the modulation depth and frequency is low enough, the minimum sensitivity function, in terms of real detector parameters, can be evaluated from the midband discriminant function.

The minimum detectable frequency deviation ($\Delta f_{min}$) for any laser system was derived to be

$$\Delta f_{min} = \frac{NEP \sqrt{B}\ \Delta f_D^2}{4(G_o \ell n\, G_o)\, I_o\, f_m\, \delta}$$

where NEP is the noise equivalent power, B is the system bandwidth, $\Delta f_D$ is the full width of the doppler gain curve at half height, $G_o$ is the total amplifier gain, $I_o$ is the detector input power (optical), $f_m$ is the modulation frequency, and $\delta$ is the modulation depth.

Earlier similar calculations, which estimated the above minimum detectable frequency deviation, were carried out based upon the limitations imposed by shot-noise-limited detectors. The analysis has been extended to the real case of readily available 10 $\mu$m detectors which have noise characteristics two to three orders of magnitude worse than shot-noise-limited devices. To obtain the desired 1 part in $10^{10}$ frequency stability, the loop bandwidths will have to be restricted to about 100 Hz and electro-optic modulators will have to be employed in order to operate at required modulation frequencies on the order of 1 MHz. The detectors would be liquid nitrogen cooled, but substantial improvement could be obtained if liquid helium cooled detectors were utilized.

Section 5

# ELECTRONIC CONTROL LOOP TECHNIQUES

## 5.1 GENERAL SYSTEM DESCRIPTION

The frequency control loop block diagram is shown in Figure 5-1. The stability of the main $CO_2$ oscillator is controlled by varying the cavity length with a piezoelectric tuning device. The control signal for the tuning device is developed from a phase modulated optical signal that is sent to a $CO_2$ amplifier from the main $CO_2$ laser beam. The development of the error signal is discussed in Section 4.

The basic error signal detected at the photo detector has the same carrier frequency as the modulating signal for the phase modulation. The side bands of the error signal have a frequency spectrum equal to the disturbance frequency spectrum of the main $CO_2$ oscillator. The disturbance spectrum includes thermal drift and acoustical noise. The disturbance sidebands are detected to a low pass spectrum by the phase detector operating at the carrier frequency.

The low frequency signals are filtered and amplified to provide correction signals for the tuning piezoelectric device. The filtering is to control the noise bandwidth and also to compensate or stabilize the closed-loop control system. The closed-loop bandwidth should be nearly equal to the disturbance bandwidth for best stabilization results.

## 5.2 PIEZOELECTRIC TUNING DEVICE

The piezoelectric stack is difficult to drive from an amplifier because the device looks like a large capacitor. Additionally there are structural resonances in the device which make it unusable at some frequencies. An electrical frequency response of a typical mechanically free-hanging piezoelectric device is shown in Figure 5-2. A source impedance of 620 ohms was used to measure the voltage drop to the device. Figure 5-3 shows an approximate electrical equivalent circuit of the device. The first -3 db point at 16 KHz represents the corner frequency of the driving impedance, R1, and the equivalent device capacitance, C1. The deep notch at 84 KHz represents a structural resonance, which is a series resonance of C2 and L1 in the equivalent circuit. The peak at 88 KHz is the parallel resonance of C1 and L1. The following notch and peak are results of a second structural resonance.

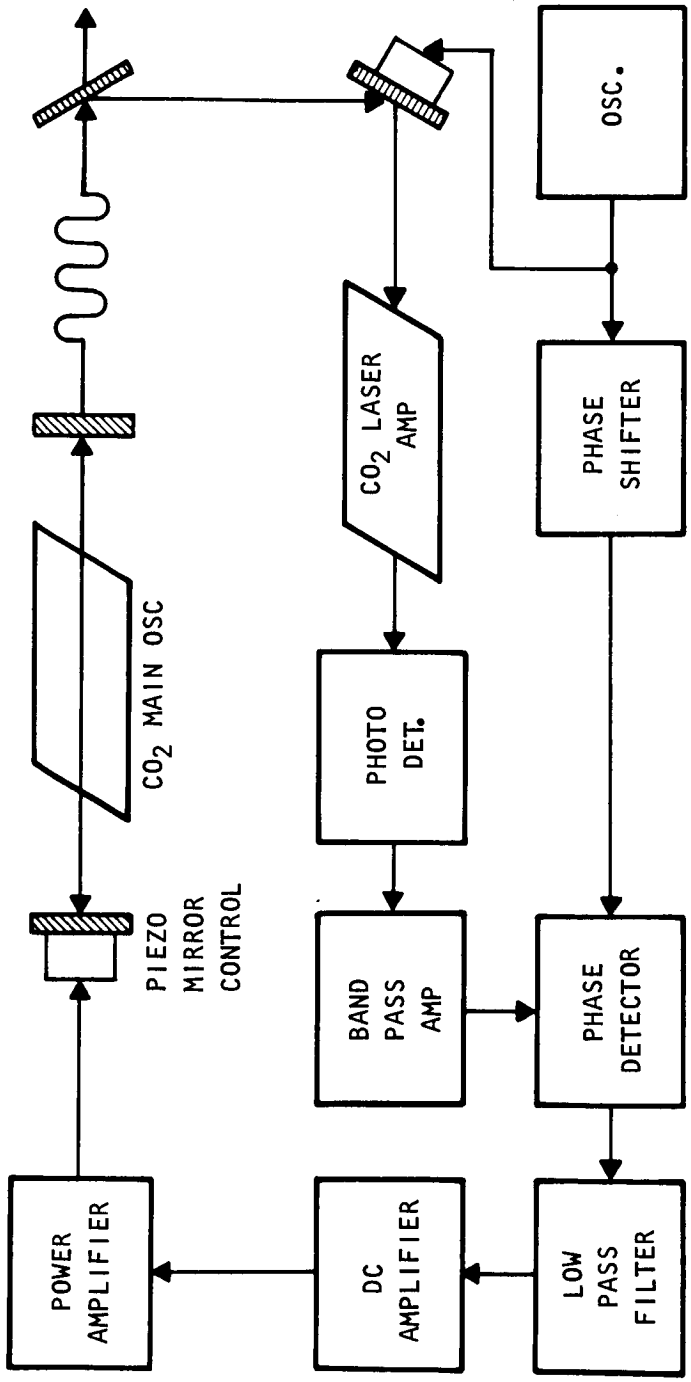


Figure 5-1. Main Frequency Control Loop Block Diagram

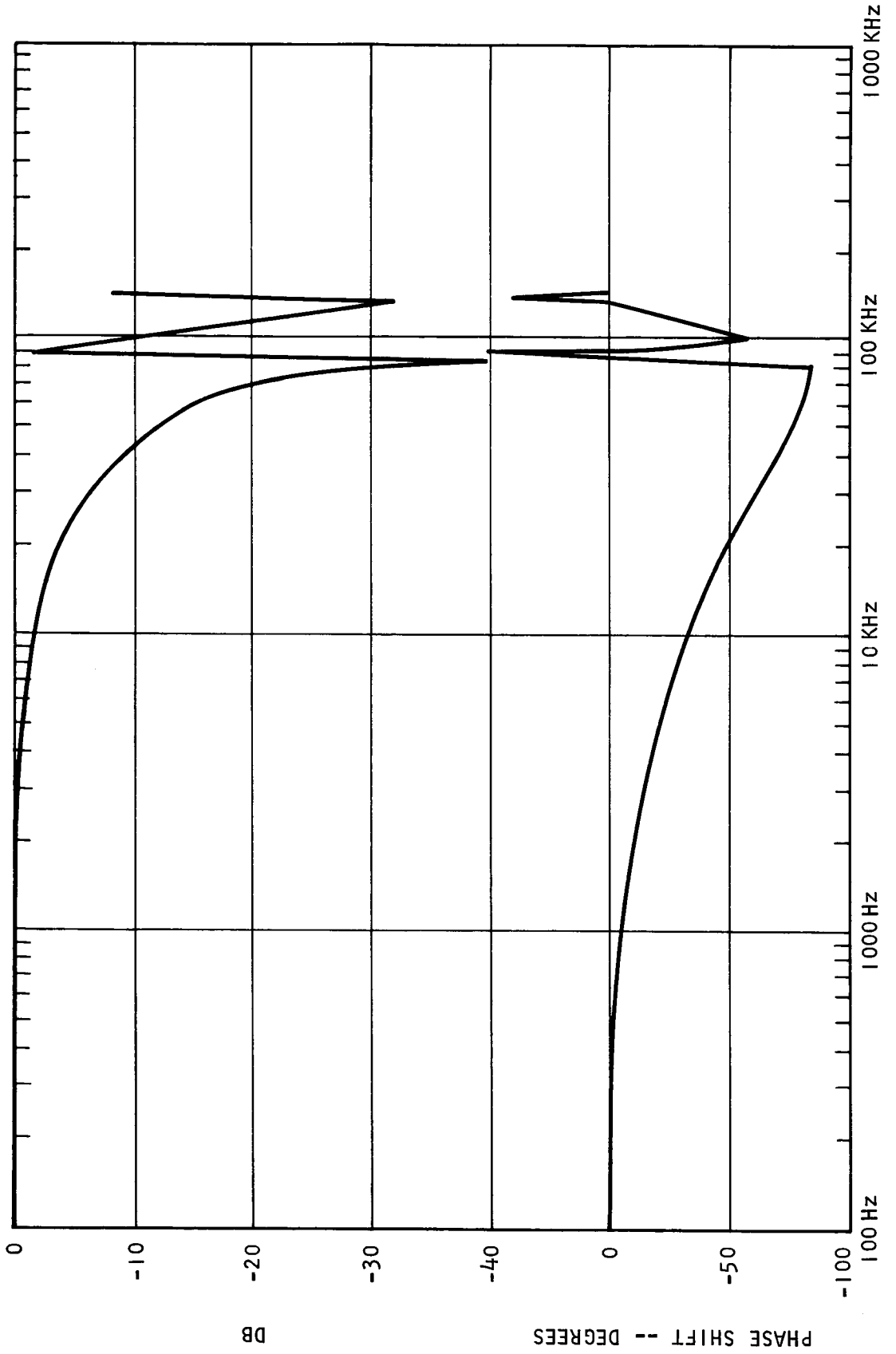


Figure 5-2. Piezoelectric Impedance Frequency Response

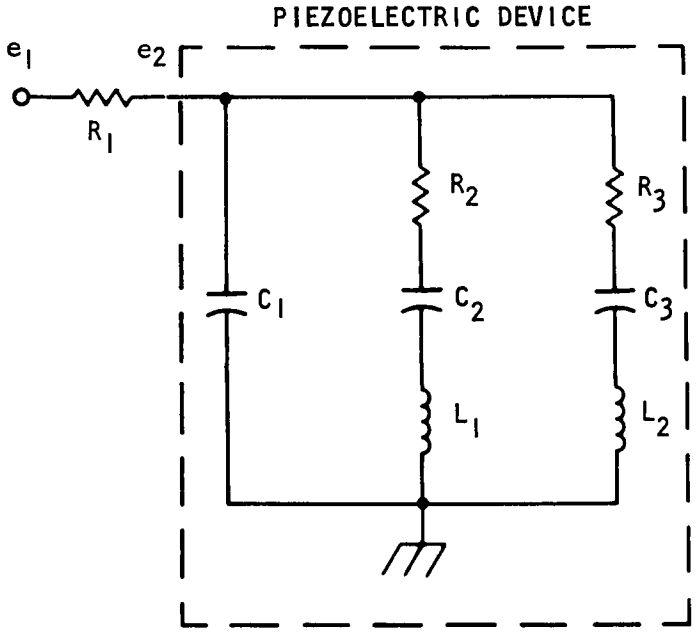


Figure 5-3. Approximate Electrical Equivalent Circuit for Free Hanging Piezoelectric Device

5.2 (Continued)

When the piezoelectric device is firmly mounted to the cavity structure and the mirror is added, the first structural resonance will occur at approximately 40 KHz. Using this fact and the electrical equivalent circuit of the device it was determined that the 16 KHz corner was not affected, and the equivalent device input capacity will still be approximately 0.016 $\mu$f. This particular device is capable of displacements on the order of 1/2 $\mu$m. Larger piezoelectric stacks would have more displacement, but with increased capacitance.

The displacement gradient of the device is approximately $2.5 \times 10^{-3}$ $\mu$/volt. A driving amplifier would have to have a voltage swing of about 300 volts to compensate for expected thermal drifts. A typical cavity length of 50 cm would require that the driving amplifier have no more ripple than 20 mv for frequency stability of $10^{-10}$.

## 5.3 PHASE MODULATOR AND CARRIER FREQUENCY

The phase modulator to be used to modulate the split optical beam could be either an electro-optic type modulator or a vibrating mirror modulator depending, primarily, on the required carrier frequency needed in the stabilization scheme.[37] If a vibrating mirror modulator is used,[44] the modulating frequencies chosen would have to produce a stable mechanical response in the device since varying displacement and phase angle would upset the closed-loop response. Mechanical techniques would be limited to frequencies no higher than about 100 kHz. However, a modulation frequency of about 100 kHz or greater would be good from a carrier standpoint. While it can be shown theoretically that a frequency bandwidth equal to the carrier frequency can be recovered through synchronous detection, practical limitations such as phase shift and distortion limit the sideband frequency information from 1/2 to 1/5 the carrier frequency. Since the closed-loop bandwidths of the probable system will be less than 20 kHz, the carrier frequency would be no limit on the system if 100 kHz or greater is utilized.

## 5.4 PHOTO DETECTOR

The photo detector has to be able to respond linearly to the carrier frequency. Any phase shift of the carrier sideband frequencies must be reflected down to the closed-loop response. The level of the carrier error signal will be very small. A rough estimate is that a one volt signal applied to the tuning piezoelectric device will produce a 200 microvolt error signal at the photo detector. At these levels it is necessary to do extensive shielding of all the detector package and connecting leads. The photo detector should also have a minimum of noise at the carrier frequency. In fact, the carrier frequency may be chosen to minimize noise.

## 5.5 BANDPASS AMPLIFIER

The bandpass amplifier will be tuned to the same frequency as the modulation frequency. The input signal levels from the photo detector are in the micro-volt range. This means that front end noise must be reduced to the absolute minimum with this amplifier. From the noise standpoint it is desirable to have the amplifier bandwidth as narrow as possible. A narrow bandwidth, however, would result in phase shift of the signal sidebands. To account for this phase shift, a low pass time constant equal to the half bandwidth -3 db point is used for the closed-loop analysis. A 10 KHz, 3 db bandwidth would result in a 5 KHz corner frequency time constant. For the 100 KHz carrier frequency, a 20 or 40 KHz, 3 db bandwidth may be used, resulting in a relatively small time constant in the control loop.

## 5.6 PHASE DETECTOR

The phase detector is a device whose dc output voltage is proportional to the phase and amplitude of the input signal with respect to a reference signal. The dc output varies as a cosine function of the angle between the input and reference signals. The phase shifter shown in Figure 5-1 is placed in the reference channel in order to minimize carrier sideband phase shift in the error signal. The low pass filter after the phase detector would have a corner frequency approximately at the noise bandwidth corner. The function of this filter is to smooth out transients.

## 5.7 DC AMPLIFIER

The major function of this amplifier is to furnish dc amplification and compensation for the closed-loop system. A plain dc amplifier would result in a Type 0 closed-loop system, resulting in a positional offset error. This would mean that for slow thermal drifts there would be an error voltage present equal to the offset error divided by the closed loop gain. If the thermal drift were 1/2 $\mu$m, the loop gain would have to be 10,000 to achieve the required frequency stability.

The closed-loop system would become Type 1 by converting the amplifier to an integrator. There would be no positional error, and the velocity error or rate of change error would be reduced by the loop gain. Also this amplifier is in an excellent place to add compensation networks for the stabilization of the closed-loop system.

## 5.8 POWER AMPLIFIER

The power amplifier is a very important part of the closed-loop system. It has to have a voltage swing in the range of several hundred volts, yet have ripple levels no

5.8 (Continued)

greater than a few millivolts. It must have high dynamic frequency response, yet be very stable. The amplifier must drive a capacitive load.

One way to achieve the high frequency response is for the amplifier to have a low output impedance. The direct capacitor load will unfortunately cause almost any amplifier to become highly underdamped and in fact oscillate at high frequencies. This is because the amplifier output impedance and the capacitor form a dominant time constant which along with the inherent amplifier time constant will result in an amplifier with no phase margin at high frequencies. A remedy to this problem is to decouple the amplifier from the load with a resistor equal to the output impedance of the amplifier. This lowers the closed-loop bandwidth, but is absolutely necessary.

Typical open-loop output impedances are from 100 to 1,000 ohms for most amplifiers. This is why the frequency response of the piezoelectric device was determined with a 620 ohm series resistor. One interesting fact to consider is that when the driving signal to the piezoelectric device is of the same frequency as the structural resonance, the series resistor will drop the driving voltage and result in less drive to the device.

## 5.9 CLOSED-LOOP SYSTEM

The closed-loop transfer functions are shown in Figure 5-4. These transfer functions include estimates of gain and time constants. A total loop gain of about 66 db is desired and the loop appears to be stable at this level. The bandpass amplifier has a 10 KHz bandwidth which results in a 5 KHz low pass time constant for the closed-loop system. The integrator was chosen to give the Type 1 system. With no compensation networks the closed-loop bandwidth is approximately 400 Hz. Compensation networks which were added to the integrator and the power amplifier are shown as part of those transfer functions.

Based on the typical components discussed above,the system frequency or Bode plot can be calculated and is shown in Figure 5-5. The closed-loop bandwidth is approximately 5 KHz. This corresponds to the bandwidth that was chosen for the bandpass amplifier. If a wider amplifier bandwidth were used,it would not greatly alter the compensation problem. Closed-loop bandwidths of 5 to 15 KHz seem possible if system noise is not an overwhelming problem.

All analysis has assumed that a specific piezoelectric tuning device would be used. It is possible that this device would not have enough total displacement to compensate for all thermal drifts. A second piezoelectric device mounted to the second mirror on the

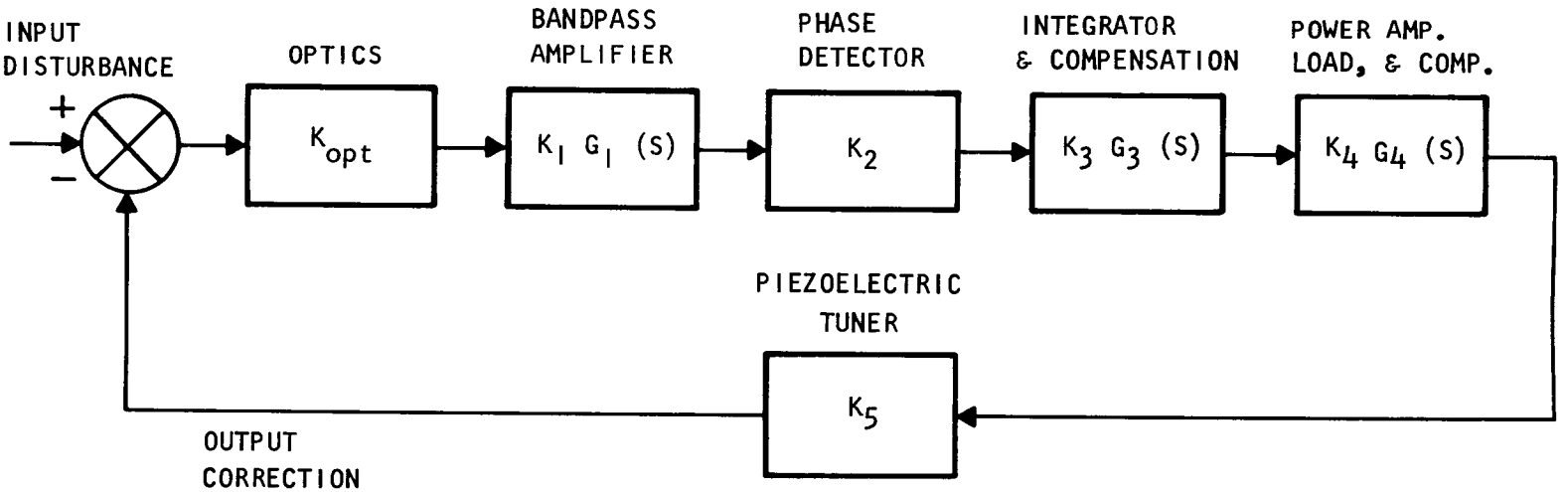


$K_{opt} = 10^{-2}$ VOLT/μ

$$K_1 G_1 (S) = \frac{K_1}{3.18 \times 10^{-5} S + 1}$$

$$K_3\ G_3\ (S) = \frac{K_3\ (0.5S+1)}{S(0.05S+1)}$$

$$K_4\ G_4\ (S) = \frac{30\ (10^{-4}\ S + 1)}{(5 \times 10^{-6} S + 1)(10^{-5} S + 1)}$$

$K_1\ K_2\ K_3 \cong 3.3 \times 10^6$

$K_5 = 2 \times 10^{-3}$ μ/VOLT

$K_{TOTAL} = 66$db

Figure 5-4. Closed Loop Transfer Functions

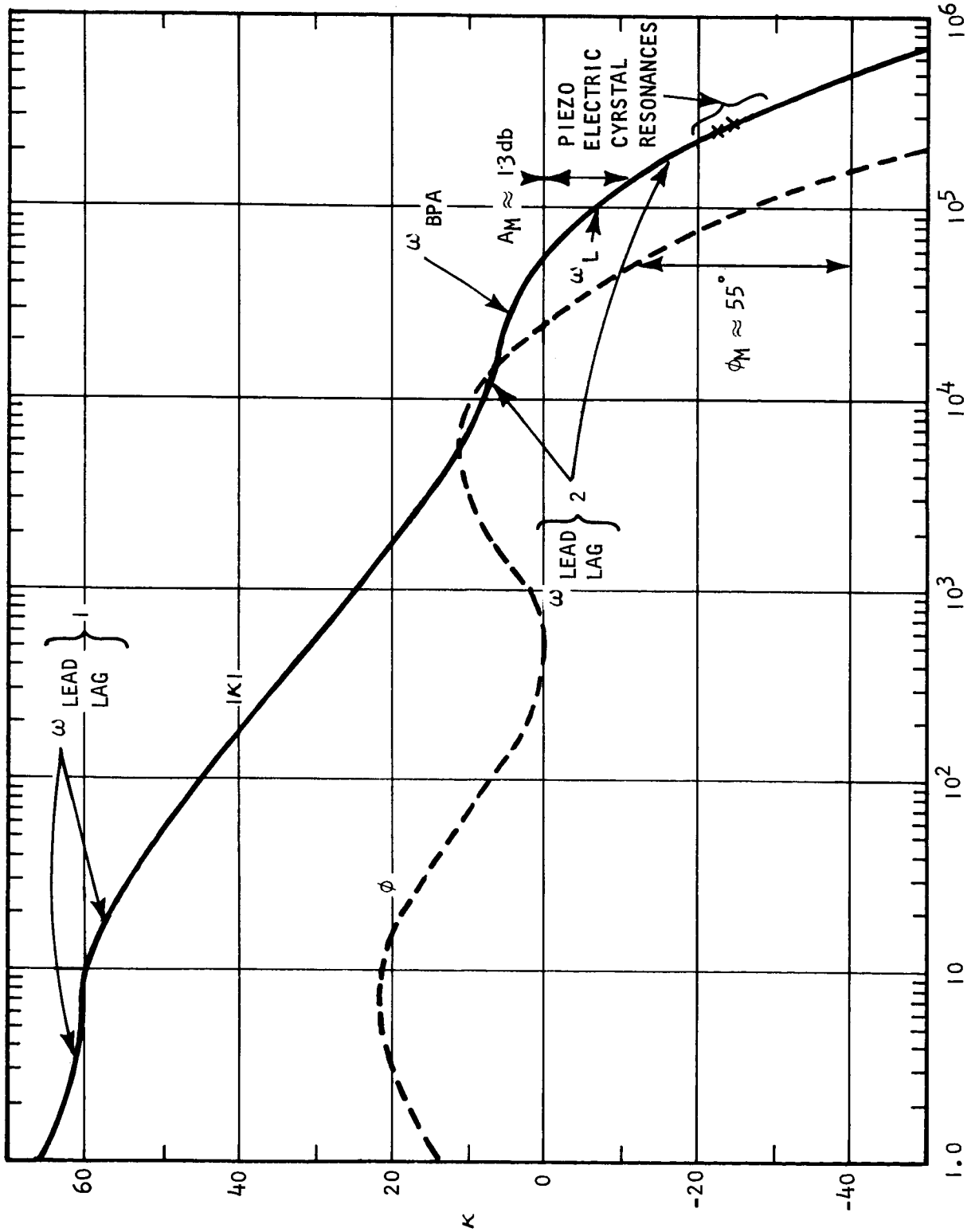


Figure 5-5. Open Loop System Transfer Function With Two Lead-Lag Networks

5.9 (Continued)

cavity could help with this problem. If it were a much larger device, it would have more displacement capability. The only problem is that it would have a very high equivalent input capacity and require some type of special drive cross-over system.

Figure 5-6 illustrates how it would be possible to use two piezoelectric devices with one error signal. Figure 5-6a shows the basic closed-loop system as it has been analyzed in this Section. All the system transfer functions are lumped into KG(s),and $G_{L1}(s)$ represents the transfer function of the first piezoelectric device with its series resistor. Figure 5-6b shows the closed-loop system as it would be with two devices and two cross-over networks. Since $G_{L1}(s)$ is the small device, it would be used only at high frequencies and $G_1(s)$ would be a high pass filter. The second device, being much larger than the first device, would be driven with the transfer function $G_{L2}(s)$, by a low pass filter. This low pass filter would be a function of the other three transfer functions.

The resulting transfer function for $G_2(s)$ shows that the two piezoelectric device approach can be used. In practice it would be possible, but care would have to be exercised in order to preserve phase and gain matching of the two channels.

## 5.10 SUMMARY

Based on the readily available components, used in similar laser systems, it appears possible to obtain a satisfactory control loop with bandwidths of at least 5 KHz. The degree to which this bandwidth can be utilized will be determined primarily by the noise characteristics of the laser amplifier, photodetector, and front end amplifier. For the case when large piezoelectric displacements may be required due to thermal drifts, two independent piezoelectric stacks could be used; one for the low frequency but large movements and the other for low amplitude but high frequency control. A cross-over scheme in the control loop appears possible; this would not seriously limit the overall gain-bandwidth product. This approach appears promising in that it could relieve some of the strain on the temperature control of the laser structure.

5-6 a

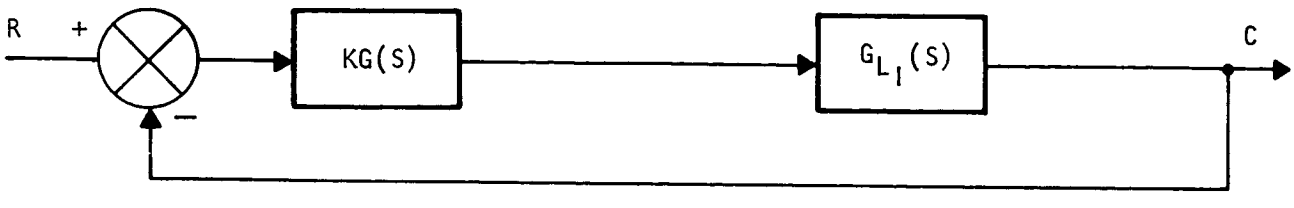


5-6 b

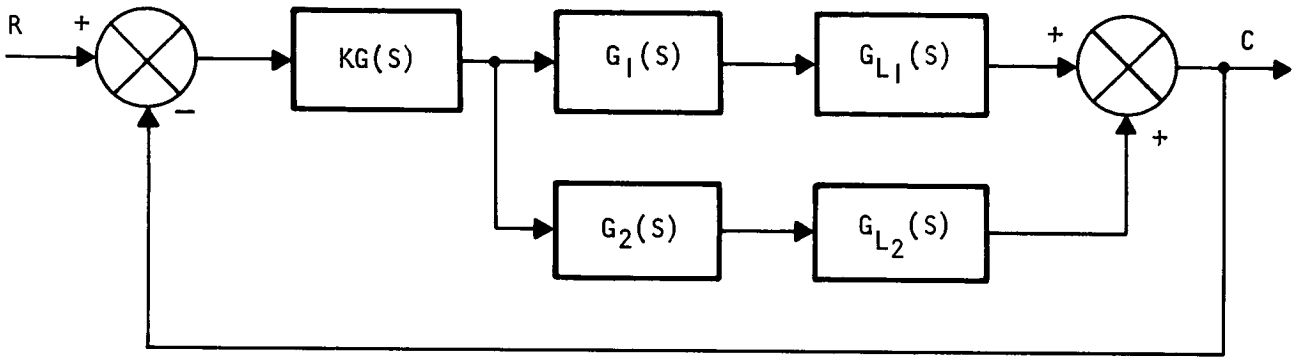


$$G_1(S)\ G_{L_1}(S) + G_2(S)\ K_{L_2}\ G_{L_2}(S) = G_{L_1}(S)$$

$$G_2(S) = \frac{G_{L_1}(S)\left[1 - G_1(S)\right]}{K_{L_2}\ G_{L_2}(S)}$$

$$G_1(S) = \frac{S\tau}{\tau S+1}$$

$$G_{L_1}(S) = \frac{1}{\tau_{L_1} S+1}$$

$$G_{L_2}(S) = \frac{1}{\tau_{L_2} S+1}$$

$$K_{L_2} = \text{GAIN DIFF. BETWEEN DEVICES}$$

$$G_2(S) = \frac{(\tau_{L_2} S + 1)}{K_{L_2}(\tau_{L_1} S + 1)} \frac{1}{(S\tau_1 + 1)}$$

Figure 5-6. Cross-Over Drive for Two Piezoelectric Devices

Section 6

# LASER WAVELENGTH AND MODE CONTROL

## 6.1 INTRODUCTION

As discussed in Section 2, the $CO_2$ laser can operate almost equally well on several different wavelengths around 10.6 $\mu$m depending on the J value of the transition. Although the laser will generally only operate on one wavelength at a time, the choice of wavelength can be a random process depending on which photon starts the lasing action. This random type of operation is not tolerable in a heterodyne system. Also, it is possible that the laser may prefer, at a given time, to oscillate on a higher order mode rather than the $TEM_{oo}$ mode unless special considerations are given to the design of the optical cavity to discourage such operation. The following sections discuss several techniques which can be applied to the design of the optical cavity of a $CO_2$ laser which would force the laser to oscillate at a particular wavelength and mode in a reproducible manner independent of surrounding conditions.

## 6.2 WAVELENGTH SELECTION

### 6.2.1 Internal Prism

A technique for wavelength selection that has been used many times in the past on He-Ne, Argon, and other lasers is to impose a high-quality prism in the laser cavity between the laser tube and one of the cavity mirrors. The natural angular dispersion of the prism is enough to detune the cavity for all wavelengths other than the one for which the mirror-prism system is aligned. In all previous cases, the separation between the adjacent wavelengths was large and no problem existed in obtaining enough loss on unwanted lines to keep them from oscillating. For the case of the $CO_2$ laser, the lasing lines are so close together that special attention must be given to the design of such an intracavity prism.

Since the wavelength separation between the adjacent J transitions is so small (.02 $\mu$m minimum), the prism must have high enough resolving power to adequately separate the lines. The resolving power of a prism is given by

$$\Delta\lambda = \frac{\lambda}{B\frac{dn}{d\lambda}}$$

6.2.1 (Continued)

where $\Delta\lambda$ is the Rayleigh limit to the separation of lines, $\lambda$ is the average wavelength, B is the base length of the prism and $\frac{dn}{d\lambda}$ is the dispersion of the prism material.

Unfortunately there are few materials which could be used for internal cavity prisms in the 10-$\mu$m range. Internal cavity work automatically requires low absorption and scattering loss and the materials which fulfill this requirement, in usable thicknesses, are limited to Germanium and several of the Ionic salts, such as Sodium Chloride and Potassium Chloride.

The dispersion characteristics at 10 $\mu$m for a large group of infrared materials has been listed in Table 6-1. Except for Lithium Fluoride, which is starting to absorb quite strongly at 10 $\mu$m, NaCl has the highest dispersion characteristics of all the other infrared materials.

Table 6-1. Dispersion Characteristics of Several Infrared Crystals at a Wavelength of 10 $\mu$m

| MATERIAL | INDEX OF REFRACTION | DISPERSION $dn/d\lambda$ ($\mu^{-1}$) |
|---|---|---|
| $BaF_2$ | 1.4195 | .0051 |
| CsI | 1.73916 | .00081 |
| CsBr | 1.66251 | .00131 |
| Ge | 4.0032 | .0004 |
| Si | 3.4179 | .0003 |
| KCl | 1.45664 | .00398 |
| NaCl | 1.49482 | .00699 |
| KRS-5 | 2.37069 | .00215 |
| LiF | 1.094 | .087 |
| Se | 2.4767 | .0009 |
| KBr | 1.52 | .00222 |

In order to resolve the nearest lines of the $CO_2$ laser ($\Delta\lambda$ = .02 $\mu$m) using a NaCl prism ($dn/d\lambda$ = .007 $\mu$m), the base width of the prism must be at least

$$B = \frac{\lambda}{\Delta\lambda \frac{dn}{d\lambda}} = 72 \text{ mm long},$$

6.2.1 (Continued)

a fairly large crystal. A big advantage is obtained by putting this prism inside the laser cavity where the multiple pass effect through the prism will increase the resolving power. For example, if the losses in the cavity run about 10 percent (including output mirror transparency losses), then the internal beam will make an average of about 18 passes through the prism. The effective length of the prism is then increased by this amount, reducing the required length of the prism to a respectable size for in-cavity operation.

If a Brewster-angle tube is used, the prism can easily be fabricated so that the beam will enter and exit the prism at Brewster's angle with respect to the prism faces. This would reduce the prism losses significantly.

Although the several laser lines would be spatially separated within the cavity, the mirror system would have to be designed with high enough angular sensitivity so that only one of the possible laser lines could oscillate. Comparing the above numbers, in terms of angular sensitivity, to those published by Sinclair[18] on the angular sensitivity of laser cavities, indicates that the required sensitivity can be obtained.

The main disadvantage to this approach is the need for use of mechanically poor materials. The salts, such as NaCl, are very brittle, extremely soft and are hygroscopic, making it very difficult to optically prepare them with high enough quality for in-cavity use. Also their thermal-mechanical characteristics are quite poor (see Section 7.3 on Brewster-angle windows). For example, with the size prism required (1-2 cm long), a one degree change in temperature of the prism corresponds to a change in optical path length equivalent to about 30 MHz change in output frequency. It is most desirable to find a scheme which can reduce this thermal effect so that the requirements on the electronic system can be kept as low as possible.

6.2.2 Internal Grating

A similar approach to the use of an internal prism is the use of an internal grating either as a third mirror in a three-mirror scheme or as one of the laser mirrors. For very long wavelengths, on the order of 50 $\mu$m and longer, gratings have been designed to act as an end mirror in a two mirror laser cavity. By choosing the proper blaze angle and groove spacing, it is possible to return approximately 90-95 percent of the cavity power back into the cavity while the remaining power is useful output. No one has reported using this procedure at 10 $\mu$m although there seems to be no fundamental reason why it could not be made to work.

6.2.2 (Continued)

The resolution of a grating is given by

$$\Delta\lambda = \frac{\lambda}{mN}$$

where $\Delta\lambda$ is the Rayleigh limit, $\lambda$ is the wavelength, m is the order and N is the number of rulings used. A typically available grating for use at 10 $\mu$m has a ruling of about $10^5$ grooves/m (100 grooves/mm) and for a $10^{-2}$ meter (1 cm) diameter laser beam the resolution would be about .01 $\mu$m for the first order, sufficient for the separation of the nearest $CO_2$ laser lines.

Although grating selection does have the necessary sensitivity, the mechanical complexities associated with installing such a device as a laser mirror inside the laser cavity would be more difficult than the effort would be worth, especially since other schemes could be implemented more easily.

6.2.3 Cavity Length Control

Because of the narrow spacing between adjacent $CO_2$ laser lines and the narrow Doppler linewidth, some discrimination in wavelength can be obtained by length tuning the cavity.

Consider, for example, the condition for which oscillation is permitted on one line, $\lambda_1$, but denied for the other, $\lambda_2$. That is, the optical separation of the cavity mirrors is chosen such that a node exists for $\lambda_1$ at each mirror (oscillation permitted), and a node at one mirror and an antinode at the other mirror for $\lambda_2$ (oscillation not permitted). The minimum mirror separation, $\ell$, for this condition is given by

$$\ell = \frac{N\lambda_1}{2} = \frac{N\lambda_2}{2} + \frac{\lambda_2}{4}$$

where N is the number of half wavelengths between the mirrors. As an example, choose $\lambda_1 - \lambda_2 = \Delta\lambda$ as 0.02 $\mu$m as a typical case for the $CO_2$ laser operating at 10.6 $\mu$m. This is the approximate separation of nearest P-type transitions in $CO_2$. The above equation can be reduced to

$$\ell = \frac{\lambda_1\lambda_2}{4\Delta\lambda} \approx \frac{\lambda^2}{4\Delta\lambda}$$

$$\ell = 1.4 \times 10^{-3} \text{ m (1.4 mm)}$$

6.2.3 (Continued)

Even multiples of this length will provide conditions for which both lines can simultaneously oscillate. Odd multiples of $\ell$ will only allow one of the two lines to oscillate at a time. The choice of which line is to oscillate is controlled by fine tuning the length over a quarterwave distance. Unfortunately, the $CO_2$ laser has several lines of about equal gain continuously spaced at about .02 $\mu$m, and it is not possible to discriminate against them all with this technique alone. However, by choosing the optical path separation between laser mirrors equal to an odd multiple of $\ell$, the number of possible lines which could oscillate for a particular mirror setting can be substantially reduced and the ones which could oscillate will not be nearest neighbors. This, in effect, serves as a gross wavelength selector which may relieve some of the strain on other wavelength selection schemes, especially prism selection.

6.2.4 Frequency-Selective Etalon Techniques

The various wavelengths which can be emitted from the $CO_2$ laser arise from the possibility of transitions from closely spaced rotational J levels of one vibrational band to another. Because of the regularity in the spacing of these J levels, the frequency separation between wavelengths is relatively constant for those transitions which would be of interest. For the 10.6 $\mu$m lines, the separation is about 53 GHz. With this regularity in frequency spread, one can consider techniques for $CO_2$ wavelength selection similar to those used to select a particular axial mode frequency in a .6328 $\mu$m He-Ne laser; namely, frequency-selective etalon techniques.

The problem then is to select one $CO_2$ Doppler line (50 MHz wide) from a group of Doppler lines separated by 53 GHz. This can be done by designing an etalon which has a free spectral range of about 48 GHz and a half-power bandpass of about 3 GHz. By accurately adjusting the length of the etalon to center on the desired Doppler line (one with highest output power), the etalon would not be aligned for any nearby Doppler lines. The nearest Doppler lines which would be in alignment would be about ±10 from the desired line. As observed by Moeller and Rigden[11], the gain of the lines at P values of ±10 from some chosen P branch with good gain is substantially below the optimum. This verifies theoretical predictions by Patel[10].

One desirable feature of this approach is that the stability requirements on the etalon are not difficult to achieve. The etalon cavity Q is only 48/3 = 16 instead of the $10^7$ or better for the He/Ne laser case. The equivalent C/2L spacing turns out to be about 3 mm.

6.2.4 (Continued)

To maintain good etalon transmission stability, the length of the etalon need only be stabilized to about 1 part in $10^3$, which is well within the range of unstabilized devices.

This general approach can be utilized with at least two different specific techniques. One would involve a three-mirror cavity scheme in which three mirrors would be placed colinear, with the separation between two of the mirrors being the required 3 mm for wavelength discrimination. The third mirror would be separated from the first two by the laser tube (see Figure 6-1). The surface of the center mirror facing the laser tube would require nearly zero reflectivity and the other mirror surfaces would have reflectivities chosen to give the required Q's in the laser and the wavelength selection cavities. The various laser wavelengths could be selected by only adjusting the linear separation of the mirrors in the two cavities.

The other approach which appears to be more easily implemented utilizes the frequency-selective etalon as a bandpass device used inside the laser cavity as shown in Figure 6-2. In this case a Fabry-Perot etalon is made such that its optical thickness is about 3 mm thick. Its two surfaces are polished flat and parallel so that the device will serve as a typical Fabry-Perot periodic pass-band filter, whose period is determined by the optical thickness. By varying the angle of the etalon with respect to the in-cavity laser beam, the optical thickness can be varied sufficiently to allow tuning over the desired wavelength range.

The Finesse, F , or Q of a lossless etalon is given[19] by

$$F = \frac{\pi \sqrt{R}}{1 - R}$$

where R is the reflectance of the surface of the plate. It is assumed that the reflectance is the same for each surface. To obtain the desired F = 16, the corresponding value of R is about 82 percent, well within the range of multi-layer dielectric coatings, even at 10 $\mu$m.

An ideally manufactured device would have a periodic pass-band characteristic as shown in Figure 6-3. The transmission peaks would be 100 percent, and the device would be lossless for the correct wavelength. The position of the transmission peaks in absolute frequency space are determined by the angle the plate makes with the beam. The wavelength for maximum transmission at first order is given by

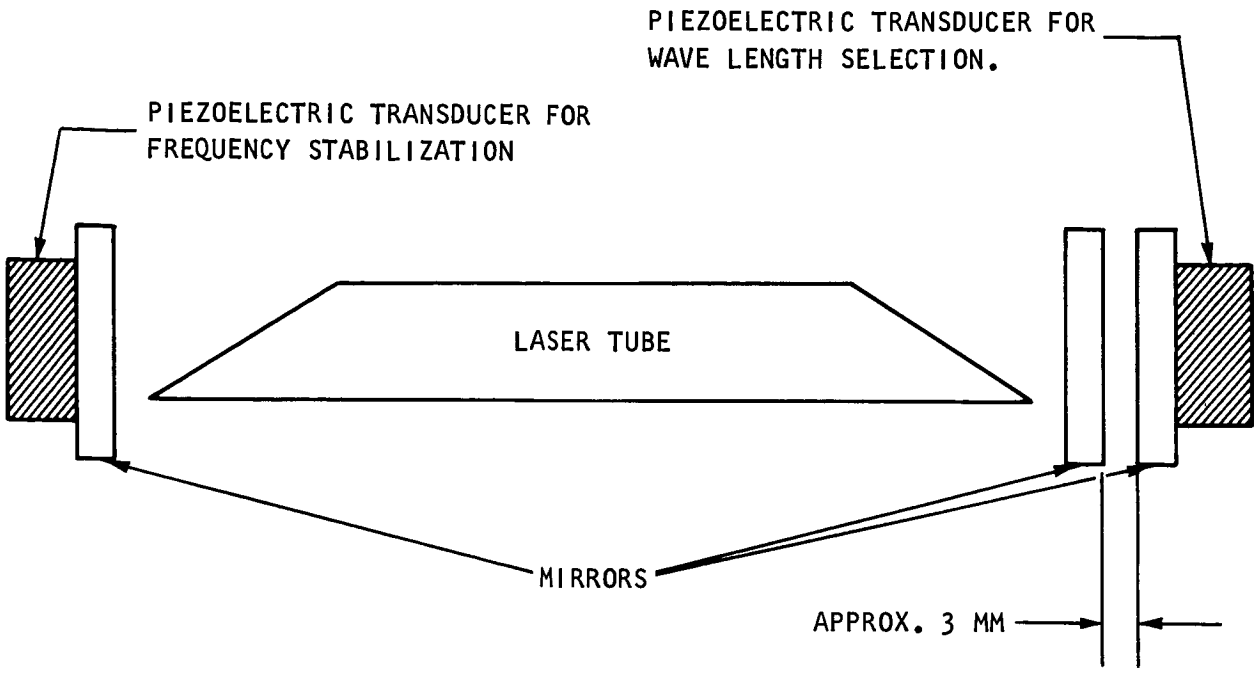


Figure 6-1. Wavelength Selection By a 3 Mirror Scheme

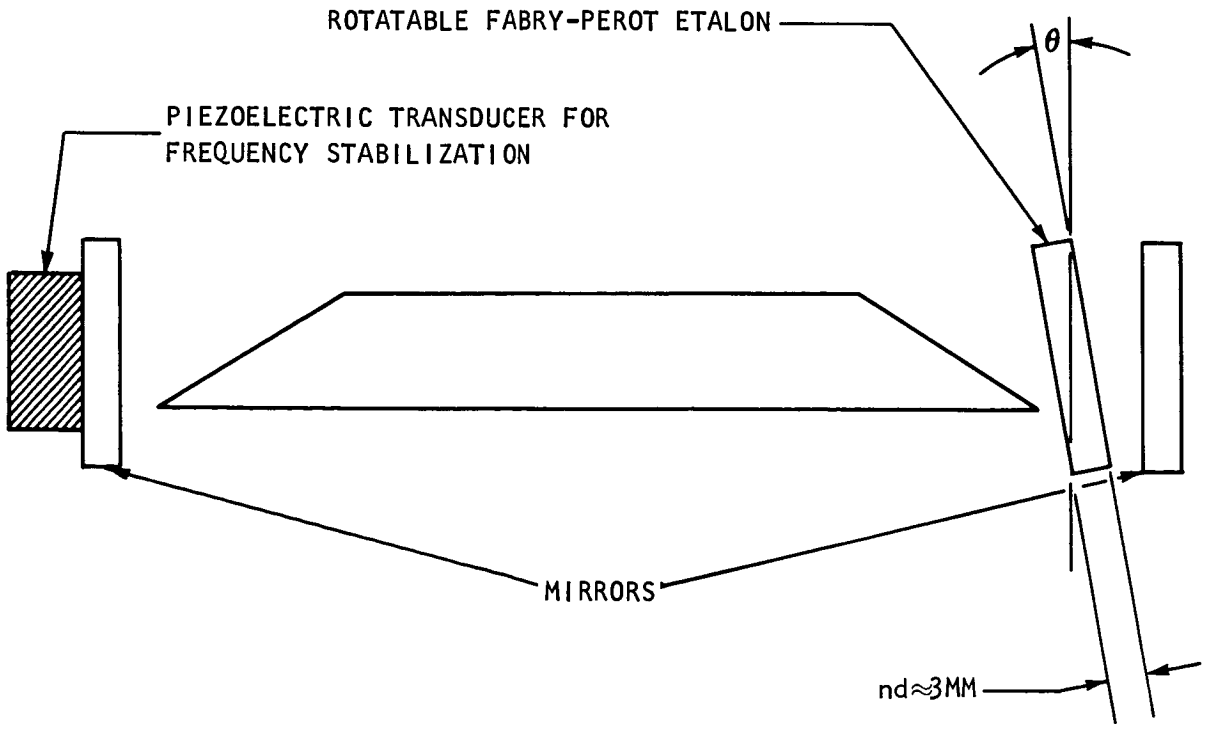


Figure 6-2. Wavelength Selection By Tunable Bandpass Filter

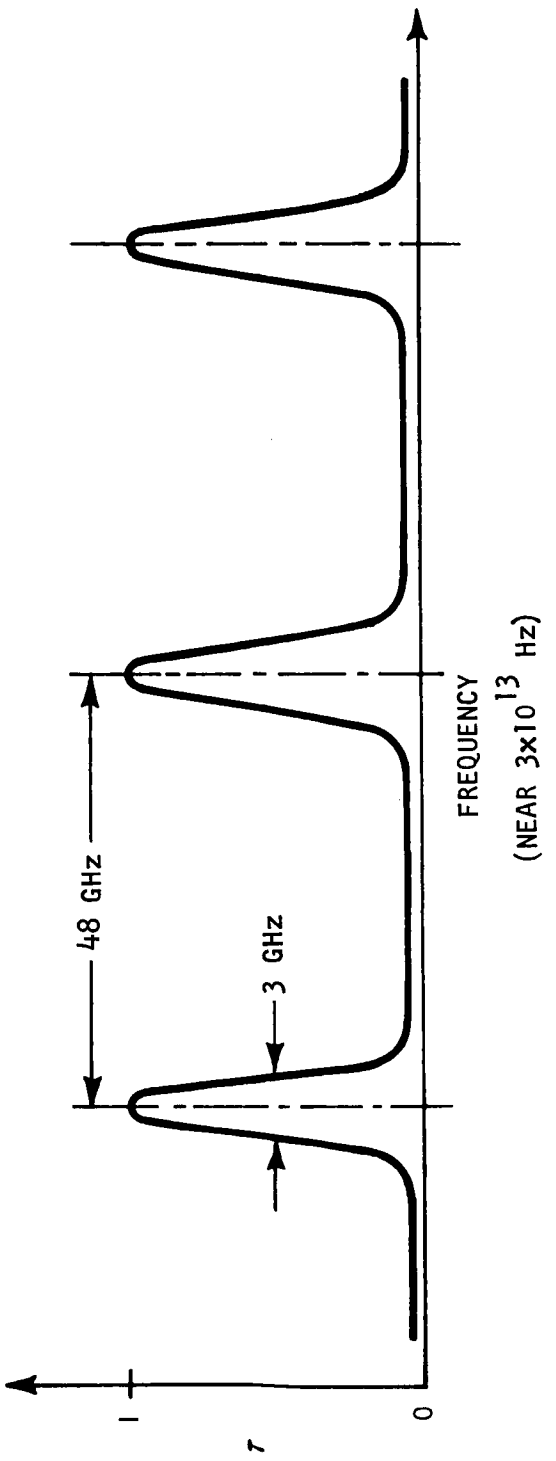


Figure 6-3. Pass Band Characteristics of a Short Fabry-Perot Etalon

6.2.4 (Continued)

$$m \frac{\lambda}{2} \cos \theta = nt$$

where $n$ is the index of refraction of the plate, $t$ is the physical thickness of the plate, $\theta$ is the angle between the plate normal and direction of the beam inside the plate and $m$ is an integer. As an example, choose Germanium as the Fabry-Perot material ($n = 4.00$). It can readily be calculated from the above formula that rotating the prism 13.5 degrees around the normal will sweep the frequency pass-band until the second order starts appearing.

The major difficulty with this approach is the attainment of high enough quality materials and precise, high reflectivity coatings. Since this device would be placed inside the cavity, the device must have very low loss. For a $CO_2$ laser about 50 cm long, the cavity loss must be less than about 5 percent for oscillation to occur. Losses can occur in the Fabry-Perot etalon primarily from two sources, absorption and reflectivity mismatch between surfaces. The transmission characteristics as a function of these variables are given as

$$\tau = \frac{(1 - a)\, T^2}{[1 - (1 - a)R]^2} \qquad \text{(transmission with absorption)}$$

and

$$\tau = \frac{T_1 T_2}{(1 - \sqrt{R_1 R_2})^2} \qquad \text{(transmission with reflectivity mismatch)}$$

For materials with no absorption ($a = 0$) and for exactly equal reflectivities $R_1 = R_2$ and $T_1 = T_2$, $\tau = 1.0$.

Generally, coating procedures will not allow reproducibility of reflectivities closer than about $\pm 1$ percent. $T_1$ and $T_2$ (therefore $R_1$ and $R_2$) can be as much as 2 percent different. Even with no absorption, the maximum $\tau$ for a mismatch in reflectivities of 2 percent at a reflectivity of about 82 percent would be about 99.5 percent.

6.2.4 (Continued)

The reduction in peak transmission due to absorption can only be estimated since accurate information on the absorption coefficient in Germanium at 10 $\mu$m is not available. Measurements which have been made[20,21] indicate that the absorption coefficient is "negligible" to 11 $\mu$m after which some structure starts to appear. Measurements in the near infrared indicate that the absorption coefficient will be less than $10^{-1}$/cm beyond 2 $\mu$m. As an estimate then, choose a very pure Germanium sample with an optical thickness of 3.0 mm (physical thickness of 3/4 mm) possessing an absorption coefficient of $10^{-1}$/cm. The total single pass absorption would then be $(1 - e^{-.075/10}) = 0.75$ percent. The peak transmission of the etalon calculates to be $\tau = 86$ percent. Although this value is too low to be of use, it must be remembered that it is derived from a pessimistic absorption number. To get $\tau$'s on the order of 95 percent, one would need materials exhibiting a total single pass absorption of less than 0.2 percent. High purity Germanium with the necessary dielectric films may indeed have absorption values of this order or better, making this technique feasible; but better measurements on the materials will have to be made.

Although there is no fundamental reason why other materials could not also be used for the etalon, the use of Germanium offers several attractive features. It is a good material to work to optical tolerances and its optical coefficient of thermal expansion (see Section 7.2) is almost an order of magnitude lower than the ionic salts.

6.2.5 Search and Acquisition Techniques

Since the choice of wavelength emitted from a $CO_2$ laser not containing a specific wavelength selection device is rather a random process, depending on which photons start the laser action, a technique which essentially turns the laser on and off until the desired output wavelength is obtained could be used. A non-critically constructed prism or grating could be placed outside the laser cavity to disperse a portion of the laser radiation on a detector. The prism or grating would be aligned with the detector in such a way as to allow the detector to "see" only the desired wavelength. If no energy fell on the detector after the laser was turned on, a feedback circuit would turn off the laser excitation power and automatically turn it back on again after a specific relaxation period had passed. The laser could be switched on and off until it emitted at the correct wavelength.

The fundamental rate at which this procedure of random searching could occur is limited by the relaxation time of the $CO_2$ laser transitions. Experiments on Q-switched $CO_2$ lasers indicate that the $CO_2$ gas would relax to its non-excited equilibrium state within a few milliseconds after the excitation was removed. This time constant would be much

6.2.5 (Continued)

lower than the breakdown time of the laser gas when the laser is excited by most normal power sources, so that the switching rate would be limited by practical rather than fundamental reasons. It is expected that the desired laser wavelength could be found in only a few seconds after initial turn-on.

The big advantage to this scheme is that no intra-cavity devices need be used to wavelength select. The detector would be the same as that used in the stabilization scheme.

## 6.3 HIGHER ORDER TRANSVERSE MODE SUPPRESSION TECHNIQUES

For the case of the $CO_2$ laser, the gain of the laser transition is nearly independent of tube diameter, indicating the desirability of going to as large a diameter as possible as long as the mode volume can be utilized. Unfortunately, the diffraction losses for the higher-order modes go down as the tube diameter is increased so that the laser tends to oscillate in many high-order transverse modes. To fabricate a relatively short, stabilized tube and still maintain high output power, special techniques in cavity design need to be developed to utilize the large diameter characteristics of the $CO_2$ laser.

There are several techniques for suppressing unwanted transverse modes. These modes can exist in a laser even when its length is such as to allow only one longitudinal mode as in the case of the $CO_2$ laser. In almost all cases, however, the basic mechanism is to obtain differential loss between the $TEM_{oo}$ mode and higher order modes by diffraction. In the case of a laser, the lowest order mode has a near Gaussian cross-sectional intensity distribution within the laser tube, i.e., with energy concentrated near the center of the tube. The higher order modes progressively have more energy concentrated further from the center of the tube and are correspondingly affected more by the presence of the tube walls or the size of the mirrors or whatever the limiting aperture of the laser cavity happens to be.

It is possible to compute the losses incurred by each cavity mode for a particular choice of mirror curvatures and separation, tube diameters, and losses due to mirror transparency, absorption, and scattering. By choosing a mirror system so that the losses for all modes higher than $TEM_{oo}$ are slightly greater than the laser gain, then only the lowest order transverse mode will oscillate. It is therefore desirable to choose a cavity configuration that will provide as much discrimination in loss as possible between the first and second order modes of a cavity. If the second-order oscillation is quenched, then all other higher order oscillations will also be quenched. The following sections discuss several techniques for suppressing the higher-order modes.

### 6.3.1 Aperturing

Li[22] has calculated the losses for the first and second order transverse modes for several symmetric mirror configurations. His results clearly indicate that the best loss discrimination can be obtained by choosing a confocal cavity. However, to obtain this high discrimination ratio, a confocal cavity requires a Fresnel number, N , in the range of 1/2 to 1. The Fresnel number is given by

$$N = \frac{a^2}{\ell\lambda}$$

where 2a is the limiting aperture diameter, $\ell$ is the mirror separation, and $\lambda$ is the laser operating wavelength.

For reasonably short cavities (say, 1/2 meter) and a wavelength of 10 $\mu$m ($10^{-3}$ cm), the diameter of the tube would be limited to about $3.5 \times 10^{-3}$ m (3.5 mm). Unfortunately, this small diameter does not take good advantage of the nearly diameter independent gain characteristic of the $CO_2$ laser. By going to large radius mirrors, the tube diameter can be increased, but at the expense of a corresponding reduction in the large differential diffraction loss between the $TEM_{oo}$ mode and higher order modes.

Another technique that provides a good mode loss discrimination ratio is the half-symmetric geometry. It is obtained by constructing a cavity with a flat mirror at one end and a concave mirror at the other end. The radius of curvature of the concave mirror is approximately equal to twice the mirror separation. In this case, the discrimination ratios are about the same as the confocal case but for Fresnel numbers of about a factor of two higher. The diameter of the tube may then be about a factor of $\sqrt{2}$ larger than for the confocal geometry or about $5 \times 10^{-3}$ m (5 mm) in diameter. This tube size is still rather small, limiting the maximum output power of the laser.

### 6.3.2 "Cats Eye" Optical System

Another approach that can provide much larger tube diameters with good discrimination ratios was described by Li and Smith[23], in which a lens is used within the cavity to provide an increase in mode volume. Figure 6-4 demonstrates their system, which was used with an He-Ne laser operating at 0.6328 $\mu$m.

6.3.2 (Continued)

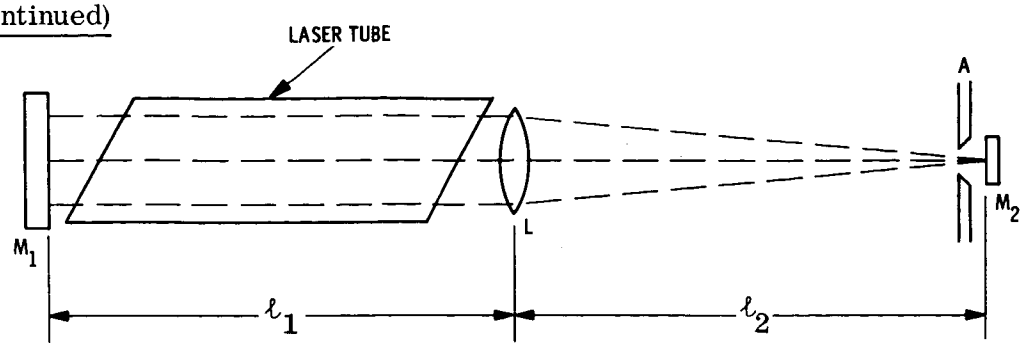


Figure 6-4. Mode Volume Enhancement Using an Internal Lens

$M_1$ is a semitransparent flat mirror, $M_2$ is a totally reflecting flat apertured by A, and L is a very high quality lens of focal length f. It has been shown that the region of stability of this laser lies in the region

$$0 \leq \left[1 - \left(\frac{\ell_1}{f}\right)\right] \qquad \left[1 - \left(\frac{\ell_2}{f}\right)\right] \leq 1$$

and when $\ell_1 = \ell_2 = \ell = f$ the system is in an equivalent confocal geometry. For this case, the optical beam is practically parallel inside the laser tube and will fill the entire laser tube volume if not vignetted by $M_1$ or L . When the aperture A is open the system runs multimode and has alignment characteristics of the confocal resonator. As A is closed, the mode pattern becomes simpler until single-mode operation is attained. Alignment of $M_1$ is then critical.

The equations for the single mode beam spot sizes are given by

$$\omega_1 = \sqrt{\left(\frac{a_1}{a_2}\right)\left(\frac{\lambda\ell}{\pi}\right)} \quad \text{and} \quad \omega_2 = \sqrt{\left(\frac{a_2}{a_1}\right)\left(\frac{\lambda\ell}{\pi}\right)}$$

where

$a_1$ is the effective radius of $M_1$

$a_2$ is the effective radius of $M_2$

$\ell = \ell_1 = \ell_2 = f$ and

$\lambda$ is the laser wavelength.

$\omega_1$ and $\omega_2$ are the radii of the 1/e points of the beam intensity on each mirror.

6.3.2 (Continued)

The effective Fresnel number for this configuration is $N_{eff} = \frac{a_1 a_2}{\ell\lambda}$ which must be chosen properly to provide sufficient diffraction losses to keep the higher order modes from oscillating.

To approximate the maximum tube diameter that could be used in this mirror configuration with a distance between $M_1$, $M_2$ and L of one-half meter, one needs to know the gain of the laser transition to choose the proper value of the Fresnel number. Because this information is not accurately established at the present time, a Fresnel number of 1/2 will again be assumed. This value will provide a pessimistic value of the tube diameter. Choosing N = 1/2,

$$a_1 a_2 = N_{eff}\ell\lambda = 1/2 \times (1/2\ m)\ (10^{-5}\ m) = 2.5 \times 10^{-6}\ m^2$$

Choosing $a_2$, the aperture radius, as some small but reasonable radius such as $0.5 \times 10^{-3}$ m (.5 mm), $a_1$ can then be calculated to be

$$a_1 = 1/2 \times 10^{-2}\ m\ (1/2\ cm)$$

or the tube diameter, 2a, can be about 1 cm. Since this represents a pessimistic number, the use of a tube diameter greater than a factor of two larger is allowed over conventional means discussed earlier. Reducing the small aperture diameter $(2a_1)$ allows even greater increases in tube diameter.

One obvious difficulty with this type of system is that the required length of the laser is about twice the length of the active laser tube. It is conceivable that the system could be folded by replacing the lens L by a converging mirror and bringing the focused beam back to an aperture and mirror at the other end of the tube. In either case this system would be limited to lower-power $CO_2$ lasers so that the power density could be kept below the damage level at the focused point.

6.3.3 Transverse Mode Control in the $CO_2$ Laser by Choice of Mirror Curvature

It is well known that the laser oscillation frequencies in the longitudinal mode are separated by the $c/2\ell$ spacing of the laser mirrors. The general expression[24] which takes into account the oscillation frequencies of the transverse modes is given by

6.3.3 (Continued)

$$\nu = \frac{c}{2\ell} [q + (1 + m + n)\ f] \tag{6.1a}$$

where

$$f = \pi^{-1} \cos^{-1} \left[(1 - \frac{\ell}{b_1})\ (1 - \frac{\ell}{b_2})\right]^{1/2} \tag{6.1b}$$

$b_1$ and $b_2$ are the radii of curvature of the two laser mirrors separated by a distance $\ell$. The transverse mode numbers m and n can take on values 0, 1, 2, ... The longitudinal number q is equal to the number of half wavelengths in the distance d. The modes are labeled $TEM_{qmn}$. For each value of $m + n$, there is a set of frequencies with a common separation $\nu_0 = c/2\ell$, corresponding to $\Delta q = 1$. Such a set can be called a transverse mode set. The frequency difference between mode sets is given by the second term of the above equation:

$$\delta\nu_{\Delta(m+n)} = (\frac{c}{2\ell}) f\, \Delta (m + n) \tag{6.2}$$

The factor f can vary between zero and 1/2 if the values of $\ell$, $b_1$ and $b_2$ remain within the boundaries of the stable regions given by

$$0 \leq (\frac{\ell}{b_1} - 1)\ (\frac{\ell}{b_2} - 1) \leq 1 \tag{6.3}$$

For the case of the $CO_2$ laser, selection of mirror curvatures can move the required oscillation frequencies outside the Doppler line for almost all but one transverse mode.

By choosing the frequency difference between mode sets equal to the Doppler linewidth, oscillation on only one set at a time can occur. Setting the requirement of $\delta\nu_{\Delta(m+n)} = 50$ MHz (the Doppler width at half height for $CO_2$), the restrictions on f and, therefore, the mirror radii can be computed.

6.3.3 (Continued)

Using Equation (6.3), the lower limit of f can be computed by choosing $\Delta(m + n) = 1$

$$\delta\nu_{\Delta(m+n)} = 50 \text{ MHz} = \left(\frac{c}{2\ell}\right) f_{min}$$

and

$$f > \frac{50 \text{ MHz}}{\left(\frac{c}{2\ell}\right)}$$

This value of f is plotted in Figure 6-5 for several cavity lengths.

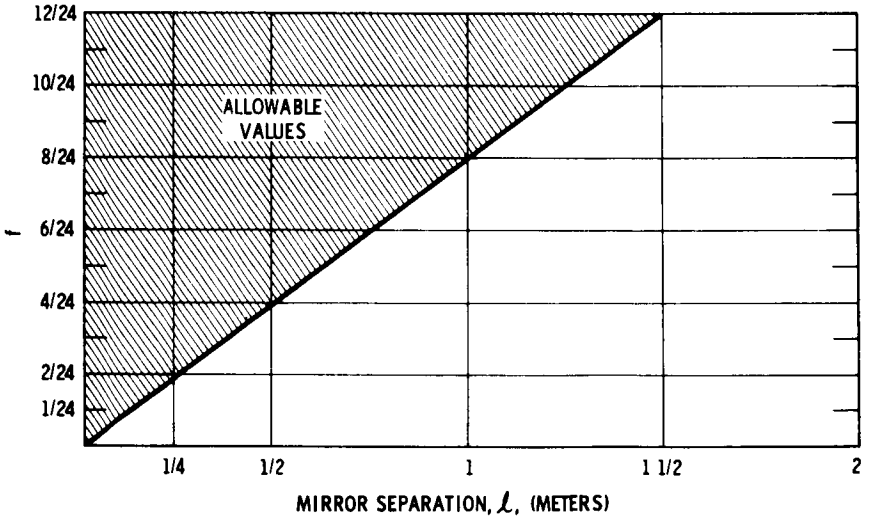


Figure 6-5. Allowable Values of f for Single Transverse Mode Operation in a $CO_2$ Laser

For greatest mode discrimination, it would be desirable to operate as close to the minimum value of f as possible. If the laser is operating on the $TEM_{oo}$ mode, there exists a combination of frequencies for each successive higher order mode separated from each other by a frequency determined by f. For example, if the laser cavity were chosen as 1/2 meter long then the $\frac{c}{2\ell}$ spacing would be 300 MHz. With the frequency separation between the higher order modes being 50 MHz, overlap of frequencies would occur after the sixth highest mode was reached. That is, the lowest order mode would oscillate as well as the 7th order mode and 13th order mode, etc. A slight amount of diffraction loss would be required to ensure that these very high order modes would not also oscillate.

6.3.3 (Continued)

For laser tubes longer than about 1-1/2 meters, multiple transverse mode operation is allowable for any mirror curvature unless other techniques, such as diffraction loss control, are used to inhibit multiple modes.

The above results indicate that a hemispherical, confocal, or relatively "fast" optical cavity should be effective in discriminating against unwanted modes. However, this technique does not allow choice of a particular transverse mode in that any mode whose frequency lies under the Doppler curve is free to oscillate. The exact spacing of the cavity mirrors could be controlled so as to choose the proper frequency.

The main disadvantage to this technique seems to be the small optical mode volume resulting from the requirement of relatively "fast" optical systems.

As an example, consider a 1/2 meter cavity with mirrors of equal radius of curvature ($b_1 = b_2 = b$). From the graph $f = 1/6$ and using equation (6.1b), the value of $b$ is calculated to be

$$b \approx 3.7 \text{ meters} .$$

That is, if the curvature of the mirrors is kept at about this value, and a small amount of diffraction loss is imposed on the higher order modes, then the laser can only operate on one transverse mode. For this length of laser, only one longitudinal mode can exist; therefore, the laser must operate single frequency.

The relatively fast optical system above results in a fairly small mode volume inside the laser tube which tends to limit the output power. In the above example, the mode radius at the 1/e power points ($\omega$) can be calculated from cavity resonator theory. The pertinent equation is

$$\omega^4 = \left(\frac{\lambda}{\pi}\right)^2 \frac{b^2 \ell}{2b - \ell} \qquad (6.4)$$

$$\omega = 1.7 \text{ mm}$$

The maximum active tube diameter would then be $\sim 4\omega$ or about 6.8 mm. Although this value is somewhat larger than seen in previous sections, the technique described in the following section allows about a factor of two improvement over this figure.

### 6.3.4 Diffraction Coupled Output Mirrors

As mentioned earlier, the practical techniques generally used to prevent the higher order TEM modes from oscillating in gas lasers usually involve aperturing of the internal laser beam, usually by the laser tube walls. Although quite effective, this technique always imposes rather large losses on the lowest order mode, substantially reducing the power output capability of the laser. This technique is especially lossy for high gain devices where large losses must be imposed to prevent higher order modes from oscillating.

The technique described below converts the energy which would ordinarily be lost internally to useful laser output, thus increasing the total output power capabilities of the laser.

For the case of the $CO_2$ laser, the value of the tube diameter is not an important parameter in the optimum gain of the tube and can be made large enough to have no effect on the field distribution within the laser. By making an output mirror with a small, 100 percent reflecting spot deposited on a transparent window, the laser output can be taken from around the spot. The size of the spot would be chosen to provide the correct amount of feedback to the laser cavity. Since the mode diameters of progressively higher order modes are increasing, thus moving their power densities to larger diameters, the higher order modes will not oscillate due to the large loss around the output mirror. The mirror size is chosen to keep all but the lowest order mode from oscillating. Then all of the power in the lowest order mode which would normally have been wasted in diffraction losses is converted to useful output.

In general, this technique of diffraction coupled output mirrors can provide the greatest single mode power output of any coupling scheme. Power enhancements in high gain lasers by a factor of 10 have been observed over conventional techniques[25]. Also, by making the mirrors with a large radius of curvature, the mode volume can be made large while still maintaining good mode discrimination. It is expected that total lowest order mode sizes inside the laser tube can be made about 12 mm in diameter using this technique on a 50 cm long tube.

Because of the blocking of the central part of the beam with the mirror spot, a near field beam pattern will have a donut shape to it. The donut ring will radiate by diffraction losses characteristic of its annular width and a bright spot will periodically appear in the center of the donut as one moves away from the laser. This alternating center intensity effect disappears when one passes into the far field region of the beam and one notices a

6.3.4 (Continued)

Fraunhoffer diffraction pattern characteristic of an annular disc. The diffraction pattern from this type of output coupler is similar to that from the standard transparent mirror coupler where the diffraction pattern is determined by the diameter of the output beam, except that slightly more power is thrown into higher order rings around the central maximum*.

Experimental studies on this type of mode discrimination will be studied during the next phase, utilizing some stable lasers being constructed on the Sylvania Independent Research and Development program.

## 6.4 SUMMARY

One of the requirements imposed on the laser is that it be capable of being heterodyned with another similar laser. This immediately puts a strong requirement on the wavelength and mode characteristics of the laser. That is, the output wavelengths of the two lasers must be identical, and they should be operating on the lowest order mode. Since the $CO_2$ laser normally will run on one of several wavelengths, special precautions must be taken to control the operating wavelength.

None of the techniques for wavelength control discussed in the previous sections has a clear cut advantage over the others in that there are some disadvantages with all techniques, even though all of them can be made to work. The search and acquisition approach may be the best in the long run primarily since no internal cavity device is needed. Some wavelength selection is automatically achieved by the basic cavity itself, easing the requirements on all of the other techniques. It should be possible to experimentally determine the capabilities of the various internal cavity schemes, such as prism selection and the novel frequency-selective etalon technique, without much difficulty once a suitable laser is available.

The preferred mode control technique is the approach utilizing a diffraction-coupled output mirror. This technique allows good mode control while still allowing large mode volumes and higher output power. It seems well suited to the high-gain $CO_2$ laser.

*See Born and Wolf, Principles of Optics (MacMillan Co., New York, 1964), p. 417.

Section 7

# LASER TUBE DESIGN AND EXCITATION TECHNIQUES

## 7.1 INTRODUCTION

The operation and construction of the $CO_2$ laser tube is uniquely different in several respects from the laser tubes which have been constructed for use in the visible portion of the spectrum. It is the purpose of this section to outline the major differences and indicate some of the preferred approaches to the design of a suitable laser tube for the purpose of this contract. Most of the information here has been gathered either from the literature on $CO_2$ lasers (see Appendix B) or from the Sylvania Independent Research and Development program on $CO_2$ lasers.

## 7.2 EXCITATION TECHNIQUES

As with other types of gas lasers, the $CO_2$ laser can be excited by an electrical discharge in the active laser region. Early experiments, however, were performed by exciting the gas in a separate tube and then pumping the gas into the optical cavity where lasing could occur. This technique was used primarily for the expediency of the experiment, and it was soon discovered that a simpler, more direct excitation scheme was possible in $CO_2$. All of the usual schemes (A. C., D. C., R. F.) of excitation have been attempted with nearly equal lasing efficiency (power dissipated in the tube vs. laser output power) for similar geometries. The overall efficiency of the A. C. or D. C. systems seems to be somewhat higher than the R. F. systems due to a higher overall conversion efficiency of prime power to gas discharge power. Tube efficiencies on the order of 13-15 percent have been observed[9] for long, high power tubes. However, shorter tubes show much lower efficiencies due to the nonlinear drop in output power as the tube is made shorter.

The advantages of the various excitation schemes are relatively straightforward. The A. C. scheme offers a big advantage in its simplicity. Readily available neon sign transformers have about the right voltage-current capabilities to drive the $CO_2$ laser. If longer, higher power tubes are desired, more transformers can be added in sections along the tube. For a pure, stable laser, the A. C. technique cannot be used since the output is 100 percent modulated at 120 cps.

7.2 (Continued)

The D. C. excitation approach, as well as the A. C., utilizes internal electrodes. In general, hot cathodes cannot be used in the laser because of cathode contamination due to the $CO_2$ gas. Usually cold cathodes are used. Inevitably, the presence of cold metal electrodes inside the laser results in some electrode sputtering when the tube is operating. The electrodes then act as an ion pump, pumping the laser tube gases by adsorption and chemical reaction. Although the rate can be reduced to fairly low values by proper electrode design, it is always present and appears to be the limiting factor in the active lifetime of the laser tube. Within periods of only several hundred operating hours, the pressure inside the tube is reduced below the required lasing level and the tube needs refilling.

With R. F. excited tubes, the sputtering problem is eliminated since the R. F. is introduced into the laser tube through the glass walls of the tube. Therefore, no metal parts whatsoever need be placed within the tube. Thus, R. F. excitation should extend the life of the tubes considerably. The disadvantage with R. F. excitation is its slightly lower efficiency and incompatibility with most liquid cooling systems. As pointed out in Section 2, the laser wall temperature has a marked effect on the output power of the laser. By keeping the tube walls cooled, the power output can be greatly enhanced — often by at least a factor of 2. Studies on the difficulties of utilizing R. F. excitation in the presence of cooling fluids with high dielectric constants such as water and techniques for solving these difficulties are major portions of the Sylvania Independent Research and Development program.

For the present program, it is expected that R. F. excitation would be most desirable not only for the lifetime considerations but also from a plasma noise viewpoint. There are indications[26,27] that schemes involving R. F. excitation provide a "quieter" plasma than other excitation schemes allowing lower system noise in any frequency stabilization scheme. However, the problems associated with R. F. pickup in the stabilization circuitry will have to be eliminated for the R. F. excitation approach to be of any significant advantage in this area.

## 7.3 BREWSTER ANGLE TUBES

As with conventional lasers, the $CO_2$ laser can be constructed with Brewster angle windows terminating the tube, providing a polarized laser output. The power output from these tubes can be made comparable to tubes with internal mirrors and allows inter-cavity experimentation.

7.3 (Continued)

The desired characteristics of the material used as Brewster angle windows are:

a. Negligible absorption and scattering loss in the thickness required (a few mm) at 10 $\mu$m.

b. High internal homogeneity (Schlieren-free).

c. Relatively low index of refraction (less than 2) so that the Brewster angle will not be too large.

d. Mechanically stable, easily worked to the required optical tolerances.

Unfortunately, none of the available materials possess all of the above qualities, and a compromise choice must be made. Germanium and some of the salts such as NaCl and KCl come the closest in that they do have very low absorptance and scattering at 10 $\mu$m.

However, Germanium has a very high index of refraction (n = 4.0), making the Brewster angle about 76 degrees. For short tubes near 1/2 meter long, approximately 30 percent of the tube is wastefully taken up by the Brewster windows. For longer tubes, the proportion can be much less, but for the present program only short tubes will be considered. The mechanical properties of Germanium are quite good, and it would be preferred from this viewpoint.

Brewster angle windows constructed from NaCl or KCl would be ideal but for their very poor mechanical stability. They are very brittle crystals and crack easily. Also they are hygroscopic and dissolve rapidly in water, and they are very soft and difficult to polish to the required optical tolerances. Even with these difficulties, the salts appear to be the better choice for short tubes. With care and much patience, high quality windows can be generated and with proper packaging techniques, the windows can be kept dry for an indefinite period of time. They offer an additional bonus in that they are transparent in the visible also, which helps in cavity alignment.

The choice between NaCl and KCl is rather arbitrary in that they have almost identical properties as far as 10 $\mu$m absorption, moisture solubility, and optical working characteristics. For the application to the present program, the combination of the coefficient of expansion and the temperature coefficient of refractive index indicates that KCl may be the better choice as demonstrated in the following paragraphs.

7.3 (Continued)

For the high stability lasers, it is important that the optical cavity be thermally compensated so that any change in temperature will result in only a very small or no change in the optical separation of the laser mirrors. The effects of the windows on the optical path can be seen by evaluating the effective optical coefficient of expansion. The optical thickness, $\ell_o$, of the Brewster window can be written as

$$\ell_o = nt/\cos\ \theta$$

where n = index of refraction and t = mechanical thickness, and $\theta$ is the internal beam angle with respect to the window normal.

The change in this thickness with temperature is

$$\frac{d\,\ell_o}{dT} = \frac{1}{\cos\ \theta}\ (n\frac{dt}{dT} + t\frac{dn}{dT})$$

From this an equivalent optical coefficient of expansion can be derived which turns out to be

$$\alpha_{op} = n\alpha_{mech} + \frac{dn}{dT}$$

where $\alpha_{mech}$ is the typical mechanical coefficient of expansion and dn/dT is the temperature coefficient of refractive index. $\alpha_{op}$ is in units of optical thickness/physical thickness/°C.

It is most desirable to choose a material for which $\alpha_{op}$ is the smallest at 10 $\mu$m. The following table compares the values for NaCl and KCl.[28,29]

Table 7-1. Several Properties of NaCl and KCl at 10 $\mu$m

| | $\alpha_{mech}$ | dn/dT | n | $\alpha_{op}$ |
|---|---|---|---|---|
| NaCl | $3.9 \times 10^{-5/°C}$ | $-2.0 \times 10^{-5/°C}$ | 1.49 | $3.8 \times 10^{-5/°C}$ |
| KCl | $3.6 \times 10^{-5/°C}$ | $-2.5 \times 10^{-5/°C}$ | 1.46 | $2.8 \times 10^{-5/°C}$ |

Although not small, the lower $\alpha_{op}$ indicates KCl has a definite advantage.

## 7.4 INTERNAL MIRROR TUBES

The problems associated with Brewster angle tubes can be eliminated by putting the cavity mirrors inside the laser tube vacuum envelope. Because of its simplicity and lower cost, this technique has most certainly been used most often on the $CO_2$ laser. Its only big disadvantage is the inaccessibility to the optical beam between the mirrors and the difficulty of manipulating the mirrors.

For this program, the stability scheme will most certainly require that one or both of the laser mirrors be mounted on piezoelectric stacks which are not manufactured with high vacuum applications in mind. Also, internal mode selecting devices would possibly be required which would be difficult to adjust externally. It is felt that the Brewster angle tube would be more desirable — at least in the earlier stages of the program.

## 7.5 SUMMARY

In general, the optimum design and excitation techniques used on the $CO_2$ laser depend on the particular application and goal. For the purposes here, where high stability and mode control characteristics are the prime objectives, it appears that the laser tube should be designed so that R. F. excitation can be used. Also, the tube should be a Brewster angle tube with special precautions taken in the packaging of the tube to eliminate deterioration of the windows. The best window material for the purposes of this program is potassium chloride.

Section 8

# MECHANICAL STABILIZATION TECHNIQUES

## 8.1 INTRODUCTION

The inherent spectral width of the output from a single frequency $CO_2$ laser is extremely narrow as demonstrated in the following paragraph. In practice, however, it is impossible to achieve this narrow spectral width. Mechanically and acoustically excited vibrations of the laser structure and mirrors considerably broaden the spectral width, and thermal changes cause the mean frequency to drift. The mechanical design of the laser structure, therefore becomes very important for a high stability laser, especially in the areas of acoustical isolation shielding and thermal control.

The fundamental reason that the output from a laser has a finite inherent spectral width rather than a pure sine wave is due to the random nature of the internal processes in the laser. The expected value of the inherent spectral width has been derived by a number of investigators using several methods. The result has been about the same in all cases. Siegman[30] has given a particularly complete analysis which shows the inherent spectral width to be:

$$\Delta f_{osc} = \frac{\pi h f \Delta f^2}{P_{osc}}$$

where h is Planck's constant, f is the oscillating frequency, $P_{osc}$ is the output power from the laser, and $\Delta f$ is the width of the cavity resonances without the gain of the laser material.

Given the cavity length L and the average loss per pass $\ell$, $\Delta f$ may be calculated by

$$\Delta f = \frac{C}{2L} \frac{\ell}{\pi}$$

Assuming, for the case of a highly stabilized $CO_2$ laser, that the cavity length is 50 cm, the average loss per pass is 30 percent, and the output power is 1 watt, the inherent spectral width is

$$\Delta f_{osc} = 5 \times 10^{-5} \text{ Hz}$$

8.1 (Continued)

or

$$\left(\frac{\Delta f}{f}\right)_{osc} = 1.7 \times 10^{-18}$$

## 8.2 VIBRATION EFFECTS

What happens in practice is that the single-frequency output with this narrow spectral width wanders in frequency due to relative optical position changes of the laser mirrors. When spectral width is measured in an experiment, these wanderings of the output frequency are averaged by the measuring instrument. The spectral width measured is a function of the amplitude and frequency spectrum of the mirror vibrations and the averaging time constant of the measuring instrument.

A lower limit for the magnitude of the frequency wandering can be predicted. Assuming no transverse vibrations of the elements of the structure supporting the laser mirrors, the spectral width due to thermal excitation of the lowest frequency longitudinal mode of the structure may be calculated. Siegman[31] has performed the calculation with the result

$$\left(\frac{\Delta f}{f}\right)_{\substack{\text{thermal}\\\text{vibration}}} = \left(\frac{kT}{2YV}\right)^{1/2}$$

where k is Boltzman's constant, T is the absolute temperature, Y is Young's modulus of elasticity and V is the volume of the supporting structure.

Assuming for a typical high stability $CO_2$ laser that V = 1700 $cm^3$ and the material is invar,

$$\left(\frac{\Delta f}{f}\right)_{\substack{\text{thermal}\\\text{vibration}}} = 3 \times 10^{-15}$$

or

$$\Delta f_{\substack{\text{thermal}\\\text{vibration}}} = 8.4 \times 10^{-2} \text{ Hz}$$

If acoustical and mechanical vibration inputs to the structure have significant power at longitudinal mode frequencies of the structure, the magnitude of the wandering of the laser frequency will be increased further. In addition, real laser structures may have elements with beam-like or plate-like geometries. Beams and plates have transverse vibration

8.2 (Continued)

modes which may occur at quite low frequencies. Also, the joints between elements may have low-frequency modes. If any of these additional vibration modes occur at frequencies included in the power spectra of the acoustical and mechanical vibration inputs, the frequency wandering of the laser will be even further increased.

There is little specific data available on $CO_2$ lasers, but the same acoustic and vibration noise problems have been measured for other lasers. A significant amount of data on spectral width has been reported for helium-neon lasers, and this data gives an indication of what can be achieved under various conditions with various designs.

Javan and Jaseja et al [32, 33, 34] have reported measurements of the spectral width of their helium-neon lasers in a series of experiments conducted in quiet to extremely quiet conditions. In the first report of the experiments[32] in January 1962, the oscillation frequency was reported to be taking place over an extremely narrow spectral width measured to be better than 1 part in $10^{14}$. This narrow frequency wandered by about 100 KHz due to microphonic or vibration effects.

In a second report on the continuing experiments[33] in November 1962 the wandering due to vibrations was reported to be less than 100 Hz. Finally, in March 1963 the spectral width due to vibrations was reported to be 20 Hz. This was only an order of magnitude larger than the value they calculated for the thermal vibration limit of their laser.

Bennett[35] reports that E.A. Ballik achieved a spectral width measurement of less than 0.5 Hz in a similar experiment. Data on the laser is not given, but this is probably close to the thermal vibration limit. Table 8-1 shows the results of these experiments.

Table 8-1. Summary of Experiments With 1.15 Micron HE-NE Laser In Quiet Surroundings

| Experimenter | $\left(\frac{\Delta f}{f}\right)_{vibration}$ | Reference |
|---|---|---|
| Javan et al | $3.8 \times 10^{-10}$ | 32 |
| Jaseja et al | $3.8 \times 10^{-13}$ | 33 |
| Jaseja et al | $7.7 \times 10^{-14}$ | 34 |
| Ballik | $1.9 \times 10^{-15}$ | 35 |

This group of experiments was conducted with moderately rugged lasers in experimental laboratories with extremely careful acoustic noise and vibration control. The experiments

8.2 (Continued)

show that isolation of the laser structure from sources of vibration excitation is an effective way of reducing the wandering of the output frequency from a laser.

Other investigators have made spectral width measurements in more usual laboratory environments and in field environments. Baird, et al[36] measured the spectral width for the beat between two of their own single frequency lasers as 10 MHz. They reported[37] similar measurements on another pair of single-frequency lasers as 200 kHz.

At the Sylvania laboratory several measurements have been made between pairs of commercial Spectra-Physics Model 119 single-frequency 6328A° lasers. Targ[38] has measured the beat width under standard laboratory conditions as 100 kHz. Kerr[39] measured the beat width as 10 kHz under good laboratory conditions and 200 kHz under field conditions with the lasers separated by 300 feet and with an automatic frequency control loop (AFC) feeding back to the internal piezoelectric length adjusting transducer in one laser. This AFC loop maintained the average offset frequency between the lasers.

Table 8-2 summarizes the results for single-frequency 6328A° helium-neon lasers. The data has been put into a standard from and adjusted to apply to a single laser by assuming the beat width is the square root of the sum of the squares of the two identical laser widths.

Table 8-2. Summary of Experiments With Single-Frequency 6328A° HE-NE Lasers

| Experimenter | $\left(\frac{\Delta f}{f}\right)_{vibration}$ | Conditions | Reference |
|---|---|---|---|
| Baird et al | $1.5 \times 10^{-8}$ | Exp. laser in lab | 36 |
| Baird et al | $3 \times 10^{-10}$ | Exp. laser in lab | 37 |
| Targ | $1.5 \times 10^{-10}$ | #119 in Stand. lab | 38 |
| Kerr | $1.5 \times 10^{-11}$ | #119 in Best lab | 39 |
| Kerr | $3 \times 10^{-10}$ | #119 in Field | 39 |

After considering the experimental results summarized in Tables I and II we come to the following conclusions concerning a $CO_2$ laser structure for frequency stability greater than 1 part in $10^{10}$:

1. The laser must be at least as insensitive to vibrational excitation as the commercial Spectra-Physics Model 119 single-frequency He-Ne laser and should be better.

8.2 (Continued)

2. Sophisticated acoustical and mechanical vibration isolation must be provided for the laser structure.

## 8.3 THERMAL EFFECTS

In addition to the wandering of the extremely narrow laser output frequency about some mean value as a result of vibration, the mean frequency will drift due to temperature variations, producing changes in the mechanical and optical lengths in the laser components. This drift must be minimized so that the total optical path variation will stay within the range of a length control servo system. For the stabilities of interest, thermally compensating structures and temperature control must be used. The following paragraphs derive the pertinent equations for thermal analysis.

The cross section of a typical $CO_2$ laser is shown in Figure 8-1. The laser is composed of a mechanical structure of length $L_s$, a thermal compensating element of length $L_c$, two laser mirrors, and a laser tube containing two Brewster angle windows of thickness W. The Brewster angle windows make an angle, $\phi$, with respect to the axis.

A light ray from one laser mirror to the other goes through an air path of length $L_a$, through one Brewster angle window, through the length of the laser tube, through the other window, through another air path $L_a$, and arrives at the other laser mirror.

Using subscripts a for air, w for Brewster angle windows, $\ell$ for inside the laser tube, c for the compensating element, and s for the structure, we may derive an equation for the optical path between the laser mirrors in terms of the mechanical and optical constants of the individual elements.

Let L equal the optical path between the two mirrors, and let n be the index of refractions. Then

$$L = 2n_a L_a + 2n_w L_w + n_\ell L_\ell \tag{8-1}$$

Now

$$n_w L_w = \frac{n_w W}{\cos \phi} \tag{8-2}$$

and

$$L_a = \frac{1}{2} (L_s - L_c - L_\ell - 4W \sin \phi) \tag{8-3}$$

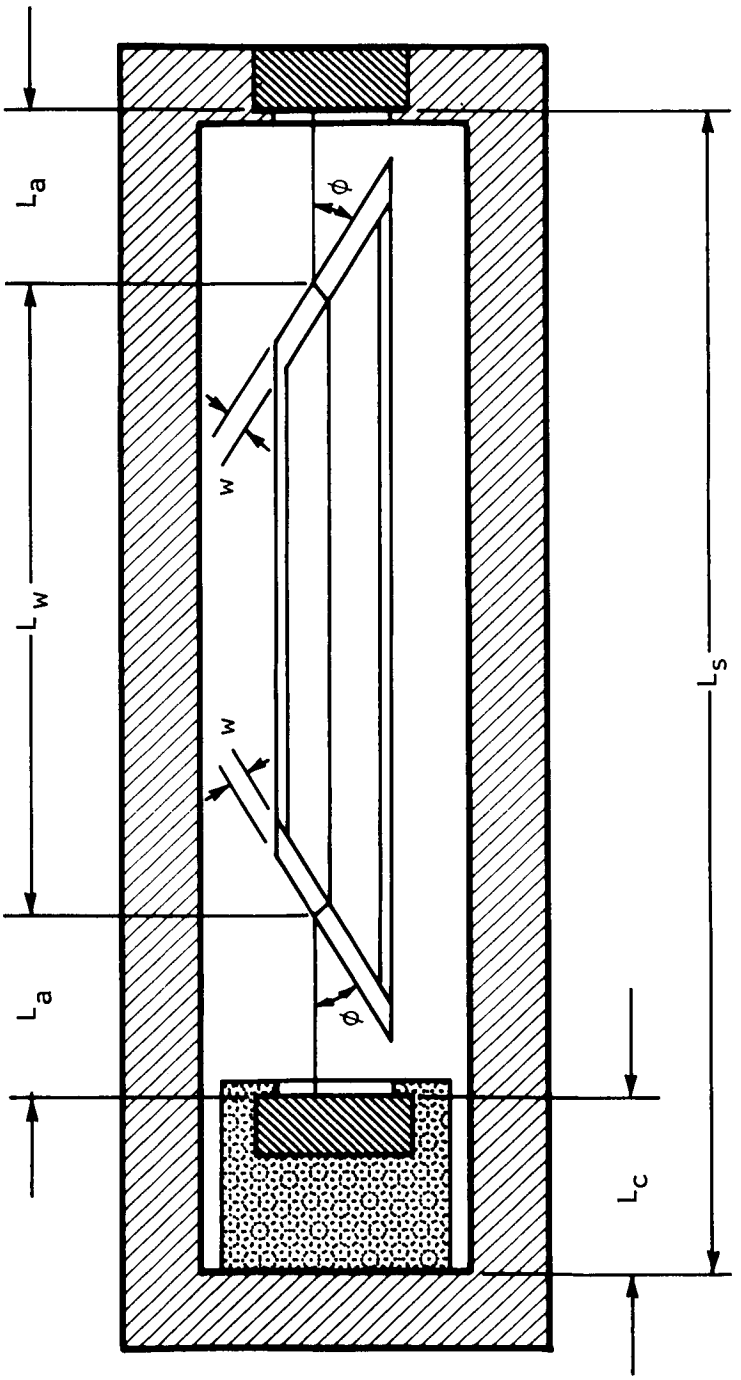


Figure 8-1. Typical $CO_2$ Laser with Brewster's Angle Tube and Thermal Compensating Element

8.3 (Continued)

Therefore,

$$L = n_a (L_s - L_c - L_\ell - 4w \sin \phi) + \frac{2n_w W}{\cos \phi} + n_\ell L_\ell \tag{8-4}$$

We are interested in the variations in L with respect to the temperature, T. Taking the derivative of L with respect to T we get

$$\frac{dL}{dT} = n_a \left( \frac{\partial L_s}{\partial T} - \frac{\partial L_c}{\partial T} \right) + (L_s - L_c - L_\ell - 4W \sin \phi) \frac{\partial n_a}{\partial T}$$
$$+ \frac{2W}{\cos \phi} \frac{\partial n_w}{\partial T} + \left( \frac{2n_w}{\cos \phi} - 4n_a \sin \phi \right) \frac{\partial W}{\partial T}$$
$$+ (n_\ell - n_a) \frac{\partial L_\ell}{\partial T} + L_\ell \frac{\partial n_\ell}{\partial T} \tag{8-5}$$

Now the coefficient of thermal expansion $\alpha$ is defined by

$$\alpha_i = \frac{1}{L_i} \frac{\partial L_i}{\partial T} \tag{8-6}$$

and Equation (8-5) can be written

$$\frac{dL}{dT} = n_a (L_s \alpha_s - L_c \alpha_c) + 2L_a \frac{\partial n_a}{\partial T} + \frac{2W}{\cos \phi} \frac{\partial n_w}{\partial T}$$
$$+ \left( \frac{2n_w}{\cos \phi} - 4n_a \sin \phi \right) W \alpha_w$$
$$+ (n_\ell - n_a) L_\ell \alpha_\ell + L_\ell \frac{\partial n_\ell}{\partial T} \tag{8-7}$$

The next to last term is negligible since $n_\ell$ and $n_a$ are both very close to 1, and the last term is negligible because the gas in the laser tube is at low pressure and hence $n_\ell$ is exceedingly close to 1. Therefore, $\partial n_\ell / \partial T$ is negligible.

8.3 (Continued)

So finally to first order

$$\frac{dL}{dT} = n_a(L_s\alpha_s - L_c\alpha_c) + 2L_a \frac{\partial n_a}{\partial T} + W \left[\frac{2}{\cos \phi} \frac{\partial n_w}{\partial T} + \left(\frac{2n_w}{\cos \phi} - 4n_a \sin \phi\right) \alpha_w\right] \quad (8\text{-}8)$$

Now frequency stability is related to length stability by

$$\frac{\Delta f}{f} = - \frac{\Delta L}{L} \quad (8\text{-}9)$$

Therefore, the change in frequency stability due to a temperature change $\Delta T$ is given by

$$\frac{\partial \left(\frac{\Delta f}{f}\right)}{\partial T} \Delta T = \frac{\partial \left(-\frac{\Delta L}{L}\right)}{\partial T} \Delta T$$

$$= -\frac{1}{L} \{ n_a (L_s\alpha_s\Delta T_s - L_c\alpha_c\Delta T_c) + 2L_a \frac{\partial n_a}{\partial T} \Delta T_a + W \left[\frac{2}{\cos \phi} \frac{\partial n_w}{\partial T} \left(\frac{2n_w}{\cos \phi} - 4n_a \sin \phi\right)\alpha_w\right] \Delta T_w \} \quad (8\text{-}10)$$

The first term represents the effect of the structure and compensating element; the second term represents the effect of the air path; and the third term represents the effect of the Brewster angle windows.

An obvious method of preventing thermally induced frequency changes is to maintain the temperature constant so that $\Delta T_s$, $\Delta T_c$, $\Delta T_a$, and $\Delta T_w$ are all zero. Then each term in the expression is identically zero. Another approach would be to have the terms cancel each other by some means so that they collectively equalled zero, or a combination of having some terms cancel and others individually equal zero could be used. Design approaches to achieve thermal stability will be discussed below in Section 8.4.

## 8.4 VIBRATION CONTROL

### 8.4.1 Structural Stability Requirements

In order for a structure to be stable against vibration, it is necessary that the mechanical resonances of the structure not be at frequencies within the main power spectrum of acoustical and mechanical vibration noise inputs.

Acoustical noise and mechanical vibration noise are actually identical quantities, but we will define them as two separate noise sources. Acoustic noise will be defined as noise energy transferred as sound waves through the air, and mechanical vibration noise will be defined as noise transferred through the structural mounting.

The main power spectrum of both acoustic and mechanical vibration noise is at low frequencies. The peak of the acoustic spectrum usually occurs at less than 500 Hz. In both types of noise, however, there will be occasional shocks with frequency components of up to perhaps 30 kHz. The fact that most of the noise power spectrum for vibrational excitation occurs at low frequencies, together with the fact that high frequency noise is easier to isolate from a structure than is low frequency noise, dictates that the $CO_2$ laser structure should be designed to make the structural frequency resonances as high as can be achieved.

The frequency of the lowest longitudinal resonance of a laser cavity structure is determined by the cavity length. This frequency is given by the equation

$$f_{L\nu} = \frac{C_s}{2L} \tag{8-11}$$

where $C_s$ is the velocity of sound in the structure, and $L$ is the structure length.

In choosing a length for the $CO_2$ laser, one must make a "trade off" between high longitudinal mode frequency and stiffness against bending distortion on the one hand and high output power on the other. Assuming a structure made of invar for thermal stability reasons, Table 8-3 shows the lowest longitudinal frequency for various cavity lengths.

Table 8-3. Lowest Longitudinal Mode Frequencies In Invar Laser Cavities

| Cavity Length | Frequency |
|---|---|
| 1 m | 2 kHz |
| 50 cm | 4 kHz |
| 20 cm | 11 kHz |
| 10 cm | 21 kHz |

8.4.1 (Continued)

Once a trade off is made and a cavity length is chosen, then a design of the remaining structure must be chosen to keep from lowering the basic first resonance. The individual elements of the structure must be chosen with geometries and methods of support (boundary conditions) such that they do not have low frequency transverse resonances. The first step is to eliminate all simple beam and thin plate elements which have low frequency transverse resonances. This usually leaves complex structures and calculations become increasingly difficult. However, by a combination of calculation, intuition, and experiment, good structural elements maintaining high frequency resonances can be designed.

When the configuration and method of support for the elements of the structure have been determined, the elements should then be redesigned using sandwich construction with visco-elastic adhesives to provide high damping of the high frequency resonances.

The joints between the elements of the structure must then be considered. These joints must be designed so that they do not have any low frequency resonances. Especially critical are the joints perpendicular to the cavity length. One particularly good design for these joints is to use large contact areas under compressional stress. The spring constant of the joint will then be high. Designs with joints using only the spring force of a few screws to connect significant masses must be avoided.

In summary, the structural designer must be extremely careful to provide a laser structure with resonances only at high frequencies. Damping must then be provided for all structural elements to minimize vibrations as much as possible.

8.4.2 Acoustic and Mechanical Vibration Noise Isolation

Once a laser structure with only damped high frequency resonances has been achieved, it is still necessary to provide acoustic and vibration noise isolation in order to achieve one part in $10^{10}$ frequency stability.

The traditional method of achieving such isolation is to mount the laser cavity in a box lined with acoustical padding and to support the mass of the box and laser on a series of damped low spring constant springs. This method was used by Rabinowitz, et. al[40] to achieve one part in $10^{10}$ or better frequency stability with a helium-neon laser.

Acoustical padding techniques are perfectly acceptable methods of isolating against acoustic noise. However, the main problem associated with using a damped spring isolator for mechanical vibration noise isolation is that the angular and spatial position of the laser

8.4.2 (Continued)

beam with respect to a base plane is very erratic and indeterminant. Such a situation is unacceptable for many applications and, if possible, techniques should be devised to mechanically stabilize the laser mounting structure.

A mechanical vibration noise isolator which does maintain rigid alignment of the laser beam with respect to the base can be made with a series of "layered media". The acoustical impedance of each layer is chosen so that a large impedance mismatch occurs at each interface. This causes large reflection of acoustic waves at the interfaces. The materials in the layers are further chosen to produce high acoustic wave absorption coefficients.

The net result is that mechanical vibration noise energy which must go through the "layered media" in the form of acoustic waves is reflected by the series of interfaces and the energy is absorbed in the layers. This is achieved while maintaining rigid alignment of the laser beam with respect to the base.

In addition to the "layered media" isolation at the bottom, the laser structure must be completely enclosed on the top and all four sides with a box containing acoustic damping material. This box may be made the main structural support member for bending if portability and ruggedness is desired. It is also desirable that the top and sides of this box be made with sandwich construction so that they will be heavily damped and not resonate.

Also extreme care must be made in the choice of components to be used near or within the laser structure which could be a source of vibration energy. A constant flowing gas system for the $CO_2$ laser would not be tolerable because of the vibration problems associated with a mechanical vacuum pump. Also the frequency modulation scheme to be used within the laser structure should be electro-optic in nature. The modulation scheme utilizing an oscillating mirror, which may be acceptable from the electronic point of view, would be a source of vibration which would be difficult to counteract.

Two $CO_2$ lasers have been built utilizing many of the ideas discussed above as part of the Sylvania Independent Research and Development Program. The laser cavities are shown in Figure 8-2. Noise isolation is achieved by putting the high resonance frequency laser cavity in an acoustic isolation box within an acoustic isolation box. The "layered media" at the bottoms and the acoustic isolation on the top and sides is clearly visible in the partially disassembled cavities.

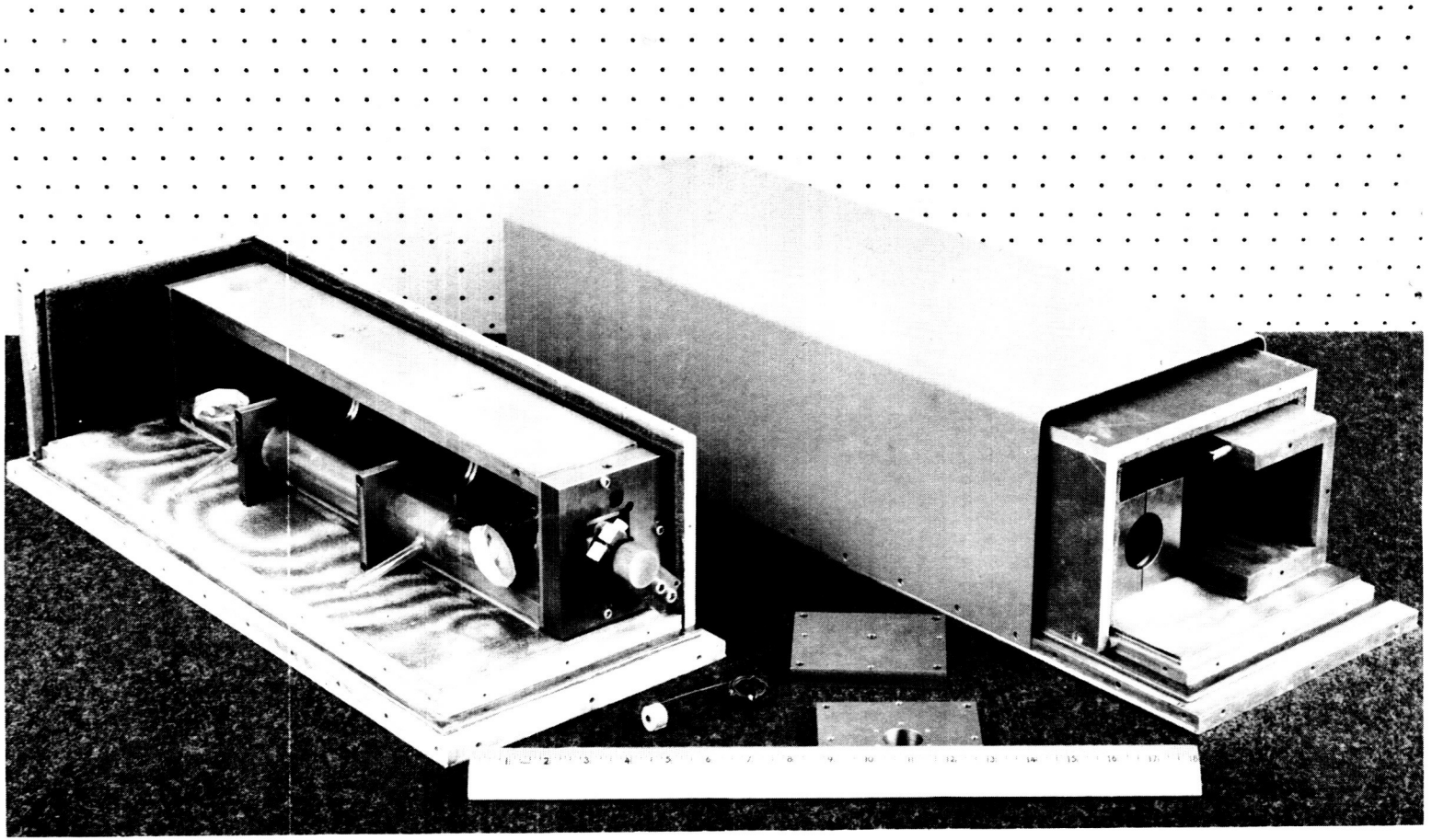

Figure 8-2. Experimental $CO_2$ Laser Structures Showing Laminations for Vibration Isolation

8.4.2 (Continued)

Construction of these cavities has only been recently completed. $CO_2$ lasers will be installed soon, and vibration isolation measurements will be made by laser heterodyne techniques.

The cavity for the stabilized $CO_2$ laser being designed for this program will be similar to these company-sponsored lasers. The design will follow the philosophy outlined above.

## 8.5 THERMAL DRIFT CONTROL

In Section 8.2 an equation was derived which related frequency stability to temperature changes for the typical $CO_2$ shown in Figure 8-1. This equation was

$$\frac{\partial\left(\frac{\Delta f}{f}\right)}{\partial T}\ \Delta T = -\frac{1}{L}\left\{\begin{array}{l} n_a(L_s\alpha_s\Delta T_s - L_c\alpha_c\Delta T_c) \\ \\ +2L_a\ \dfrac{\partial n_a}{\partial T}\ \partial T_a \\ \\ +W\left[\dfrac{2}{\cos\phi}\ \dfrac{\partial n_w}{\partial T} + \left(\dfrac{2n_w}{\cos\phi} - 4n_a\sin\phi\right)\alpha_w\right]\Delta T_w \end{array}\right\} \quad (8\text{-}12)$$

Thermal changes occur slowly and can be compensated for relatively easily by an automatic length control system, provided the range over which the length must be compensated is limited.

It is important that the relative magnitude of the terms in the equation be known. As an example, a typical case has been computed. In Table 8-4 the dimensionless form of each term is shown for a one°C temperature change in that element. Again assumptions more or less typical for high-stability $CO_2$ lasers have been made. We have assumed that the structure is made of special high-purity invar[41] such that $\alpha_s = 1.8 \times 10^{-7}$/°C and have assumed $L_s = 50.3$ cm. The compensator is assumed to be made of aluminum with $\alpha_c = 24 \times 10^{-6}$/°C and $L_c = 0.3$ cm. The Brewster windows are assumed to be made of KC1 3 mm thick with $n_w = 1.46$, $\partial n_w/\partial T = -25 \times 10^{-6}$/°C and $\alpha_w = 36 \times 10^{-6}$/°C. We have assumed $L_a = 3$ cm, $n_a = 1.00027$, and $\partial n_a/\partial T = 9.3 \times 10^{-7}$/°C. The mirror separation L is 50 cm.

For the $CO_2$ laser case assumed, all the terms are on the order of $10^{-7}$/°C. The structure and compensator terms can of course be varied by changing dimensions and coefficient of expansions. The Brewster angle window term can be varied slightly by changing window thickness, or it can be eliminated by changing to an internal mirror laser tube.

8.5 (Continued)

The effect of the air path term can be eliminated by evacuating the path or by changing to an internal mirror laser tube, or it can be reduced by using a helium-filled path.

Table 8-4. Relative Magnitude of Thermal Frequency Drift Terms for One°C Temperature Change

| Term | Magnitude |
|---|---|
| $\frac{n_a L_s \alpha_s \Delta T_s}{L}$ | $1.8 \times 10^{-7}$/°C |
| $\frac{-n_a L_c \alpha_c \Delta T_c}{L}$ | $-1.4 \times 10^{-7}$/°C |
| $\frac{2L_a \frac{\partial n_a}{\partial T} \Delta T_a}{L}$ | $1.1 \times 10^{-7}$/°C |
| $\frac{W\left[\frac{2}{\cos \phi} \frac{\partial n_w}{\partial T} + \left(\frac{2n_w}{\cos \phi} - 4n_a \sin \phi\right)\alpha_w\right] \Delta T_w}{L}$ | $-3.57 \times 10^{-7}$/°C |
| Sum of Above Terms | $-1.1 \times 10^{-7}$/°C |

8.5.1 External Temperature Control

One method of designing a low thermal drift $CO_2$ laser is to provide external temperature control. The compensating element can be eliminated and the temperatures maintained constant on the structure, the air path, and the Brewster angle windows. By this method, the total range of drift can be held so that it does not exceed the range of the control system.

Most control systems of this type have only the ability to add heat. They must, therefore, be operated at an elevated temperature in order to use the environment as a heat sink.

8.5.1 (Continued)

The use of an elevated temperature can be a problem. Some materials can decompose and optical surfaces can become contaminated due to migration of volatiles.

In the case of the $CO_2$ laser, however, the elevated temperature may be an asset in that the drier air would prevent attack by water vapor of any salt Brewster windows attached to the laser tube.

A good temperature-controlling system should be capable of maintaining the temperature within the laser cavity (laser tube on or off) to within a few degrees Celsius. For the example in Table 8.5, then, the expected drift from thermal changes would be about 5 parts in $10^7$ which corresponds to about 15 MHz for the $CO_2$ wavelength.

8.5.2 Thermally Compensating Structures

Another method of designing a low thermal drift $CO_2$ laser can be obtained by choosing the terms of the thermal drift equation to exactly cancel each other for as broad a temperature range as possible. For one element to compensate one or more other elements the temperature changes experienced by each must be identical. Such an assumption of several elements all experiencing identical temperature changes may not be bad if the changes are due to very slowly varying environmental changes or to slowly varying changes of a liquid temperature control fluid which is controlling the temperature of each of the elements. Such an assumption would certainly be bad if cyclical variations in temperature with significant thermal lag between the elements was occurring.

The simplest thermal compensation method is the so-called "bimetallic" compensation provided by adjusting the compensator term to just cancel the structure term. The assumption of equal temperature changes in the two elements may be very good if they are metals with insulating material, such as air around them. In this case they will essentially be isothermal items.

This "bimetallic" compensation method can be used for internal mirror laser tubes where the last two terms in the equation are zero, or for the case when the air path temperature and the Brewster angle window temperature are externally controlled.

## 8.6 ATMOSPHERIC PRESSURE VARIATION EFFECTS

Another somewhat related problem is frequency drift due to atmospheric pressure variations. The air path is the only portion affected, and the equation for such drifts is

8.6 (Continued)

$$\frac{\partial(\frac{\Delta f}{f})}{\partial p} \Delta p = \frac{2L_a}{L} \frac{\partial n_a}{\partial p} \Delta p \qquad (8\text{-}13)$$

The value of this equation for the assumed conditions for Table 8.5 with $\partial n_a/\partial p = 3.56 \times 10^{-7}$/mm Hg* is

$$\frac{\partial(\frac{\Delta f}{f})}{\partial p} = 4.27 \times 10^{-8}/\text{mm Hg} \qquad (8\text{-}14)$$

In the worst climates, monthly variations in pressures exceeding 40 mm Hg are extremely rare.[42]

So

$$\Delta(\frac{\Delta f}{f})_{p\ max} = 1.7 \times 10^{-6} \qquad (8\text{-}15)$$

The automatic length control system must have at least this range if pressure effects are to be compensated for.

As for the air path term in the thermal drift equation, this effect can be eliminated by using internal mirror laser tubes or evacuating the air path. The effect can also be greatly reduced by using a helium-filled path.

8.7 SUMMARY

To design a $CO_2$ laser with frequency stability of one part in $10^{10}$, the problems of acoustic and mechanical vibration noise and thermal frequency drifts must be carefully considered in designing a mechanical structure for the laser.

The structure should be designed so that its resonances fall at high frequencies where noise input power spectra are low, preferably about 2-3 kHz. The structure must be isolated from the acoustic noise and mechanical vibration noise environment, but must still maintain rigid alignment of the laser beam with the base of the instrument. Laminated structures with a high acoustic mismatch between layers appears to be a good approach. If possible, modulators used within the laser structure should be electro-optic in nature.

*Derived from Barrell, H. and I.E. Sears, Phil. Trans., A238, 1 (Feb 1934) and Edlen, B., J. Opt. Soc. Am., 43, 339 (May 1963)

8.7 (Continued)

The range of thermal frequency drifts must be restricted so that an automatic control system can compensate for the drifts by length adjustment. The range of the thermal drifts should be limited by external temperature control or by a combination of external temperature control and thermally compensating elements. The latter approach is the preferred.

Atmospheric pressure changes can produce a sizable frequency drift with lasers utilizing Brewster angle windows and must be considered in designing the range of the automatic control system.

Considering the available materials for use in a $CO_2$ laser structure and the capability of relatively simple temperature control systems, the source which has the greatest effect, in magnitude, on the laser frequency drift appears to be atmospheric pressure changes. The minimum range on the electronic control system appears to be about $10^{-6}$ meters for a 50-cm long laser. Larger ranges would be desirable.

# Section 9

# CONCLUSIONS

The previous sections discuss in detail the many areas which would affect the design of a frequency stabilized $CO_2$ laser. It has been determined that most of the stabilization schemes used previously on gas lasers are either not suitable for use with the $CO_2$ laser or would not be able to achieve the desired stability levels. However, a stabilization scheme which stabilizes the $CO_2$ laser output to an appropriate line in an external $CO_2$ amplifier appears to offer the best approach. A detailed analysis on the characteristics of this scheme has led to a design formulation which allows prediction of the minimum stabilization levels which can be achieved by this scheme. Since many of the design parameters of such a system can be left to the discretion of the designer, limitations based on a knowledge of "practical" systems have been imposed in the prediction of the lower stability limits.

The goal of a frequency stability level of 1 part in $10^{10}$ can be reached using system parameters as follows:

a. Servo-loop bandwidth to be 100 Hz or less.
b. Modulation frequency of external modulator to be $\geq$ 1 MHz.
c. Frequency modulation index to be greater or equal to unity.
d. The effective single-pass amplifier length is to be $\geq$ 1.8 meters.

The above requirements are based on the use of existing liquid nitrogen cooled, gold-doped-germanium detectors, chosen for highest D* at 10.6 $\mu$m.

Unfortunately, the noise characteristics of these detectors limit the system bandwidth by at least two orders of magnitude over the available liquid helium cooled detectors, placing a strong burden on the mechanical package design. It is felt, however, that because of the extreme operational difficulties associated with liquid helium cooled detectors, every effort should be made to operate with detectors which only need be cooled with liquid nitrogen. Since the electronic stabilization network will be limited to frequencies less than 100 Hz, the mechanical package will be required to essentially eliminate all vibrational influences which occur at frequencies higher than 100 Hz. Specialized techniques involving multilayered baffling will be necessary, but information gained from stability measurements on the He-Ne laser indicate that the desired results can be achieved.

9. (Continued)

To maintain high sensitivity, the modulation frequency should be chosen as high as the detector will allow, to a limit of about 20 MHz. The use of an electro-optic type modulator such as GaAs appears to be most suitable, especially if an extension to greater stability levels is desired in the future. Although not readily available, these modulators have been demonstrated to work very well at 10.6 $\mu$m.

In order to reduce the noise on the laser beam and increase tube life, r-f excitation techniques should be used for both the laser tube and the amplifier tube. The laser tube should be filled to an appropriate pressure utilizing a mixture of $CO_2$, $N_2$, and He for maximum output power. The amplifier should also be filled to an appropriate pressure and gas composition to provide for a maximum single-pass gain. The best operating conditions for the amplifier have not yet been determined and need to be examined during the course of the amplifier fabrication. Since heterodyne operation between two such lasers is contemplated, the $CO_2$ amplifiers for both lasers should be made and processed simultaneously. Unequal internal pressures can result in relatively large differences in output frequency (a few MHz per torr, typically). Fortunately, the effects of external magnetic fields and electric fields on the frequency stability of the laser will be negligible.

The cavity length for the laser should be chosen as long as possible, for highest output power, without running into mechanical resonance problems. A cavity length of about 1/2 meter seems to be a reasonable compromise. This cavity length should allow single-frequency power output levels on the order of 1/4 to 1/2 watt.

The $CO_2$ laser is capable of operation on many wavelengths, although only one at a time; and since heterodyne experiments will be performed with the laser, wavelength control and selection will be necessary. The technique for choice of a particular line can be accomplished in many ways, but no one technique appears to be outstanding. Wavelength control either by internal-cavity, frequency-etalon techniques or by externally activated search and acquisition techniques seem to be the most applicable. Further tests should be performed in this area during future portions of the program.

The technique which appears most suitable for higher order mode control utilizes a diffraction coupled output mirror. This technique allows mode control without restricting the power output capabilities of the laser.

Standard control-loop techniques can be used in the servo-control system and will not be a limiting factor in the operation of the system. Loop bandwidths on the order of 5 to

9. (Continued)

10 kHz are possible and could be utilized if better optical detectors were used. Bandwidths greater than 10 kHz would require specialized techniques.

It appears that "stretching" the design numbers to their limit and by utilizing the best available detectors (liquid helium cooled), the external amplifier scheme would be capable of a frequency stability on the order of 1 part in $10^{12}$.

# Section 10

## PLANS FOR THE NEXT PHASE

The next phase (Phase II) will be concerned with the design of a frequency-stabilized $CO_2$ laser. The design will be based on the findings of the study phase and the future requirement that two such lasers will be used in laboratory-type heterodyne experiments.

A design package complete with assembly and detailed drawings of mechanical and electrical components will be submitted at the conclusion of the phase. A final report on the work performed during the study and design phases of this program will be submitted, along with the design package. This report will be the concluding effort on this program.

## Section 11

## REFERENCES


1. Herzberg, G. "Molecular Spectra and Molecular Structure II, Infrared and Raman Spectra of Polyatomic Molecules," D. VanNostrand & Co. Inc., Princeton, N.J. 1945.

2. Patel, C. K. N., "Selective Excitation Through Vibrational Energy Transfer and Optical Maser Action in $N_2$- $CO_2$," Phy. Rev. Letters, 13, 617 (November 1964).

3. Barchewitz, P., et al., "Emission Infrarouge de CO et $CO_2$ laser continu a $CO_2$ par action directe d'une excitation haute frequence," C. R. Acad. Sc. Paris, t. 260, (29 March 1965), p. 3581.

4. Patel, C. K. N., "CW High Power $N_2$ $CO_2$ Laser," Appl. Phy. Let., Vol. 7, No. 1, (July 1965), pp. 15-17.

5. Bridges, T. J., and C. K. N. Patel, "High-Power Brewster Window Laser at 10.6 Microns," Applied Physics Letters, Vol. 7, No. 9, (November 1965), pp 244-245.

6. Moeller, G., and J. D. Rigden, "High-Power Laser Action in $CO_2$-He Mixtures," Applied Physics Letters, Vol. 7, No. 10, (November 1965), pp. 274-276.

7. Patel, C. K. N., P. K. Tien, and J. H. McFee, "CW High-Power $CO_2$-$N_2$-He Laser," Applied Physics Letters, Vol. 7, No. 11, (December 1965), pp. 290-292.

8. Barchewitz, P., et al., "Emission Laser continue par excitation haute frequence directe de $CO_2$ et $N_2O$ dans les transitions vibrationneles 00°1 - 10°1 - 02°0," C. R. Acad. Sc. Paris, t. 260, (24 May 1965), p. 5491.

9. Rigden, J. D., "State of the Art in $CO_2$ Lasers," WINCON Conference, Los Angeles, (4 February 1966).

10. Patel, C. K. N., "Interpretation of $CO_2$ Optical Maser Experiments," Phy. Rev. Let. Vol. 12, No. 21, (May 1964) pp. 588-590.

11. Moeller, G. and D. Rigden, "Observation of Laser Action in the R-Branch of $CO_2$ and $N_2O$ Vibrational Spectra," Applied Physics Letters, Vol. 8, No. 3, (Feb. 1966), pp. 69-70.

12. Gerry, E. T. and D. A. Leonard, "Measurement of 10.6$\mu$ $CO_2$ laser transition Probability and Optical Broadening Cross Sections", Appl. Phys. Lett., 8, 227 (1 May 1966)

11. (Continued)

13. White, A. D., "Frequency Stabilization of Gas Lasers," IEEE Journal of Quantum Electronics, QE-1, 349 (November 1965).

14. Bennett, W. R., "Mode Pulling in Gas Lasers", in Quantum Electronics III, P. Grivet and N. Bloembergen, Eds. New York, Columbia University Press, 1964, p. 441.

15. Bennett, W. R., S. F. Jacobs, J. T. Latourette, and P. Rabinowitz, "Dispersion Characteristics and Frequency Stabilization of a Gas Laser," Appl. Phys. Letters, Vol. 5., P. 56 (Aug. 1964).

16. White, A. D., E. I. Gordon, and E. F. Labuda, "Frequency Stabilization of Single Mode Gas Lasers," Appl. Phys. Letters, Vol. 5, P. 97 (Sept. 1964).

17. Farreng, R., et al, "Amplification du rayonnement d'un laser à $CO_2$ par du gaz carbonique excité en haute frequence", C. R. Acad. Sc. Paris, 261, 2617-2620 (4 Oct. 1965).

18. Sinclair, D. C., Prism Selection Section, "Choice of Mirror Curvatures for Gas Laser Cavities", Appl. Optics, 3, 1067 (1964).

19. Born, M., and F. Wolf, Principles of Optics, Pg 328 (Macmillan Co, N. Y. 1964).

20. Briggs, H. B., "Infrared Absorption in high Purity Germanium" J. Opt. Soc. Am. 42, 686 (1952).

21. Dash, W. C., and R. Newman, "Intrinsic Optical Absorption in Single Crystal Germanium and Silicon at 77°K and 300°K", Phys. Rev., 99, 1151 (1955).

22. Li, T., "Diffraction Loss and Selection of Modes in Maser Resonators with Circular Mirrors," Bell System Technical Journal, 45, 917, (May 1965).

23. Li, T., and P. W. Smith, "Mode Selection and Mode Volume Enhancement in a Gas Laser with Internal Lens," Proceedings of the IEEE, 53, 399, (April 1965).

24. Goldsborough, J. P., "Beat Frequencies between Modes of a Concave-Mirror Optical Resonator," Applied Optics, 3, 267 (February 1964).

25. Latourette, J. T., S. F. Jacobs, Sec. 62.4, P. Rabinowitz, "Improved Laser Angular Brightness through Diffraction Coupling", Appl. Optics, 3, 981 (Aug. 1964).

26. Prescott, L. J., and A. Vanderziel, "Detection of Spontaneous Emission Noise in He-Ne Lasers", Phys. Lett, 12, 317 (Oct. 1964).

11. (Continued)

27. Bellisio, J. A., C. Freed, and H. A. Hans, "Noise Measurements on He-Ne Laser Oscillators", Appl. Phys. Lett., 5, 5 (Jan. 1964).

28. American Institute of Physics Hand Book, 2nd Ed.

29. Smakula, A., "Synthetic Crystals and Polarizing Materials", Optica Acta, 9, 205 (July 1962).

30. Siegman, A. E., et al, Laser Material (Spectroscopy) Semi-annual Report No. 1 (December 15, 1964 to June 15, 1965), Contract DA28-043-AMC-00446(E), U. S. Army Electronics Command, Fort Monmouth, New Jersey. M. L. Report No. 1346, Microwave Laboratory, W. W. Hansen Laboratory of Physics, Stanford University.

31. Siegman, A. E., et al, Laser Material (Spectroscopy) Semi-annual Report No. 2 (June 15, 1965 - December 15, 1965), Contract DA28-043-AMC-00446(E), U. S. Army Electronics Command, Fort Monmouth, New Jersey. M. L. Report No. 1401, Microwave Laboratory, W. W. Hansen Laboratory of Physics, Stanford University.

32. Javan, A., E. A. Ballik, and W. L. Bond, "Frequency Characteristics of a Continuous-Wave He-Ne Optical Maser," J. Opt. Soc. Am., Vol. 52, No. 1, pp. 96-98, January 1962.

33. Jaseja, T. S., A. Javan, J. Murray and C. H. Townes, "Stability and Resettability of He-Ne Masers," Bull. Am. Phys. Soc., Ser. II, Vol. 7, No. 8, p. 553, November 1962.

34. Jaseja, T. S., A. Javan, and C. H. Townes, "Frequency Stability of He-Ne Masers and Measurement of Length," Phys. Rev. Letters, Vol. 10, No. 5, pp. 165-167, March 1963.

35. Bennett, W. R., "Inversion Mechanisms in Gas Lasers," Appl. Optics Supp. on Chem. Lasers, pp. 3-33, 1965.

36. Baird, K. M., D. S. Smith, G. R. Hanes, and S. Tsunekane, "Characteristics of a Simple Single-Mode He-Ne Laser," Appl. Optics, Vol. 4, No. 5, pp. 569-571, May 1965.

37. Smith, D. S., K. M. Baird, and W. E. E. Berger, "Electrodeless Excitation of He-Ne Gas Lasers," Appl. Optics, Vol. 4, No. 12, p. 1673, December 1965.

38. Russell Targ, Private Communication.

11. (Continued)

39. Kerr, J. R., "Microwave Optical Receiver Techniques," Sylvania Electric Products Inc Technical Report AFAL-TR-66, June 1966, Contract AF 33(615)-3108, Air Force Avionics Laboratory, Wright-Patterson Air Force Base, Ohio.

40. Rabinowitz, P., et al, "Theoretical and Experimental Investigation of Optical Heterodyning," Technical Report No. AFAL-TR-64-276, TRG Inc., Contract No. AF 33(657)-11372, Air Force Avionics Laboratory, Wright-Patterson AFB, Ohio (December 1964).

41. Foster, J. D., and I. Finnie, "Determination of Small Thermal Expansion Coefficients With a Single-Frequency Helium-Neon Gas Laser," (to be published).

42. Scott, C. A., C. J. Decarli, and R. N. Tone, "Four Barometric Pressure Environments for an Industrial Fringe-Counting Laser Interferometer", Sandia Corp. Tech. Memo SCL-TM-64-86, (Nov. 1964).

# Appendix A

## EVALUATION OF THE FUNCTION K ($\tilde{\alpha}$)

We have defined the function

$$\tilde{K}\ (\tilde{\alpha}) \equiv \int_{-\infty}^{\infty} \frac{1}{\tilde{\alpha} - jy}\ e^{-y^2}\ dy$$

In general, this function cannot be evaluated in any simple form. However, the following expansions do exist.

For large values of $\tilde{\alpha}$ one can expand the first term in the integrand in a Taylor series in powers of $y/\tilde{\alpha}$, and then integrate this series term by term. The result is

$$\tilde{K}\ (\tilde{\alpha}) \approx \frac{\sqrt{\pi}}{\tilde{\alpha}} \left[ 1 + \sum_{n=1}^{\infty} \frac{1 \cdot 3 \cdot 5 \cdots (2n-1)}{(j\sqrt{2}\ \tilde{\alpha})^{2n}} \right] \quad |\tilde{\alpha}| >> 1$$

It is important to note, however, that this series is only asymptotically convergent. That is, for any large value of $|\tilde{\alpha}|$ this series will at first converge as additional terms are included. If too many terms are taken, however, the factor $1 \cdot 3 \cdot 5 \cdot \cdots (2n-1)$ in the numerator will eventually become larger than the denominator, and the series will begin to diverge as still more terms are included. Hence, the above expansion must be applied with care.

Useful series expansions for small $\tilde{\alpha}$ can be obtained as follows. An integral expression for $d\tilde{K}(\tilde{\alpha})/d\tilde{\alpha}$ can be obtained by differentiating with respect to $\tilde{\alpha}$ inside the integral for $\tilde{K}\ (\tilde{\alpha})$. An integration by parts on the $d\tilde{K}(\tilde{\alpha})/d\tilde{\alpha}$ integral will then yield the differential equation

$$\frac{d\tilde{K}(\tilde{\alpha})}{d\tilde{\alpha}} = 2\tilde{\alpha}\,\tilde{K}(\tilde{\alpha}) - 2\sqrt{\pi}$$

A. (Continued)

Let $\tilde{K}(\tilde{\alpha}) = \exp(\tilde{\alpha}^2)\ \tilde{L}(\tilde{\alpha})$. Then

$$\frac{d\,\tilde{L}(\tilde{\alpha})}{d\tilde{\alpha}} = -2\sqrt{\pi}\ \exp(-\tilde{\alpha}^2)$$

Integrating both sides of this, and using the fact that $\tilde{K}(o) = \tilde{L}(o) = \pi$, gives

$$\tilde{L}(\tilde{\alpha}) = \pi - \int_o^{\tilde{\alpha}} 2\sqrt{\pi}\ e^{-t^2}\ dt$$

But, the definition of the error function, erf z, is

$$\text{erf } z \equiv \frac{2}{\sqrt{\pi}} \int_o^z e^{-t^2}\ dt$$

Hence, we obtain

$$\tilde{K}(\tilde{\alpha}) = \pi \exp(\tilde{\alpha}^2)\ \left[1 - \text{erf}\ \tilde{\alpha}\right]$$

Abramowitz and Stegun* give the series expansions

$$(7.1.5) \qquad \text{erf}\ \tilde{\alpha} = \frac{2}{\sqrt{\pi}} \sum_{n=o}^{\infty} \frac{(-1)^n\ \tilde{\alpha}^{2n+1}}{n!\ (2n+1)}$$

$$(7.1.6) \qquad \text{erf}\ \tilde{\alpha} = \frac{2}{\sqrt{\pi}} \exp(-\tilde{\alpha}^2) \sum_{n=o}^{\infty} \frac{2^n\ \tilde{\alpha}^{2n+1}}{1 \cdot 3 \cdot \cdots (2n+1)}$$

*Milton Abramowitz and Irene Stegun, Handbook of Mathematical Functions, Dover Publications.

A. (Continued)

By using either of these equations for small values of $\tilde{\alpha}$, together with the asymptotically convergent series given above for large $\tilde{\alpha}$, we obtain the asymptotic expressions:

$$K(\tilde{\alpha}) \approx \begin{cases} \pi - 2\sqrt{\pi}\,\tilde{\alpha}\,, & \tilde{\alpha} \to 0 \\ \dfrac{\sqrt{\pi}}{\tilde{\alpha}}, & \tilde{\alpha} \to \infty \end{cases}$$

The small $\tilde{\alpha}$ approximation is used in Section 4-4 of the text.

Appendix B

BIBLIOGRAPHY FOR MOLECULAR LASERS AND AMPLIFIERS


1. P. Barchewitz, et. al., "Infrared Emission of CO and $CO_2$ and CW $CO_2$ Laser Action by Direct High Frequency Excitation," Comp. Rend. 260 (13), 3581-3582, March 29, 1965 (in French).

2. P. Barchewitz, et. al., "Continuous Laser Action in $N_2O$ Produced by Direct High-Frequency Excitation," Comp. Rend. 260 (15), 4179-4181, April 12, 1965 (in French).

3. P. Barchewitz, et. al., "Continuous Laser Emission Through H. F. in $CO_2$ and $N_2O$ in the Vibrational Transition Domain 00°1-10°0 and 00°1-02°0," Comp. Rend. 260 (21), 5491-93, May 24, 1965 (in French).

4. T. J. Bridges and C. K. N. Patel, "High-Power Brewster Window Laser at 10.6 Microns," Appl. Phys. Letters 7, 244, 1 November 1965.

5. A. B. Callear, "Measurement of Energy Transfer in Molecular Collisions," Appl. Optics (Supplement 2: Chemical Lasers), 145-170, 1965.

6. P. K. Cheo and H. G. Cooper, "Excitation Mechanisms of Population Inversion in CO and $N_2$ Pulsed Lasers," Appl. Phys. Letters 5 (3), 42, August 1, 1964.

7. R. Farrenz, et. al., "Amplification of the Radiation From a $CO_2$ Laser by $CO_2$ Gas Under High Frequency Excitation," Comp. Rend. 261 (14), 2617-2620, October 4, 1965 (in French).

8. G. W. Flynn, M. A. Kovacs, C. K. Rhodes, and A. Javan, "Vibrational and Rotational Studies Using Q Switching of Molecular Gas Lasers," Appl. Phys. Letters 8 (63), 1 February 1966.

9. E. T. Gerry, "Pulsed-Molecular-Nitrogen Laser Theory," Appl. Phys. Letters 7 (1), 6-8, July 1, 1965.

10. A. Henry, et. al., "Laser Emission by Carbon Monoxide in the Visible Region," Comp. Rend. 261 (6), 1495-1497, August 9, 1965 (in French).

11. John A. Howe, "Effect of Foreign Gases on the $CO_2$ Laser: R-Branch Transistions," Appl. Phys. Letters 7 (1), 21-22, July 1, 1965.

B. (Continued)

12. M. A. Kovacs, G. W. Flynn, and A. Javan, "Q Switching of Molecular Laser Transitions," Appl. Phys. Letters 8, 62, 1 February 1966.

13. F. Legay and N. Legay-Sommaire, "The Possibility of an Optical Maser Utilizing the Vibrational Energy of Gases Excited by Activated $N_2$," Comp. Rend. 259 (2), 99, July 6, 1964 (in French).

14. N. Legay-Sommaire, L. Henry, and F. Legay, "A Laser Utilizing the Vibrational Energy of a Gas Excited by Activated Nitrogen (CO, $CO_2$, $N_2O$)," Comp. Rend. 260 (12), 3339-3342, March 22, 1965 (in French).

15. W. Lenz, Zeitshrift fur Physik 25, 299 (1924), and 80, 423 (1933).

16. D. A. Leonard, "Saturation of the Molecular Nitrogen Second Positive Laser Transition," Appl. Phys. Letters 7 (1), July 1, 1965.

17. L. E. S. Mathias and J. T. Parker, "Visible Laser Oscillations from Carbon Monoxide," Phys. Letters 7 (3), 194, November 15, 1963.

18. L. E. S. Mathias, A. Crocker, and M. S. Wills, "Laser Oscillations from Nitrous Oxide at Wavelengths Around 10.9 Microns," Phys. Letters 13 (4), 303, December 15, 1964.

19. A. C. G. Mitchell and M. W. Zemansky, Resonance Radiation and Excited Atoms, Chapter 4, Cambridge University Press, 1961.

20. G. Moeller and J. D. Rigden, "High-Power Laser Action in $CO_2$ -He Mixtures," Appl. Phys. Letters 7 (10), 274-276, November 15, 1965.

21. G. Moeller and J. D. Rigden, "Observation of Laser Action in the R-Branch of $CO_2$ and $N_2O$ Vibrational Spectra," Appl. Phys. Letters 8, 69, 1 February 1966.

22. C. K. N. Patel, "Interpretation of $CO_2$ Optical Maser Experiments," Physical Rev. Letters 12 (21), 588, May 25, 1964.

23. C. K. N. Patel, "Laser Oscillation on $X^1\Sigma^+$ Vibrational-Rotational Transitions of CO," Appl. Phys. Letters 5 (4), 81, August 15, 1964.

24. C. K. N. Patel, "Selective Excitation Through Vibrational Energy Transfer and Optical Maser Action in $N_2$ -$CO_2$," Physical Rev. Letters 13 (21), 617, November 23, 1964.

B. (Continued)

25. C. K. N. Patel, "Continuous-Wave Laser Action on Vibrational Rotational Transitions of $CO_2$," The Physical Review 136 (5A), A1187-A1193, November 30, 1964.

26. C. K. N. Patel, "CW Laser Action in $N_2O$ ($N_2$-$N_2O$ System), Appl. Phys. Letters 6 (1), 12-13, January 1, 1965.

27. C. K. N. Patel, "CW High-Power $N_2$-$CO_2$ Laser, Appl. Phys. Letters 7 (1), 15-17, July 1, 1965.

28. C. K. N. Patel, P. K. Tien, and J. H. McFee, "CW High-Power $CO_2$-$N_2$-He Laser," Appl. Phys. Letters 7 (11), 290-292, December 1, 1965.

29. C. K. N. Patel, "Efficient Phase-Matched Harmonic Generation in Tellurium with $CO_2$ Laser at 10.6 Microns," Physical Review Letters 15 (26), 1027-1030, December 27, 1965.

30. C. K. N. Patel, "Vibrational-Rotational Laser Action in Carbon Monoxide," The Physical Review 141 (1), 71-83, January 1966.

31. J. C. Polanyi, "Vibrational-Rotational Population Inversion," Appl. Optics (Supplement 2: Chemical Lasers), 109-127, 1965.

32. W. T. Wittenman, "Increasing Continuous Laser Action on $CO_2$ Rotational Vibrational Transitions Through Selective Depopulation of the Lower Laser Level by Means of Water Vapor," Phys. Letters 18 (2), 125-127, August 15, 1965.

33. G. Herzberg, Molecular Spectra and Molecular Structure. I. Spectra of Diatomic Molecules, D. Van Nostrand Company, Inc., New York, 1950.

34. G. Herzberg, Molecular Spectra and Molecular Structure. II. Infrared and Raman S Spectra of Polyatomic Molecules, D. Van Nostrand Company, Inc., New York, 1945.

35. A. E. Ruark and H. C. Urey, Atoms, Molecules and Quanta, second edition, Dover Publications, Inc., New York, 1964.

36. V. Kondratyev, The Structure of Atoms and Molecules, Gordon and Breach, New York (no date).

37. J. C. D. Brand and J. C. Speakman, Molecular Structure, Edward Arnold, Ltd., London, 1960.

8/5/67

SYLVANIA ELECTRONIC SYSTEMS

Government Systems Management

*for* GENERAL TELEPHONE & ELECTRONICS

40 SYLVAN ROAD, WALTHAM, MASS.